REMOVAL OF HALOACETONITRILES (HANs) AND
DISSOLVED ORGANIC NITROGEN (DON) IN WATER
BY VACUUM ULTRAVIOLET (VUV)

Miss Pradabduang Kiattisaksiri

A Dissertation Submitted in Partial Fulfillment of the Requirements
for the Degree of Doctor of Philosophy Program in Environmental Management
(Interdisciplinary Program)
Graduate School
Chulalongkorn University
Academic Year 2016
Copyright of Chulalongkorn University

การกำจัดสารฮาโลอะซิโตไนไตรล์และสารไนโตรเจนอินทรีย์ที่ละลายน้ำในน้ำ

ด้วยแวคคูอัมอัลตราไวโอเลต

นางสาวประดับดวง เกียรติศักดิ์ศิริ

Thesis Title	REMOVAL OF HALOACETONITRILES (HANs) AND DISSOLVED ORGANIC NITROGEN (DON) IN WATER BY VACUUM ULTRAVIOLET (VUV)
By	Miss Pradabduang Kiattisaksiri
Field of Study	Environmental Management
Thesis Advisor	Assistant Professor Thunyalux Ratpukdi, Ph.D.
Thesis Co-Advisor	Professor Eakalak Khan, Ph.D.
	Associate Professor Patiparn Punyapalakul, Ph.D.

Accepted by the Graduate School, Chulalongkorn University in Partial Fulfillment of the Requirements for the Doctoral Degree

⋯⋯⋯⋯⋯⋯⋯⋯⋯⋯⋯⋯⋯⋯⋯⋯ Dean of the Graduate School
(Associate Professor Sunait Chutintaranond, Ph.D.)

THESIS COMMITTEE

⋯⋯⋯⋯⋯⋯⋯⋯⋯⋯⋯⋯⋯⋯⋯⋯ Chairman
(Assistant Professor Chantra Tongcumpou, Ph.D.)

⋯⋯⋯⋯⋯⋯⋯⋯⋯⋯⋯⋯⋯⋯⋯⋯ Thesis Advisor
(Assistant Professor Thunyalux Ratpukdi, Ph.D.)

⋯⋯⋯⋯⋯⋯⋯⋯⋯⋯⋯⋯⋯⋯⋯⋯ Thesis Co-Advisor
(Professor Eakalak Khan, Ph.D.)

⋯⋯⋯⋯⋯⋯⋯⋯⋯⋯⋯⋯⋯⋯⋯⋯ Thesis Co-Advisor
(Associate Professor Patiparn Punyapalakul, Ph.D.)

⋯⋯⋯⋯⋯⋯⋯⋯⋯⋯⋯⋯⋯⋯⋯⋯ Examiner
(Assistant Professor On-anong Larpparisudthi, Ph.D.)

⋯⋯⋯⋯⋯⋯⋯⋯⋯⋯⋯⋯⋯⋯⋯⋯ Examiner
(Associate Professor Jin Anotai, Ph.D.)

⋯⋯⋯⋯⋯⋯⋯⋯⋯⋯⋯⋯⋯⋯⋯⋯ External Examiner
(Assistant Professor Bunyarit Panyapinyopol, Ph.D.)

ประดับดวง เกียรติศักดิ์ศิริ : การกำจัดสารฮาโลอะซิโตไนไตรล์และสารไนโตรเจนอินทรีย์ที่ละลายน้ำในน้ำด้วยแวคคูอัมอัลตราไวโอเลต (REMOVAL OF HALOACETONITRILES (HANs) AND DISSOLVED ORGANIC NITROGEN (DON) IN WATER BY VACUUM ULTRAVIOLET (VUV)) อ.ที่ปรึกษาวิทยานิพนธ์หลัก: ผศ. ดร. ธัญลักษณ์ ราษฎร์ภักดี, อ.ที่ปรึกษาวิทยานิพนธ์ร่วม: ศ. ดร. เอกลักษณ์ คาน, รศ. ดร. ปฏิภาณ ปัญญาพลกุล, 155 หน้า.

งานวิจัยนี้มีวัตถุประสงค์หลักในการศึกษาความเป็นไปได้ในการใช้แสงแวคคูอัมอัลตราไวโอเลต (VUV) และแสงอัลตราไวโอเลต (UV) เพื่อกำจัดสารฮาโลอะซิโตไนไตรล์ (HANs) และสารไนโตรเจนอินทรีย์ที่ละลายน้ำ (DON) ซึ่งเป็นสารตั้งต้นในการก่อตัวของ HANs

งานวิจัยส่วนที่ 1 มีเป้าหมายในการใช้ VUV และ UV เพื่อกำจัด HANs 4 ชนิด ได้แก่ โมโนคลอโรอะซิโตไนไตรล์ (MCAN) ไดคลอโรอะซิโตไนไตรล์ (DCAN) ไตรคลอโรอะซิโตไนไตรล์ (TCAN) และไดโบรโมอะซิโตไนไตรล์ (DBAN) โดยประสิทธิภาพในการย่อยสลายสารด้วย VUV และ UV เรียงลำดับได้ดังนี้ DBAN > TCAN > DCAN > MCAN ซึ่งค่าคงที่อัตราการย่อยสลายสารด้วย VUV มากกว่า UV 2-7 เท่า และการเติมก๊าซไนโตรเจนร่วมกับการฉายแสงรังสี VUV มีประสิทธิภาพในการย่อยสลายสารได้มากกว่าการเติมอากาศ เมื่อเปรียบเทียบระหว่าง HANs แบบสารผสมและสารเดี่ยว พบว่า VUV ย่อยสลายสารผสมได้น้อยกว่าสารเดี่ยว โดยกลไกหลักในการย่อยสลาย DBAN และ MCAN คือ รังสี UV (254 nm) และไฮดรอกซิลเรดิคอลตามลำดับ ในขณะที่ VUV (185 nm) เป็นกลไกสำคัญในการย่อยสลาย DCAN และ TCAN นอกจากนี้ยังพบว่าสารมัธยันตร์ที่เกิดจากการย่อยสลาย HANs ด้วย VUV เป็นผลจากปฏิกิริยาการแทนที่ ปฏิกิริยาการเติม และปฏิกิริยาการเกิดพอลิเมอร์

สืบเนื่องจากปัญหาการขาดแคลนน้ำ การนำน้ำเสียกลับมาใช้ประโยชน์จึงเป็นประเด็นที่น่าสนใจศึกษาในแง่ของการเกิดสารพลอยได้จากการปรับปรุงคุณภาพน้ำ โดยงานวิจัยในส่วนที่ 2 จะเน้นการกำจัด DON ในน้ำผิวดิน (SW) และน้ำทิ้ง (WW) ด้วยวิธี VUV และ UV ร่วมกับการเติมไฮโดรเจนเปอร์ออกไซด์ (VUV VUV/H_2O_2 UV และ UV/H_2O_2) จากการศึกษาพบว่าการลดลงของคาร์บอนอินทรีย์ละลายน้ำ (DOC) DON ลักษณะความไม่ชอบน้ำ (Hydrophobicity) การดูดซับรังสี 254 nm (UV_{254}) และองค์ประกอบของสารอินทรีย์จากการวิเคราะห์ FEEM มีค่าลดลงหลังการบำบัดตัวอย่างน้ำทั้งสองแหล่งด้วย VUV มากกว่า UV นอกจากนี้ยังพบว่าการเติม H_2O_2 ช่วยเพิ่มประสิทธิภาพของทั้งสองระบบ โดยระบบที่มีประสิทธิภาพสูงสุด คือ VUV/H_2O_2 และในการศึกษา HANFP สังเกตได้ว่า HANFP มีแนวโน้มที่เพิ่มขึ้นในช่วงแรกและลดลงในช่วงท้าย (60 นาที) ซึ่งการลดลงของ HANFP มีความสัมพันธ์กับการลดลงของค่า DOC DON Hydrophobicity และ UV_{254} จากผลการวิเคราะห์ FEEM พบว่าการลดลงของสารอินทรีย์กลุ่มทริปโตเฟนมีความสัมพันธ์อย่างมากกับการลดลงของ HANFP ซึ่งอาจกล่าวได้ว่าสารอินทรีย์กลุ่มทริปโตเฟนน่าจะเป็นสารตั้งต้นในการเกิด HANs

สาขาวิชา	การจัดการสิ่งแวดล้อม	ลายมือชื่อนิสิต _____
ปีการศึกษา	2559	ลายมือชื่อ อ.ที่ปรึกษาหลัก _____
		ลายมือชื่อ อ.ที่ปรึกษาร่วม _____
		ลายมือชื่อ อ.ที่ปรึกษาร่วม _____

5487780020 : MAJOR ENVIRONMENTAL MANAGEMENT

KEYWORDS: VACUUM ULTRAVIOLET / HALOACETRONITRILES / DISSOLVED ORGANIC NITROGEN / NITROGENOUS DISINFECTION BYPRODUCTS / DEGRADATION MECHANISM / DISINFECTION BYPRODUCTS FORMATION

PRADABDUANG KIATTISAKSIRI: REMOVAL OF HALOACETONITRILES (HANs) AND DISSOLVED ORGANIC NITROGEN (DON) IN WATER BY VACUUM ULTRAVIOLET (VUV). ADVISOR: ASST. PROF. THUNYALUX RATPUKDI, Ph.D., CO-ADVISOR: PROF. EAKALAK KHAN, Ph.D., ASSOC. PROF. PATIPARN PUNYAPALAKUL, Ph.D., 155 pp.

The main objective of this dissertation was to investigate the feasibility of using vacuum ultraviolet (VUV, 185+254 nm) and ultraviolet (UV, 254 nm) for removal of haloacetronitriles (HANs) and dissolved organic nitrogen (DON). The first part of the work aimed to study the degradation of four HANs species (monochloroacetonitrile (MCAN), dichloroacetonitrile (DCAN), trichloroacetonitrile (TCAN), and dibromoacetonitrile (DBAN)) directly by VUV and UV. The order of degradation rate was DBAN>TCAN>DCAN>MCAN for both systems. Degradation rate constants of HANs under VUV were 2-7 times greater than UV. HANs removal under nitrogen purging was much higher than under air purging. The removal efficiencies of mixed HANs were lower than that of single HANs. The major degradation mechanism of DBAN and MCAN was 254 nm (direct photolysis) and hydroxyl radical, respectively. DCAN and TCAN were more susceptible to degradation by 185 nm (direct photolysis). The intermediates from HANs removal by VUV were produced from substitution, addition, and polymerization reactions.

The second part focused on DON removal by VUV, VUV/H_2O_2, UV and UV/H_2O_2 to reduce HANs formation potential (HANFP). This part was conducted using not only surface water (SW) but also treated wastewater effluent (WW) for water reclamation application. The results showed that the reduction of dissolved organic carbon (DOC), DON, hydrophobicity, absorbance at 254 nm (UV_{254}), and fluorescence excitation-emission matrix (FEEM) of both water samples by VUV was higher than UV. Addition of H_2O_2 improved the performances of VUV and UV. VUV/H_2O_2 exhibited the highest removal efficiency for all parameters studied. Even though HANFP increased at the early stage, its concentration decreased at the end of treatment (60 min). Decreases in DON, DOC, hydrophobicity, and UV_{254} led to HANFP reduction. Moreover, FEEM revealed that substantial reduction in tryptophan (nitrogen-rich organic) had strong correlation with HANFP reduction, implying this group of compounds act as a precursor of HANs.

Field of Study: Environmental Management   Student's Signature ----------------------------

Academic Year: 2016   Advisor's Signature ----------------------------

                                                 Co-Advisor's Signature ----------------------------

                                                 Co-Advisor's Signature ----------------------------

ACKNOWLEDGEMENTS

CONTENTS

LIST OF TABLES

LIST OF FIGURES

LIST OF ABBREVIATIONS

AOPs	Advanced oxidation processes
BAC	Biologically activated carbon
BDCM	Bromodichloromethane
BCAN	Bromochloroacetonitrile
BF	Bromoform
C-DBPs	Carbonaceous disinfection byproducts
CF	Chloroform
DBAA	Dibromoacetic acid
DBCM	Dibromochloromethane
DBAN	Dibromoacetonitrile
DBPs	Disinfection byproducts
DCAA	Dichloroacetic acid
DCAcAm	Dichloroacetamide
DCAN	Dichloroacetonitrile
DIN	Dissolved inorganic nitrogen
DO	Dissolved oxygen
DOC	Dissolved organic carbon
DON	Dissolved organic nitrogen
FEEM	Fluorescent excitation emission matrix
GC-ECD	Gas chromatography-electron capture detector
GC/MS	Gas chromatography/mass Spectrometry
HAAs	Haloacetic acids
HAcAms	Haloacetamides
HANs	Haloacetronitriles
HANFP	Haloacetronitriles formation potential
HPI	Hydrophilic
HPO	Hydrophobic
IAN	Iodoacetonitrile
LP-Hg	Low pressure mercury lamp
LP-Hg-VUV	Low pressure mercury VUV lamp

LP-Hg-UV	Low pressure mercury UV lamp
MB	Methylene blue
MBAN	Monobromoacetonitrile
MCAA	Monochloroacetic acid
N-DBPs	Nitrogenous disinfection byproducts
NDEA	*N*-nitrosodiethylamine
NDMA	*N*-nitrosodimethylamine
NOM	Natural organic matter
TCAcAm	2,2,2-trichloroacetamide
TCAA	Trichloroacetic acid
TCAN	Trichloroacetonitrile
TBA	*Tert*-butanol
TDN	Total dissolved nitrogen
THMs	Trihalomethanes
U.S.EPA	United States Environmental Protection Agency
UV	Ultraviolet
UV/H_2O_2	Ultraviolet/Hydrogen peroxide
UV/H5	Ultraviolet/Hydrogen peroxide 5 mg L^{-1}
UV/H10	Ultraviolet/Hydrogen peroxide 10 mg L^{-1}
UV/H20	Ultraviolet/Hydrogen peroxide 20 mg L^{-1}
UV/H50	Ultraviolet/Hydrogen peroxide 50 mg L^{-1}
VUV	Vacuum ultraviolet
VUV+Air	Vacuum ultraviolet with air purging
VUV+N_2	Vacuum ultraviolet with nitrogen gas purging
VUV/H_2O_2	Vacuum ultraviolet/Hydrogen peroxide
VUV/H5	Vacuum ultraviolet/Hydrogen peroxide 5 mg L^{-1}
VUV/H10	Vacuum ultraviolet/Hydrogen peroxide 10 mg L^{-1}
VUV/H20	Vacuum ultraviolet/Hydrogen peroxide 20 mg L^{-1}
VUV/H50	Vacuum ultraviolet/Hydrogen peroxide 50 mg L^{-1}
VUV+TBA	Vacuum ultraviolet with *tert*-butanol addition
WHO	World Health Organization

CHAPTER 1
INTRODUCTION

1.1 Background

Disinfection byproducts (DBPs) are a group of chemical contaminants formed in water during the disinfection processes in drinking water treatment. Chlorine and chloramines are the most widely used as disinfectants because they are effective in killing harmful microorganisms, and their ability to provide residuals in water distribution system. However, disinfectants themselves can react with organic precursor in water to form undesirable chemical DBPs. Two groups of carbonaceous DBPs (C-DBPs), trihalomethanes (THMs) and haloacetic acids (HAAs) are considered to be the dominant DBPs in drinking water. Most previous studies have focused on them; therefore, the formation and control of these regulated DBPs have been well studied. In addition to THMs and HAAs, emerging unregulated nitrogenous DBPs (N-DBPs) such as *N*-nitrosodimethylamine (NDMA), haloacetronitriles (HANs), halonitromethanes (HNMs), and haloacetamides (HAcAms) have received research attention. It is because they are significantly more genotoxic and cytotoxic than regulated C-DBPs and the order of their toxicity was iodine > bromine > chlorine (Muellner et al., 2007; Plewa et al., 2004). Although these N-DBPs often occur at a lower level than those regulated C-DBPs, they should be a concern owing to their greater toxicity.

HANs is one group of a high priority DBPs included in a United State (U.S.) nationwide DBP occurrence study (Richardson, 2003). A survey on 12 drinking water treatment plants in the U.S. found that HANs had the highest formation of the three major N-DBP groups (HANs, HNMs, and HAcAms), with the maximum values of 14 µg L^{-1} (Krasner et al., 2006). In the U.S. EPA's Information Collection Rule (ICR), HANs ranged from <0.5 to 41 µg L^{-1} (Muellner et al., 2007). ICR data are collected as part of a national research project to support development of national drinking water standards which protect public health. In addition, HANs formation potential (HANFP) from 166 samples collected from both potable water and wastewater treatment plants across the U.S. ranged from 0.5 to 70 µg L^{-1} (Chen & Westerhoff, 2010). Despite no

regulation for any types of HANs, the World Health Organization (WHO) has suggested the guideline value of 70 µg L^{-1} for dibromoacetonitrile (DBAN), and a provisional guideline value of 20 µg L^{-1} for dichloroacetonitrile (DCAN) (WHO, 2011). However, due to their occurrence, formation and potential health effects to human health, they may be considered in future regulations.

N-DBPs formed when chemical disinfectants react with N-DBP precursors. For HANs, they can be produced from either chlorination or chloramination. DCAN formation was higher by chlorination than chloramination (Dotson, Westerhoff, & Krasner, 2009; Huang et al., 2012; Yang et al., 2012). Dissolved organic nitrogen (DON) is one of the most significant parameters in drinking water treatment due to its potential to form N-DBPs. DON such as amino acids is the main precursor of HANs (Chen & Westerhoff, 2010; Lee, Westerhoff, & Croué, 2007).

Generally, there are two main methods to control DBPs: (1) removal of precursor prior to disinfection; and (2) removal of DBPs after their formation. Nowadays, various techniques are available for removing DBPs and precursor from water. Among them, advanced oxidation processes (AOPs) seem to be a powerful technique for the disinfection of drinking water and degradation of DBPs and precursor. The treatments by light, especially ultraviolet (UV) radiation at 200 to 400 nm, appear to be one of the most popular technologies for water purification. There are no chemicals used in the UV process. Therefore, it does not produce significant levels of DBPs.

Besides UV, vacuum UV (VUV) is an attractive process. VUV is associated with the emission of the radiation in the wavelength of 100 to 200 nm. Water treatment by VUV radiation can result in the photolysis of pollutants and the formation of oxidizing species. The VUV radiation can photolyze water molecules to form hydroxyl radical (OH$^{\bullet}$) (Gonzalez, Oliveros, Wörner, & Braun, 2004). The direct photolysis is dependent on the ability of compounds or medium to absorb the emitted light. Fortunately, water absorbs UV light strongly at wavelengths lower than 190 nm (Kutschera, Börnick, & Worch, 2009). A previous study proved that the mineralization rate of dissolved organic carbon (DOC) provided by the VUV process was higher than that provided by the UV process (Ratpukdi, Siripattanakul, & Khan, 2010). In addition, a number of previous studies have demonstrated that VUV treatment was effective in the removal of many pollutants such as organic azo dye, perfluorooctanoic acid, taste and odor compounds

(Kutschera, Börnick, & Worch, 2009), natural organic matter (NOM), THMs and HAAs (Buchanan, Roddick, & Porter, 2006; Buchanan, Roddick, Porter, & Drikas, 2005; Dobrović, Juretić, & Ružinski, 2007).

1.2   Research problem statement

HANs are one of the emerging N-DBPs group. They were reported to be more toxicity than currently regulated DBPs such as THMs or HAAs. Although HANs are not currently regulated, it has potential to be included in the drinking water standard in the future. Therefore, controlling or removing HAN is important for better safe drinking water and to meet with future regulations.

To the best of our knowledge, there has been no research related to the application of VUV for the degradation of HANs and DON and also the characteristic of DON after VUV treatment has never been studied. Therefore this work has been divided into two parts to determine the most appropriate approach to control HANs. The first part was to investigate the HANs removal by VUV in comparison with conventional UV. The main objective of this part was to investigate the removal efficiency, kinetic rate constants, degradation mechanisms (direct and indirect photolysis), and intermediate photolysis products of HANs.

The second part was to investigate the removal of DON (HANs precursor) and reduction of HANFP. The effect of hydrogen peroxide (H_2O_2) addition to enhance the removal of DON and HANFP was studied. Relationships of HANFP and DON reduction was determined. Moreover, NOM characteristics (i.e. DOC, UV absorbance at 254 nm (UV_{254}), hydrophilic (HPI) and hydrophobic (HPO) fractions, and fluorescent excitation emission matrix (FEEM)) after treatment by VUV, VUV/H_2O_2, UV and UV/H_2O_2 were also examined to better understand of HANFP.

AOPs are capable of reducing the concentration of N-DBPs in drinking water and reclaimed water. The most popular AOPs are UV photolysis and UV with H_2O_2 addition (Afzal, Kang, Choi, & Lim, 2016; Fang, Ling, & Shang, 2013; Hou et al., 2017; Ling, Sun, Fang, & Shang, 2016; Zhou et al., 2012). VUV is a relatively new AOP that has an advantage in degrading the contaminants without additional chemicals to generate OH$^{\bullet}$. It shows high efficiency in the degradation of various organic pollutants. In addition, the elimination of HANs precursor in this research focused on

not only drinking water but also treated wastewater. Because of water shortage in different parts of the world, the reclamation of wastewater has increased. This research attempted to investigate the feasibility of using VUV-based AOPs for treating high DON in treated wastewater. The formation of HANs after treatments is also examined in order to find out whether or not VUV-based AOPs can control HANs formation in drinking water and treated wastewater.

1.3 Research objectives

The main objective of this research is to investigate the feasibility of using VUV process for the control of HANs and DON in water and treated wastewater. The sub-objectives are as follows:

(1) To determine the effect of dissolved oxygen (DO) on the degradation of HANs water by VUV in comparison with UV.

(2) To clarify the role of direct photolysis and OH$^\bullet$ on the degradation of HANs under VUV and UV systems.

(3) To study the effect of H_2O_2 on the removal of DON and HANFP by VUV, VUV/H_2O_2, UV, and UV/H_2O_2.

(4) To elucidate the link between DON characteristics and HANFP after treatment by VUV, VUV/H_2O_2, UV, and UV/H_2O_2.

1.4 Research hypotheses

The hypotheses of this study were formulated corresponding to the objectives:

(1) VUV process can remove HANs in water better than UV process. The increasing of DO level could enhance the degradation efficiency of HANs by VUV and UV.

(2) The formation of OH$^\bullet$ under VUV light could play a dominant role in the degradation of HANs.

(3) VUV system performs better on the removal of DON than UV. The addition of H_2O_2 could enhance the reduction of DON due to the increasing of OH$^\bullet$ formation under VUV and UV systems.

(4)   The more hydrophilic DON, and proteinaceous components of DON could affect the treatability by VUV. The removal of these DON components could reduce the formation of HANs after chlorination.

1.5   Dissertation organization

This dissertation is divided into 6 chapters.

Chapter 1 includes background, research problem statement, research objectives, research hypotheses and dissertation organization (this section).

Chapter 2 provides a literature review on HANs and DON. This chapter describes formation and control of HANs and DON by AOPs. A review on DON is also described in details particularly on the occurrence and structural characterization.

Chapter 3 illustrates an overall research framework, scope of the study, and experimental design and set up.

Chapter 4 presents the results from the degradation of HANs by VUV and UV processes. The competitive effect among mixed HANs is included. Moreover, the effects of DO and nitrogen purging are also described. The work described in this chapter is based on a manuscript titled **"Photodegradation of haloacetonitriles in water by vacuum ultraviolet irradiation: Mechanisms and intermediate formation"**. This manuscript has been published in *Water Research* (Kiattisaksiri et al., 2016).

Chapter 5 deals with the reduction efficiency of DON by VUV and UV with and without H_2O_2 addition. The links between NOM characteristics (i.e. DOC, HPI and HPO fractions, UV_{254}, and FEEM) and HANFP are also touched on. This chapter is based on a manuscript under preparation titled **"Reduction of dissolved organic nitrogen (DON) and haloacetonitriles (HANs) formation in drinking water and treated wastewater by VUV-based AOPs"**, which will be submitted to *Water Research.*

Chapter 6 concludes the key results of the study and proposes recommendations for future research.

CHAPTER 2
LITERATURE REVIEW

2.1   Conventional water treatment process

Source waters contain a wide range of contaminants that may make the water unsafe to drink or use for daily life. Such contaminants include suspended solids content, bacteria, algae, organic matter, creating bad taste and odor. Source water may be treated differently in different communities depending on the water quality which enters the plant. However, conventional water treatment process typically consists of the following unit process: coagulation, flocculation, sedimentation, filtration, and disinfection. The conventional water treatment process is shown in Figure 2.1.
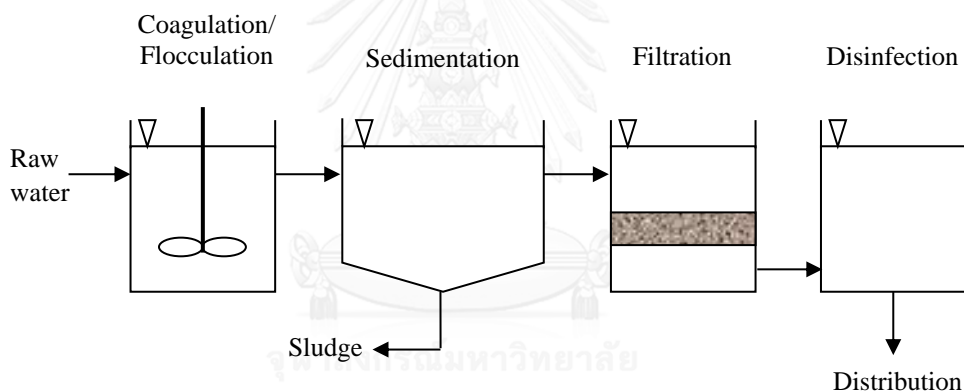
Figure 2.1 The conventional water treatment process

In brief, coagulation is the process of rapidly mixing coagulants (e.g. iron, aluminum salts, and polymer) to raw water, causing the neutralization of water. During flocculation, slow mixing brings the small particles together to form larger particles called floc. In sedimentation unit, mixing is stopped and allows the floc settles to the bottom. The clear water moves to filtration which removes particulate matter by forcing the water to pass through porous media (e.g. sand, gravel, and charcoal). Finally, water is disinfected before it distributed to public. The main reason for water disinfection is to prevent the transmission of waterborne disease through the inactivation of pathogenic microorganisms, such as viruses, bacteria and protozoa that can cause serious illnesses or death to human.

2.2 Disinfection and disinfection byproducts formation

2.2.1 Disinfection

Disinfection is an important step for ensuring that water is safe to drink. There are two kinds of disinfection: primary and secondary disinfection. The purpose of primary disinfection is to kills or inactivates disease-causing organisms, while secondary disinfection is to maintain a disinfectant residual in the finish water along the distribution system to prevent the re-growth of microorganism.

There is a wide range of disinfectants used in water treatment including chlorine, chloramines, chlorine dioxide and ozone. The most commonly employed disinfectant is chlorine. It is used as a primary disinfectant in the majority of all surface water treatment plants. Chlorine at a lower concentration (1 to 3 mg L^{-1}) is usually maintained as a secondary disinfectant in most water systems. Chlorine has successfully protected public health against waterborne disease. Although it is effective and cheapest among other disinfectants, chlorine poses significant hazards to human life since it can reacts with organic compounds in water and form carcinogenic disinfection byproducts (DBPs). Other alternatives disinfectants such as chloramines, chlorine dioxide, and ozone also produce their own set of DBPs. The detail of DBPs types and formation is presented in the next section.

2.2.2 Formation of DBPs

Disinfection byproducts (DBP) is a term used to describe a group of organic and inorganic compounds formed during the disinfection processes of water (Xie, 2004). These byproducts are produced by the reactions between disinfectants and precursors in water, as simply shown in Equation (2.1).

$$\text{Disinfectants + precursor} \longrightarrow \text{DBPs} \qquad (2.1)$$
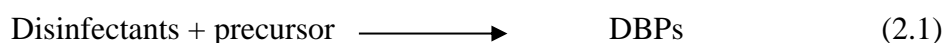
There are two kinds of precursors: organic and inorganic precursor. NOM (e.g. humic and fulvic materials, algal-derived organic matter), serves as the organic precursor, while bromide ion serves as the inorganic precursor in water. All commonly used disinfectants react with these precursors to form the different types of DBPs. Table

2.1 is a list of significant DBPs produced by the different types of disinfectants (Sadiq & Rodriguez, 2004).

Table 2.1 Formation of DBPs from different types of disinfectants

Class of DBPs (Example)	Types of disinfectants			
	Chlorine	Ozone	ClO$_2$	Chloramines
Trihalomethanes (THMs)	✓[a]	✓[b]		✓
Other haloalkanes	✓			
Haloalkenes	✓			
Haloacetics acids (HAAs)	✓			✓
Haloaromatic acids	✓			
Other halomonocarboxylic acids	✓			✓
Unsaturated halocarboxylic acids	✓			✓
Halodicarboxylic acids	✓			✓
Halotricarboxylic acids	✓			
MX and analogues	✓		✓	✓
Other halofuranones	✓			
Haloketones	✓	✓	✓	
Haloacetonitriles (HANs)	✓	✓		✓
Other halonitrile (cyanogen chloride)	✓			✓
Haloaldehyde (chloral hydrate)	✓			✓
Haloalcohols	✓			✓
Phenols	✓	✓		
Halonitromethane	✓			
Inorganic compounds (e.g. bromate, hypobromite, chlorite and chlorate)		✓	✓	
Aliphatic aldehyde (formaldehyde)	✓	✓	✓	
Other aldehydes	✓	✓	✓	
Aliphatic and aromatic ketones (acetone)	✓	✓	✓	

Class of DBPs (Example)	Types of disinfectants			
	Chlorine	Ozone	ClO$_2$	Chloramines
Carboxylic acids (acetic acid)	✓	✓	✓	
Aromatic acids (benzoic acid)	✓	✓	✓	
Aldo and ketoacids		✓	✓	
Hydroxyl acids	✓	✓	✓	
Others	✓	✓	✓	✓

Remark:

Major classes of DBPs are shown in bold.

[a] There are four regulated THMs, but if iodomethanes are included in THMs, then there will be nine compounds.

[b] Bromoform is produced if bromide ion is presented.

There are more than 500 different types of DBPs have already been identified in water (Richardson, 2003). THMs and HAAs, are two main groups of C-DBPs in drinking water. Their formation is linked to the reactions between chlorine and NOM. For brominated THMs and HAAs, their formation is due to the bromide ion in chlorinated water. In order to reduce the formation of regulated THMs and HAAs, many drinking water facilities are changing the disinfectant from chlorine to alternative disinfectants. However, these alternatives can lead to the formation of other potentially DBPs. For example, DBPs detected from the use of chloramines as water disinfectants are HANs, HNMs, and nitrosamine. These emerging unregulated byproducts are categorized as N-DBPs. Generally, the important precursor of N-DBPs is DON (Lee, Westerhoff, & Croué, 2007).

A number of factors, both water quality parameters and treatment operating conditions, can affect the formation of DBPs. These factors include disinfectant type and dose, contact time, temperature, pH, concentrations of organic matter and other precursors present in water, and length of the distribution network.

2.2.3 Toxicity of DBPs

Adverse effects from toxicological laboratory studies of some important DBPs are summarized in Table 2.2 (Sadiq & Rodriguez, 2004).

Table 2.2 Toxicological information for DBPs

Class of DBPs	Compound	Rating
Trihalomethanes (THMs)	Chloroform (CF)	B2
	Dibromochloromethane (DBCM)	C
	Bromodichloromethane (BDCM)	B2
	Bromofrom (BF)	B2
Haloacetics acids (HAAs)	Dichloroacetic acid (DCAA)	B2
	Trichloroacetic acid (TCAA)	C
Haloacetonitriles (HANs)	Trichloroacetonitrile (TCAN)	C
Inorganic compound	Bromate	B2
	Chlorite	D

Remark:

A = Human carcinogen

B1 = Probable human carcinogen (with some epidemiological evidence)

B2 = Probable human carcinogen (sufficient laboratory evidence)

C = Possible human carcinogen

D = Non classifiable

2.2.4 Regulation and standard of DBPs

Due to the toxicological information and adverse health effect, many institutes set regulation, guideline and standard for significant DBPs as summarized in the table below (Richardson, 2003; WHO, 2011).

Table 2.3 DBPs regulations, guideline, and standard

Class of DBPs / Compound	U.S.EPA regulation ($\mu g\ L^{-1}$)	WHO guideline ($\mu g\ L^{-1}$)	EU standard ($\mu g\ L^{-1}$)
Total THMs[a]	80	1[c]	100
Chloroform (CF)	-	300	-
Bromoform (BF)	-	100	-
Bromodichloromethane (BDCM)	-	60	-
Dibromochloromethane (DBCM)	-	100	-
Five HAAs[b]	60	-	-
Monochloroacetic acid (MCAA)	-	20	-
Dichloroacetic acid (DCAA)	-	50[d]	-
Trichloroacetic acid (TCAA)	-	200	-
Dichloroacetonitrile (DCAN)	-	20[d]	-
Dibromoacetonitrile (DBAN)	-	70	-
Bromate	10	10[d]	10
Chlorite	1000	700[d]	-
Chloral hydrate	-	10[d]	-
Trichloroethane	-	20[d]	-
Tetrachloroethene	-	40[d]	-
2,4,6-Trichlorophenol	-	200	-
Formaldehyde	-	900	-

Remark:

[a] The sum of four THMs species: CF, BF, BDCM, and DBCM.

[b] The sum of five HAAs species: MCAA, DCAA, TCAA, monobromoacetic acid (MBAA), and dibromoacetic acid (DBAA).

[c] WHO guidelines on THMs state that the sum of the ratio of the concentration of each THM (CF, BF, BDCM, DBCM) to its respective guideline value should not exceed unity. For authorities wishing to establish a total THM standard to account for additive toxicity, the following fractionation approach could be taken:

$$\frac{C_{CF}}{GV_{CF}} + \frac{C_{BF}}{GV_{BF}} + \frac{C_{BDCM}}{GV_{BDCM}} + \frac{C_{DBCM}}{GV_{DBCM}} \leq 1$$

Where, C is concentration and GV is guideline value.

Authorities wishing to use a guideline value for total THMs should not simply add up the guideline values for the individual compounds in order to arrive at a standard.

[d] Provisional guideline value

2.3   Haloacetonitriles (HANs)

2.3.1   Physio-chemical properties of HANs

HANs is a group of N-DBPs detected in drinking water. They can produce during water chlorination or chloramination from naturally occurring substances, such as algae, amino acid, fulvic acid and proteinaceous material. There are many type of HANs commonly found in water including MCAN, DCAN, TCAN and DBAN. DCAN is the most prevalent HANs species that are often identified. The molecular structure of four HANs is shown in Figure 2.2 and physical and chemical properties of HANs are summarized in Table 2.4**.**
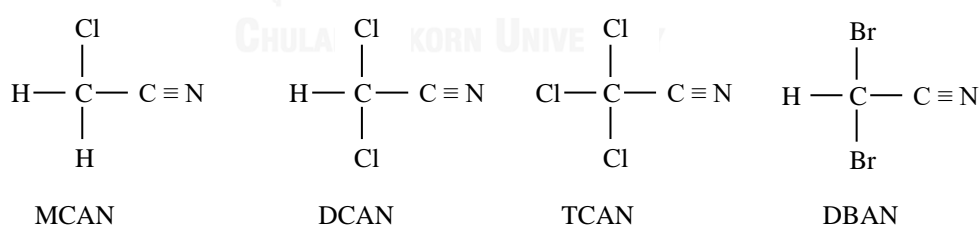
Figure 2.2 Molecular structures of HANs

Table 2.4 Physical and chemical properties of HANs

Properties	MCAN	DCAN	TCAN	DBAN
Formula	C_2H_2ClN	C_2HCl_2N	C_2Cl_3N	C_2HBr_2N
Molecular weight (g mol^{-1})	75.5	109.94	144.39	198.84
Density (g mL^{-1})	1.203	1.396	1.440	2.296
Boiling point (^{o}C)	124-126	110-112	83-84	163.1
Flash point (^{o}C)	56	36	10.5	31.9
Vapor pressure (mmHg)	11.6	21.7	58	2.1
Water solubility (mg mL^{-1})	insoluble	10-50	< 1	9.6
Log K_{ow}[a]	0.45	0.29	2.09	0.47

Remark:

[a] K_{ow} is octanol/water partition coefficient. It is representing the ratio of the solubility of a compound in octanol (a non-polar solvent) to its solubility in water (a polar solvent). Log K_{ow} values are generally inversely related to aqueous solubility and directly proportional to molecular weight.

2.3.2 Toxicity of HANs

HANs have been reported to be more genotoxicity and cytotoxicity than regulated HAAs (Muellner et al., 2007). The chronic cytotoxicity and acute genotoxicity of seven HANs: DBAN, MCAN, DCAN, TCAN, iodoacetonitrile (IAN), monobromoacetonitrile (MBAN), and bromochloroacetonitrile (BCAN) were analyzed. The order of cytotoxic potency (from microplate-based Chinese hamster ovary cell assays) were DBAN > IAN ≈ MBAN > BCAN > DCAN > MCAN > TCAN. Moreover, the rank order of declining genotoxicity potency (from single cell gel electrophoresis assay) was IAN > MBAN ≈ DBAN > BCAN > MCAN > TCAN > DCAN.

2.3.3 Formation of HANs

HANs can be produced from chlorination, chloramination, UV, and ozonation process. In the U.S., water samples were collected from potable water and wastewater treatment plants to study HANFP. The result shows that HANFP in chlorinated water range from 0.5 to 70 μg L^{-1} from 166 water samples (Chen &

Westerhoff, 2010). Chlorination conditions and raw water characteristic influenced the amount of HANFP. In Korea, HANFP was detected in the range from 10.3 to 33.6 µg L^{-1} after chlorination of raw water at pH 8. The highest formation was found in drinking water source contaminated with industrial waste effluent and domestic sewage. As the pH decreased, the concentration of HANFP increased. The highest HANFP at 55 µg L^{-1} was observed at pH 5.5 after 24 hr contact time (Kim et al., 2003). High DCAN concentrations are formed at high chlorine doses and low pH values (Xu et al., 2012). There are literature reported that the formation of DCAN increased and then decreased with increasing chlorine dose and contact time (Chu, Gao, & Deng, 2010; Huang, et al., 2016) . However, the opposite results was found in the study of Reckhow et al. (2001). They reported that DCAN formation did not increase with increasing contact time or chlorine dose due to hydrolysis effect.

    Chlorine and chloramines exposure provide different results in the formation of HANs. DCAN formation from chlorination and chloramination water was compared. Some research found that DCAN formed in chloramination were five times higher than chlorination. Upon chloramination, average concentration of DCAN was 106 nmol^{-1} (11.65 µg L^{-1}). However, amino acid or organic nitrogen content of NOM did not correlate with DCAN formation in chloramination water. The literature implies that nitrogen from monochloramine was the main precursor of DCAN. In chlorination water, organic nitrogen-rich isolates in NOM are precursors of DCAN. As the ratio of dissolved organic carbon to dissolved organic nitrogen (DOC/DON) decreased, the DCAN formation increased (Lee, Westerhoff, & Croué, 2007). However, other research shows different results. Dotson's work found that DCAN formation was higher during chlorination than chloramination. In addition, hydrophilic base (HPIB) isolated from NOM tends to form more HANs yield than other fractions (Dotson, Westerhoff, & Krasner, 2009) . Similar results obtained in the study of Huang and co-workers . The results shown that chlorination tend to form DCAN higher than chloramination. The potent precursors of DCAN during chlorination were wastewater effluents (a model for wastewater impact) and extracellular polymeric substance (a model for algal-derived precursor). In chloramination water, humic acid was a significant precursor of DCAN. DCAN concentration during chlorination was range from 1.4 to 5.5 µg L^{-1}. During the application of chloramines, DCAN formation was range from 0.1 to 2.7 µg L^{-1}, lower

than chlorine application (Huang, Wu, Hu, & Mitch, 2012). The similar result was observed in the study of Yang and colleague (Yang et al., 2012). This research proves that DCAN formation was higher in chlorination than chloramination. Besides, this study found that organic nitrogen compounds such as tryptophan, tyrosine, asparagine, and alanine generated more DCAN than other model compounds (Yang et al., 2012).

The research on the formation of DCAN from chlorination, chloramination and UV of amino acid tyrosine was evaluated in the study of Chu and colleague. Amino acids are an important component of the DON and it is a significant precursor of HANs. DCAN formation in chloramination with amino acid tyrosine was higher than chlorination. When apply chlorination and UV simultaneously, the DCAN yields decrease with increasing pH (Chu et al., 2012) . The pH shows an effect on HANs formation. The formation of DCAN decreased with increase pH from 5 to 9. When increase pH from 5 to 9, the formation of DCAN first increased and then decreased, and the maximum yield observed at pH 6 (2.4%). At pH 9, TCAN yields were not detected due to the hydrolysis effect at alkaline pH (Yang, Shang, & Westerhoff, 2007). Other research on model organic-N precursors (creatinine, L-arginine, L-histidine, glycine, and urea) found that treatment of these model compounds promotes the formation of DCAN in chlorination water (Weng, Li, & Blatchley, 2012).

A few study conducted a formation of HANs by ozonation (Chiang et al., 2010). This study found that DOC removal was low after ozonation, indicating that ozonation might change the properties of NOM, therefore might affects in the production of DCAN. The formation of DCAN was reduced significantly at high ozone dose of 25 mg-O_3 L^{-1}.

2.4 Dissolved organic nitrogen (DON)

2.4.1 Composition of DON

DON (chemicals where nitrogen is bound to carbon) is general organic nitrogen compound in natural water. DON is a complex mixture of compounds including amino acids, amine, amide, nitrile, proteins, amino sugars, purines and pyrimidine. The major portion of DON is amino acids. Amino acids concentration in rivers and lakes are in range of 50 and 1000 μg L^{-1}, which account for 15% and 35% of

DON (Westerhoff & Mash, 2002). A significant amino acid species include glutamic acid, glycine, serine, and aspartic acids.

2.4.2 Concentration of DON in water

DON is found in varying concentrations in different water sources. DON concentrations in surface waters are higher than that in groundwater. The median DON levels in deep groundwater, shallow, and surface water are 0.18, 0.24, and 0.37 mg-N L^{-1}, respectively. Secondary and tertiary treated wastewater effluents contains 5 to 25 and < 4 mg-N L^{-1}, respectively. High concentrations of DON in surface water (>1 mg-N L^{-1}) associated with agricultural runoff and wastewater effluents contamination (Westerhoff & Mash, 2002). The average DON concentrations in raw water and in finished water were 0.19 and 0.15 mg-N L^{-1}, respectively (Lee & Westerhoff, 2005).

Nitrogenous substances can be released from algae. Not only blue green algae, but also green algae can excrete DON. A correlation of algal populations and DON concentrations was studied in the previous work. The results shown that eutrophic lakes have higher levels of DON (~ 0.7 to 1.2 mg-N L^{-1}) than mesotrophic (~ 0.4 to 0.7 mg-N L^{-1}), oligotrophic (~ 0.2 to 0.4 mg-N L^{-1}), and ultra-oligotrophic (< 0.2 mg-N L^{-1}) lakes (Westerhoff & Mash, 2002).

Excretion of algae products in eutrophic water and wastewater discharge are the major sources of DON in raw water supplies. Waters containing high levels of effluent organic matter (EfOM) and algal organic matter (AOM) will have high concentration of DON, and consequently generate high amount of N-DBPs. The average DON level in water contaminated with algal or wastewater influence (290 μg-N L^{-1}) was higher than that of non-impacted water (186 μg-N L^{-1}). In addition, for river subjected to wastewater effluent, DON concentration was varied from 0.7 to 1.47 mg-N L^{-1} (Bond, Templeton, & Graham, 2012).

2.4.3 Characteristic of DON

The characteristic of DON in wastewater was studied in previous research. The molecular weight (MW) distribution of DON measured by a high-performance size exclusion chromatography (HP-SEC) indicated that the majority (87%) fraction of DON compounds was low MW fraction (MW < 1000 Da), which regarded for 67±24%

of DON. Moreover, the HPO and HPI fractions of DON accounted for about 10%, and 90%, respectively (Pehlivanoglu-Mantas & Sedlak, 2008). Another research found that low MW acid and neutrals were a significant portion of the DON fraction in wastewater effluent samples (Chon, Lee, Traber, & Von Gunten, 2013).

Previous research suggests that the ratio of carbon and nitrogen (C:N) can act as an indicator for organic matter source. A low C:N ratio refers to proteinaceous DON, while a high C:N ratio represents allochthonous humic-like DON (Liu et al., 2012) . The fluorescent spectroscopy was used for observed the nature of DON fraction. The low C:N HPO fractions were more proteinaceous than the high C:N HPO fractions in the case that the fluorescent ratio between tryptophan and humic substance was higher in HPI than HPO fraction (Liu et al., 2012).

2.4.4 Relationships between DON characteristics and N-DBPs formation

The characteristic of DON related to N-DBPs formation were reported. The fractions of molecular weight wastewater-derived DON (<1000 Da) were the main precursors of NDMA during the chlorination and chloramination of wastewater as well as potable water (Pehlivanoglu-Mantas & Sedlak, 2008).

High organic nitrogen content in water will lead to N-DBP formation. The formation of HANs results from the reaction of DON and oxidants (Chen & Westerhoff, 2010; Lee, Westerhoff, & Croué, 2007). Amino acids (e.g. aspartic acids, tyrosine and tryptophan), as DON species, were proved to be the main precursor of HANs in chlorinated water (Bond, Templeton, & Graham, 2012). Some study found that algae cells that are enriched in organic nitrogen content generated high concentration of DCAN (Fang, Ma, Yang, & Shang, 2010; Yang, Guo, & Shen, 2011). Previous study reported that hydrophilic fraction in secondary effluent is the major precursor of DCAN because it can produced the highest DCAN level compared with other fractions (Huang et al., 2016).

2.5   Vacuum ultraviolet (VUV)

VUV is one of AOPs which emitting radiation at wavelength between 100 to 200 nm. The advantage of VUV over conventional UV 254 nm is it can in situ generation of highly reactive oxidizing species (OH$^{\bullet}$) by water homolysis (Equation 2.2) (Gonzalez, Oliveros, Wörner, & Braun, 2004).

$$H_2O + hv\ (\lambda < 190\ nm) \longrightarrow H^{\bullet} + OH^{\bullet} \tag{2.2}$$

Water can absorb light strongly in VUV region. The molar absorption coefficient of water at 185 nm is 0.032 L mol^{-1} cm^{-1} (calculated with a concentration of water of 55.49 mol L^{-1} at a density of 1 kg L^{-1} (Zoschke, Börnick, & Worch, 2014). The quantum yield of OH$^{\bullet}$ at a wavelength of 185 nm is 0.33 L mol^{-1} cm^{-1} (Gonzalez, Oliveros, Wörner, & Braun, 2004).

VUV photon can be generated by two main types of lamps. The commonly used in advanced oxidation is excimer lamp and low pressure mercury (LP-Hg) lamp. For excimer lamp, Xe-excimer radiators which emits a radiation at 172 nm is mainly applied in advanced oxidation process (Gonzalez, Oliveros, Wörner, & Braun, 2004; Oppenländer, 2003). Another one is LP-Hg lamp which emits polychromatic light wavelength at 185 nm (10%) and 254 nm (80 to 90%) (Imoberdorf & Mohseni, 2012). The LP-Hg VUV lamp coated with high purity synthetic quartz (suprasil quartz) that transmits the emission of 185 nm. In contrast to LP-Hg UV lamp which emits only 254 nm due to low quality quartz enveloped. The LP-Hg VUV or UV lamps has a partial pressure of mercury about 1 Pa, which corresponded to liquid mercury vapor pressure at 40°C at the lamp wall (Oppenländer, 2003).

2.6   Control of DBPs and DBPs precursors by AOPs

Advanced oxidation processes (AOPs) are a very promising technology for remediation of contaminated water, soil, and air containing chemically stable compound. A number of AOPs are commercially available such as homogeneous UV-based system, ultrasound irradiation, heterogeneous photocatalysis (TiO$_2$/UV), Fenton process (H$_2$O$_2$/Fe^{2+}), and ozone-based applications (O$_3$/H$_2$O$_2$, O$_3$/UV, and O$_3$/H$_2$O$_2$/TiO$_2$).

All AOPs involve the generation of very reactive oxidizing species or oxidants, especially OH$^\bullet$. The OH$^\bullet$ is a powerful oxidizing intermediate, short-lived and non-selective chemical oxidant that acts rapidly with a wide range of toxic compounds (Oppenländer, 2003). The reaction rate of OH$^\bullet$ and organic compounds are in the range of 10^8 to 10^{10} M^{-1} s^{-1} (Munter, 2001). In general, when applied in properly conditions, the OH$^\bullet$ is able to degrade or transform harmful pollutants to harmless end products such as carbon dioxide (CO_2) and water (H_2O). The overall process often leads to the mineralization of toxic molecules.

The degradation of organic compound by AOPs initiated with the production of strong oxidants (e.g. OH$^\bullet$). The second step is the reaction of the oxidants with degradable organic pollutants in water. The reaction occurs until mineralization or stable oxidation products are formed (Grote, 2012).

2.6.1 Vacuum ultraviolet (VUV)

VUV oxidation has been applied in the degradation of NOM. NOM in raw water was reduced by increased VUV dose from 0 to 128 J cm^{-2}, leading to THMs and HAAs formation reduction (Buchanan, Roddick, & Porter, 2006). When compare to UV process, NOM was reduced about 45% by VUV process which 10 times faster than UV treatment (Dobrović, Juretić, & Ružinski, 2007). Nine model organic compounds (i.e. glutamic acid, aspartic acid, glycine, leucine, serine, mannose, xylose, tannic acid and resorcinol) were used to study the efficiency of VUV on surrogate NOM reduction (Bond et al., 2009). After the application of VUV at 48 J cm^{-2}, the reduction of model compounds was about 97% higher than in UV/H_2O_2 (91%) and UVC (13%) processes. The treatment of NOM by biologically activated carbon (BAC) follow by VUV system was studied in some research (Buchanan, Roddick, & Porter, 2008). The result reveals that this system led to the production of more hydrophilic biodegradation molecules from high molecular weight hydrophobic molecules, reducing the overall DOC concentration by about 50%. Furthermore, VUV-BAC process decreased the formation potential of THMs and HAAs by 60 to 70% and 74%, respectively.

2.6.2 Ultraviolet (UV)-based AOPs

UV photolysis has been investigated to treatment of various N-DBPs such as *N*-nitrosodiethylamine (NDEA), HNMs, and HANs. NDEA can be completely degraded within 20 min by the direct UV photolysis using low pressure mercury lamps as a light source (Xu, Chen, Qi, & Yang, 2008). The effect of NOM on NDEA removal was tested. The result shown that humic substance as NOM compound inhibited the degradation efficiency of NDEA due to its photo-activity. Moreover, the main degradation products of NDEA were methylamine (MA), dimethylamine (DMA), ethylamine (EA), diethylamine (DEA), nitrite and nitrate.

Another group of N-DBPs that can be removed by UV was HNMs (Krasner et al., 2006). At pH 7, HNMs can be removed by hydrate electrons (e^-_{aq}) and $OH^\bullet$ generated from UV process at the rate constant of 2.2 to $3.3 \times 10^{10}\,M^{-1}\,s^{-1}$ and 10^7 to $10^8\,M^{-1}\,s^{-1}$, respectively (Mezyk et al., 2006). For pH-dependent HNMs degradation, some study found that the removal of HNMs were slowly at pH 3 to 5 (Fang, Ling, & Shang, 2013).

For HANs, the removal rate of four HANs by the medium pressure UV was found in this order: DBAN>TCAN>DCAN. DBAN was removed faster than chlorinated-acetonitrile. The highest and the lowest kinetic constants of HANs were found in DBAN at 0.2 min^{-1} and DCAN at 0.02 min^{-1}, respectively (Hansen et al., 2013). This implies that the presence of bromine in the molecular structure of HANs increased the photolytic decay of HANs, because bromine species are more photosensitive than chlorinated HANs (Chen et al., 2010).

Not only DBPs but also DBPs precursor (e.g. NOM) was treated by UV photolysis. The efficiency of the process in the reduction of NOM was measured in term of UV absorbance at 254 nm (UV_{254}) and DOC. NOM in raw water was treated by LP-Hg UV lamps at 254 nm (Goslan, Gurses, Banks, & Parsons, 2006). The results shown that a removal of NOM in term of UV_{254} and DOC were 94% and 78%, respectively when applied a UVC dose at 22 J cm^{-2}. Increase a UVC dose up to 37 J cm^{-2} results in an increase of DOC removal, but did not significantly effect on UV_{254} reduction at a UVC dose higher than 22 J cm^{-2}. A same result found in the experiment of Bond and his co-workers (Bond et al., 2009). The study found that a UVC dose of 21 J cm^{-2} results in 78% DOC reduction. DOC reduction up to 91% was achieved when

applied high UVC dose at 47 to 48 J cm^{-2}. Moreover, partial oxidation of NOM surrogate increased the formation potential of HAAs.

The efficiency of UV is enhanced when irradiation combined with H_2O_2 due to the promotion of OH$^\bullet$ formation. When compare to direct photolysis, the combination of UVC and H_2O_2 increase the rate of UV_{254} and DOC reduction. At UVC dose of 22 J cm^{-2}, UV_{254} and DOC reduction was reach to 94% and 78% in the presence of 2 mM H_2O_2 (Goslan, Gurses, Banks, & Parsons, 2006). NOM in raw surface water was partially oxidized, but not mineralized, by UV/H_2O_2 process. This partial reduction led to a decrease in very hydrophobic acids (VHA) fraction of NOM. The diminution of VHA fraction (i.e. TOC reduction) led to the drop of DBPs formation (e.g. THMs and HAAs) (Sarathy & Mohseni, 2010). However, some study found that excess H_2O_2 may have led to less effectiveness of the process due to OH$^\bullet$ scavenger effect. The optimal H_2O_2 concentration for the degradation of humic acid was in the range between 0.0032 to 0.0163 M. High H_2O_2 dose at 0.0082 M could absorb more UVC energy, and generate more OH$^\bullet$ (Wang, Liao, Chen, & Yang, 2006) .

2.6.3 Ozone-based AOPs

Nowadays, ozone-based applications have received attention in the degradation of organic matter in water. Ozone (O_3) combined with VUV shown a better performance in the removal of NOM when compared to the O_3, VUV, O_3-UV and UV processes (Ratpukdi, Siripattanakul, & Khan, 2010). Moreover this study found that the highest DOC mineralization rate was observed at pH 7. After the oxidation, the major fraction of NOM was hydrophilic neutral.

Ozonation combined with biological activated carbon (O_3-BAC) subsequent to a conventional water treatment process was conducted to improve the removal of N-DBPs precursor in water (Chu et al., 2012). The study found that O_3-BAC process can enhance the removal of DON (58 to 72%) and DOC (35 to 74%). Moreover, the formation potential of DCAN was significantly reduced by this process (80%) when compared with the conventional treatment process (50%).

The effectiveness of ozonation and TiO_2-catalyzed ozonation (TiO_2/O_3) on the structure and amount of NOM and HANs precursor were examined (Molnar et al., 2012). The result found that the later process can reduce the total NOM content

compared to ozonation alone. However, both processes result in the change of NOM structure (i.e. an oxidation of humic acid fraction and an increase of the hydrophilic fraction up to 70%). Consequently, the formation potential of HANs increased due to an increase of the most reactive HAN precursor (i.e. hydrophilic fraction) when compared to the raw water.

Recent study on the application of ozonation integrated with photocatalytic was reported as an effective oxidation technique in the removal of DCAN (Shin et al., 2013). In this study, the test results of the indoor system found that the $UV_{solar}/TiO_2/O_3$ process had the highest removal rate (0.033 min^{-1}) of DCAN at the optimal TiO_2 and O_3 doses at 1 g L^{-1} and 1.13 g L^{-1} h^{-1}, respectively. The results from the outdoor system test indicated that the $solar/TiO_2/O_3$ process provided complete DCAN removal (within 2 hr) two times faster than those obtained with $solar/TiO_2$. In addition, the electrical energy per mass (EE/M) value showed that the $solar/TiO_2/O_3$ process had higher energy efficiency than $solar/TiO_2$ process about 5 times.

CHAPTER 3
RESEARCH FRAMEWORK AND EXPERIMENTAL DESIGN

3.1 Research framework

Research framework of this dissertation is shown in Figure 3.1. Since the main objective of this work was to investigate the feasibility of using VUV for removing of HANs and HANs precursor, this work is divided into 2 major parts includes (1) degradation of HANs and (2) reduction of DON and HANFP. The scope of each part of experiment is described in subsections 3.1.1 and 3.1.2.
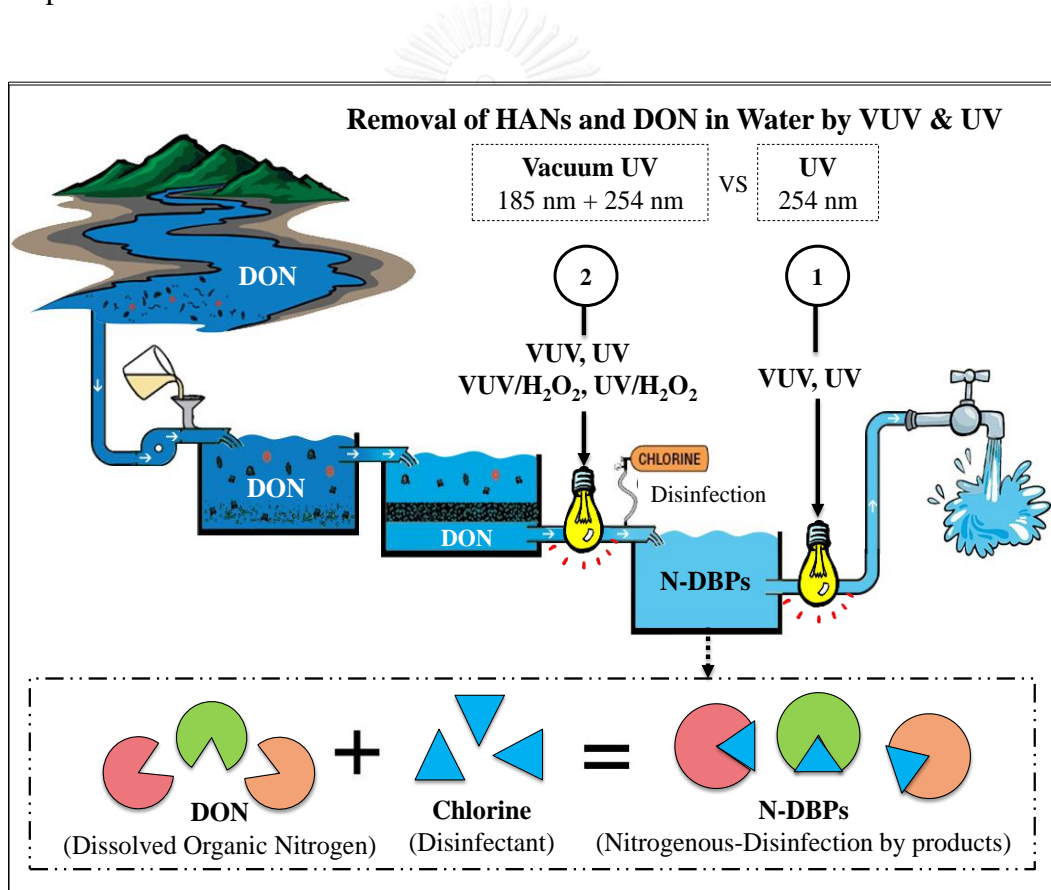
Figure 3.1 Research framework.

3.1.1 Part 1: Degradation of HANs by VUV and UV

This part studied the degradation of HANs by VUV in comparison with UV. The scope of work (Figure 3.2) is as follows:

(1) Four different species of HANs were selected as model compounds. These HANs species were MCAN, DCAN, TCAN, and DBAN.

(2) Synthetic water samples containing HANs species were prepared either in a single-solute or mixed-solute solution in order to compare the competitive effect among HANs compounds.

(3) The initial concentration of each HANs species was 100 µg L^{-1}.

(4) The photolytic experiments of HANs were investigated under a batch condition at 120 min of irradiation time. The volume of HANs solution was 6 L for each batch test.

(5) VUV (185 and 254 nm) and UV (only 254 nm) lamps were used as light sources. Details about lamps and experimental design are in section 3.2.

(6) The effect of DO was studied by purging air and nitrogen gas until the DO level higher than 8 mg L^{-1} and less than 1 mg L^{-1}, respectively.

(7) The degradation mechanisms including direct photolysis by light 185 nm or 254 nm and indirect photolysis by $OH^•$ were elucidated. The methylene blue (MB) and *tert*-butanol (TBA) were used as a $OH^•$ probe compound and a $OH^•$ scavenger, respectively.

(8) The concentrations of HANs after treatments were measured by a gas chromatography-electron capture detector (GC-ECD).

(9) The intermediate products of each HANs species after VUV treatment were identified qualitatively by GC-mass spectrometer (GC-MS).
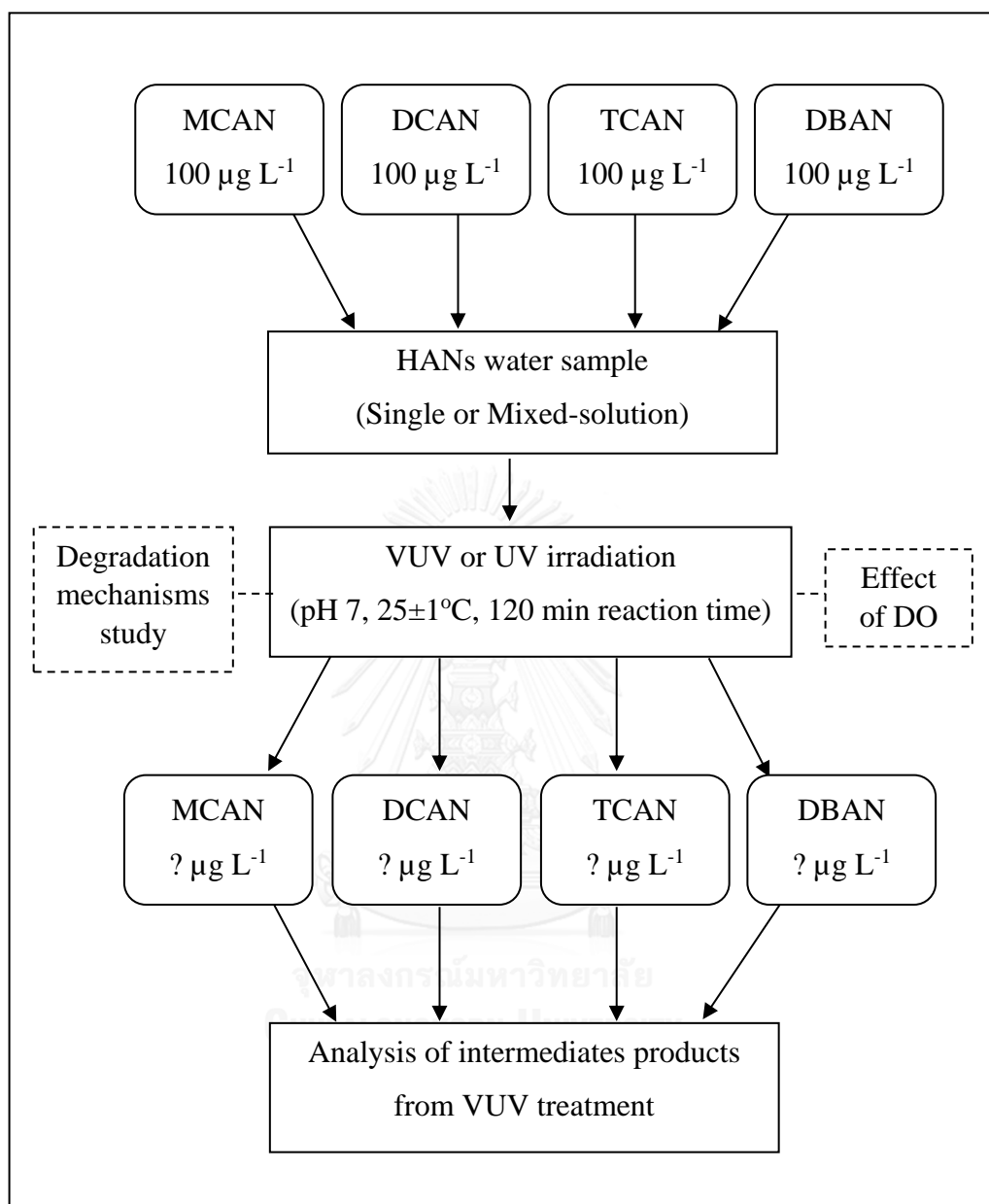
Figure 3.2 Scope of work for part 1: Degradation of HANs

3.1.2 Part 2: Reduction of DON and HANFP by VUV, VUV/H_2O_2, UV, and UV/H_2O_2

The second part of this research focused on the reduction of DON by VUV and UV with and without H_2O_2 addition. Reduction of DON and HANFP was examined. The scope of this part (Figure 3.3) is as follows:

(1)   Two different sources of water samples were selected: (a) surface water (SW) collected after sedimentation, coagulation, and filtration processes of a water treatment plant and (b) secondary treated wastewater effluent (WW) collected from a sedimentation pond of an aerated lagoon wastewater treatment plant.

(2)   Two different sources of water samples were treated by VUV, VUV/H_2O_2, UV, and UV/H_2O_2.

(3)   The experiment was conducted in a bath mode with 6 L of water samples and 60 min of reaction time. (Details in section 3.2).

(4)   The concentrations of H_2O_2 added in VUV and UV systems for treatment of surface water were 5, 10, and 20 mg L^{-1} and 10, 20, and 50 mg L^{-1} for treated wastewater.

(5)   The properties of NOM in water before and after treatment with VUV, VUV/H_2O_2, UV, and UV/H_2O_2 were characterized. They included DON, DOC, UV_{254}, HPI and HPO fractions, and FEEM.

(6)   The impact of VUV, VUV/H_2O_2, UV, and UV/H_2O_2 on HANFP was observed. HANFP was conducted at pH 7, $20\pm1^{o}C$, and 24 hr in the dark. Chlorine dosage was based on the concentrations of DOC and ammonia nitrogen (NH_3-N) in water samples (Details in Chapter 5).

(7)   The link between reduction of HANFP and NOM characteristics (i.e. DON, DOC, UV_{254}, HPI and HPO fractions, and FEEM) was examined.
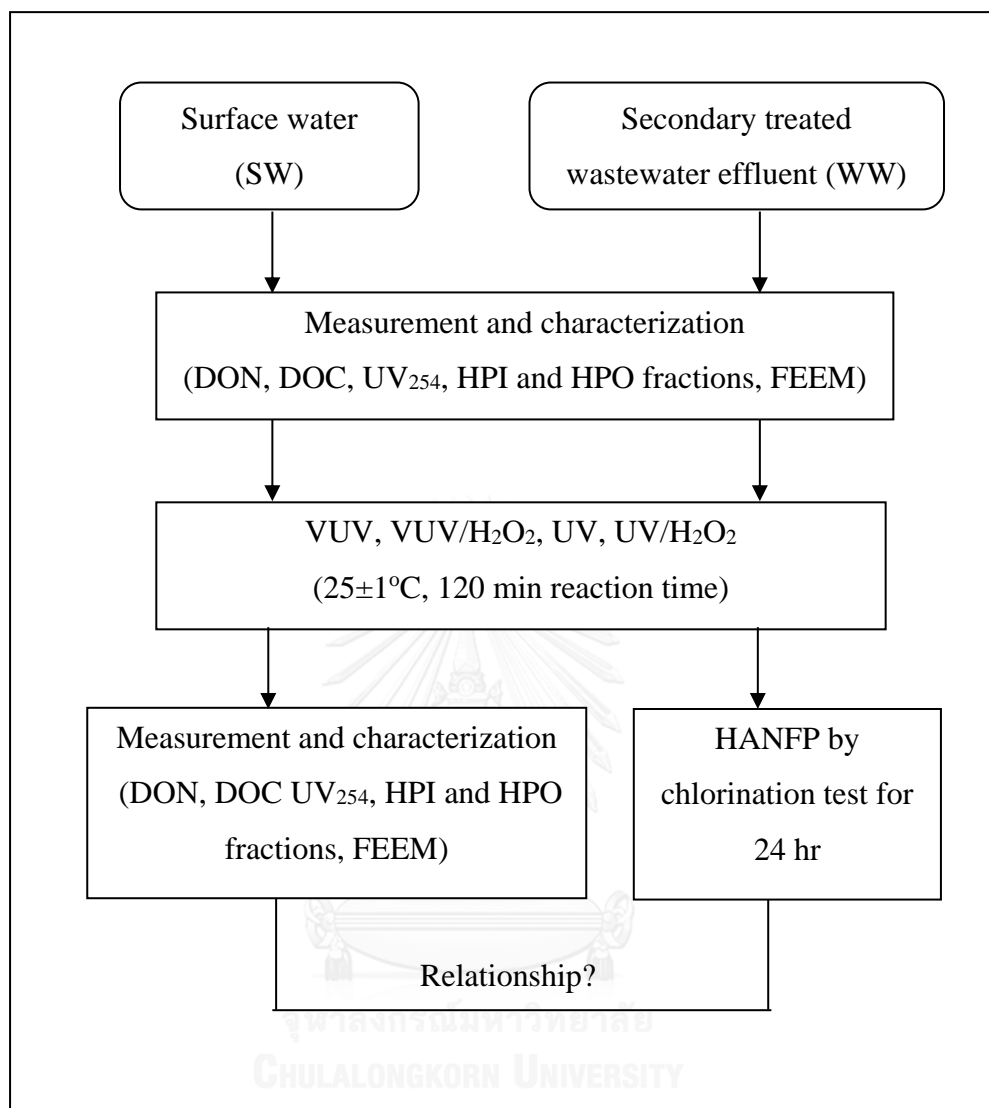
Figure 3.3 Scope of work for part 2: Reduction of DON and HANFP

3.2 Experimental design and setup

The experimental design and setup for parts 1 and 2 was the same (Figure 3.4). The photodegradation reaction was performed in a tubular borosilicate reactor (15 cm I.D.× 45 cm). Low pressure mercury VUV (LP-Hg-VUV) lamps (model GPH383T5/VH/HO, Universal Lights Source, Inc., San Francisco, CA, USA) were used as a light source for VUV. Low pressure mercury UV (LP-Hg-UV) lamps (model GPH383T5/L/HO) were used for UV experiments. The VUV lamp emits polychromatic light wavelengths at 185 nm and 254 nm, while the UV lamp emits only 254 nm. Two lamps were installed in the reactor providing total power input of 60 W (30 W/lamp). The lamps were turned on for 10 minutes before starting each batch experiment to ensure the constant light output. The photon flux of the UV lamps determined by a H_2O_2 actinometer was 1.8×10^{-6} E $L^{-1}s^{-1}$. For the VUV lamps, photon flux of 185 nm was estimated to be 10% of UV 254 nm radiation which was 1.8×10^{-7} E $L^{-1}s^{-1}$. These photon fluxes are equivalent to the intensities for UV (254 nm) and VUV (185+254 nm) system of 5.84 and 6.64 mW cm^{-2} (5.84+0.80 mW cm^{-2}), respectively.
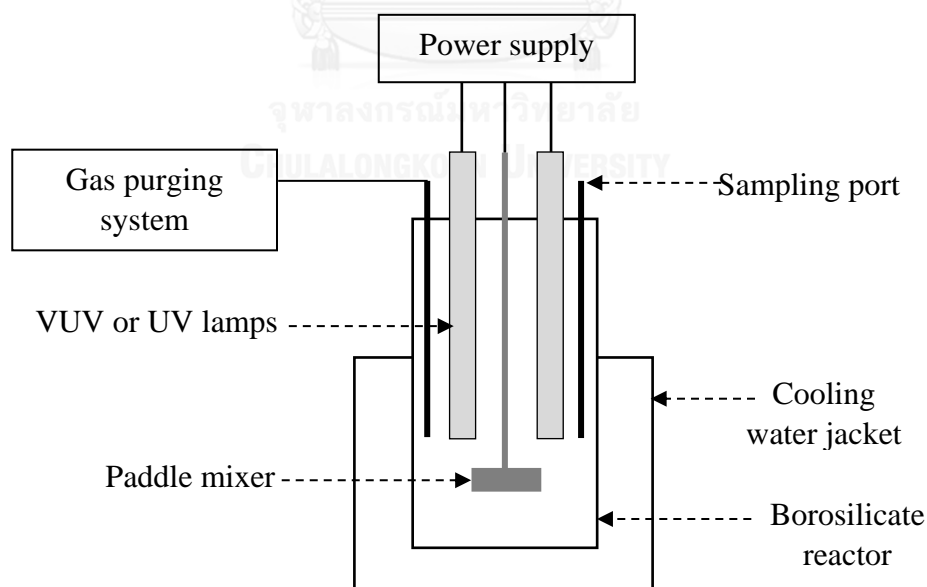
Figure 3.4 Experimental setup

CHAPTER 4
DEGRADATION OF HANs BY VUV AND UV

4.1   Introduction

During the last decade, emerging unregulated N-DBPs, such as HANs, HNMs, HAcAms, and nitrosamines, have gained attentions than regulated C-DBPs (THMs and HAAs). This is because N-DBPs have higher toxicity than C-DBPs (Muellner et al., 2007). The first three groups of N-DBPs were surveyed at 12 drinking water treatment plants in the U.S. and HANs were the group with the highest concentration (Krasner et al., 2006). As high as 14 mg L^{-1} was observed for total HANs (THAN), including DCAN, DBAN, BCAN, and TCAN. The most prevalent species among HANs detected was DCAN, which accounted for >90% of THAN detected (Baytak, Sofuoglu, Inal, & Sofuoglu, 2008; Krasner et al., 2006). HANs level in treated water could be from few microgram per liter to almost a hundred microgram per liter (Baytak, Sofuoglu, Inal, & Sofuoglu, 2008; Guilherme & Rodriguez, 2014). A relatively high THAN concentration of 88.4 mg L^{-1} was observed in tap water of Izmir, Turkey (Baytak, Sofuoglu, Inal, & Sofuoglu, 2008). Based on studies in the U.S. (Krasner et al., 2006) and Canada (Guilherme & Rodriguez, 2014), the concentration of THAN was >10 times less than those of THMs and HAAs. The cytotoxicity of HANs is nearly 200 times higher than that of regulated HAAs (Muellner et al., 2007). Due to their adverse health effects, WHO suggests a guideline value of 70 mg L^{-1} for DBAN, and a provisional guideline value of 20 mg L^{-1} for DCAN (WHO, 2011). These guidelines have not been adopted and there is no standard for HANs in any countries. HANs have been included in the U.S. EPA ICR and will potentially be regulated in the future.

The formation of HANs is tied to the reaction between chlorine or chloramine and DON in water (Lee, Westerhoff, & Croué, 2007). The HPI fraction (accounts for >80% of DON) was the main precursor of HANs formation (Huo et al., 2013). To control the concentration of HANs in water, there are two approaches including removal of HANs precursors and removal of HANs directly (after they are formed). However, the removal of precursors by conventional water treatment processes of coagulation, sedimentation, and filtration may be difficult since they are mostly

hydrophilic (Westerhoff & Mash, 2002). Therefore, posttreatment or point of use treatment for HANs removal is needed. Various methods to treat N-DBPs have been studied such as biological treatment (Webster, Condee, & Hatzinger, 2013), reduction by zero-valent zinc (Han et al., 2013), and adsorption by silica materials (Prarat, Ngamcharussrivichai, Khaodhiar, & Punyapalakul, 2011). Although these methods can reduce N-DBPs concentration, but it is costly, time consuming, and generating waste.

Recently, AOPs have been reported to be effective for the removal of N-DBPs in water. Examples of such AOPs used to treat HANs include solar photolysis (Chen et al., 2010), sonolytic ozonation (Park, Shin, Cho, & Khim, 2012), and photocatalysis ozonation (Shin et al., 2013). Complete removal of DCAN was reported under photocatalysis ozonation with less energy consumption (high energy efficiency) (Shin et al., 2013). Nevertheless, most of AOPs require additional chemical/catalyst to generate OH$^{\bullet}$. VUV is an alternative treatment of AOPs that generate OH$^{\bullet}$ in situ by water homolysis. VUV emits light at the wavelength (λ) lower than 200 nm causing water molecules to break into hydrogen atom (H$^{\bullet}$) and OH$^{\bullet}$, as shown in Equation (4.1) (Zoschke, Börnick, & Worch, 2014). Therefore, contaminants could be degraded through direct photolysis or by oxidation with OH$^{\bullet}$ (indirect photolysis).

$$H_2O + h\nu \ (\lambda < 190 \text{ nm}) \longrightarrow H^{\bullet} + OH^{\bullet} \tag{4.1}$$

Low pressure mercury (LP-Hg) lamp is one of VUV light sources. The lamp emits polychromatic light at 185 nm (10%) and 254 nm (90%) (Oppenländer, 2003). The advantages of LP-Hg VUV (hereafter referred to as VUV) is that it can generate OH$^{\bullet}$ without additional of chemicals and therefore reduces the operation cost. Also, its setup and installation are simple and can be retrofitted to an existing UV disinfection chamber. During the past decade, a number of previous studies have demonstrated that VUV are effective for degradation of many contaminants such as pharmaceutical compounds (Szabó et al., 2011), taste and odor compounds (Kutschera, Börnick, & Worch, 2009), and NOM (Ratpukdi, Siripattanakul, & Khan, 2010). Therefore, VUV could be a promising technology for post treatment of N-DBPs including HANs. UV photolysis for the removal of HANs (Chen et al., 2010), HNMs (Fang, Ling, & Shang, 2013), and iodinated THMs (Xiao et al., 2014) have been studied. Some of DBPs could

be removed by UV photolysis at the same dose for UV disinfection at neutral or alkaline pH. Their removal rate constants depend upon the type and number of halogen atoms. However, no information is available on the application of VUV for the removal of HANs.

The main objective of this part was to investigate photodegradation of four model compounds of HANs (MCAN, DCAN, TCAN, and DBAN) by VUV in comparison with conventional UV which is typically used for disinfection. The removal efficiency and the kinetic rate constants of single and mixed-HANs were compared. The effect of gas purging was studied. The degradation mechanism of HANs by direct and indirect photolysis was elucidated. In addition, the intermediate products from VUV treatment were examined.

4.2   Material and methods

4.2.1   Water samples

Four HANs species; MCAN (98%, Wako, Japan), DCAN (98%, Sigma-Aldrich, USA), TCAN (98%, Sigma-Aldrich, USA), and DBAN (90%, Acros Organics, USA), were chosen according to the occurrence data and toxicity (Krasner et al., 2006; Muellner et al., 2007). Water samples were prepared as either single or mixed solutions by firstly dissolved in acetone and subsequently diluted with de-ionized (DI) water. The degradation efficiency of HANs under VUV and UV was carried out at an initial concentration of 100 μg L^{-1} for each compound. For intermediate identification, only VUV treatment was examined at high initial concentrations of HANs species (100 and 500 mg L^{-1}). To maintain pH around 7 throughout the reaction, the samples were prepared in a phosphate buffer solution (ionic strength at 10 mM) (Prarat, Ngamcharussrivichai, Khaodhiar, & Punyapalakul, 2011). The buffer solution was prepared from disodium hydrogen phosphate heptahydrate (Na$_2$HPO$_4$.7H$_2$O, Panreac, Spain) and sodium dihydrogen phosphate monohydrate (NaH$_2$PO$_4$.H$_2$O, Carlo Erba, France).

To study the degradation mechanism by direct and indirect photolysis, methylene blue (MB, Merck, Germany) as OH$^\bullet$ probe compound was prepared in deionized water, and spiked into the HANs solutions at a concentration of 10 μM (Keen, Love, & Linden, 2012). Tert-butanol (TBA, 99%, Fluka, Germany), as OH$^\bullet$ scavenger,

was also added into the HANs solutions at 20 mM prior to VUV irradiation (Liao et al., 2013). The photon flux and an effective optical path length were determined by the degradation of H_2O_2 (>30% w/v, Fisher, UK) in water (Xiao et al., 2015).

4.2.2 Experimental procedure

All experiments were operated in a batch mode using 6 L of the phosphate buffer solutions containing HANs. The pH of the solution was adjusted at 7 and monitored by a pH meter (HACH sension2, USA). No change of pH during the reaction was observed. The solution was mixed using a paddle at 400 rpm. The temperature of the reactor was controlled at $25\pm1°C$ by a cooling water system. Forty milliliters of water samples were collected at different reaction times (0 to 120 min). All the tests were at least duplicated and the average and standard deviation were determined. The sample was preserved with 0.5 mL of 1 M glacial acetic acid (Merck, Germany) to prevent the hydrolysis of HANs after collection.

The effect of gas purging (air and nitrogen) on the photodecomposition of mixed-HANs was examined for the VUV system. Air and nitrogen saturated solutions were produced by bubbling the solution with an air pump or nitrogen gas (99.999%) via glass tubes. The gas/air flow rate was 4 L min^{-1}. Gas/Air was purged prior to the irradiation until the desired DO concentration (monitored by a DO meter, YSI 550A, USA) was reached and continued during the course of experiment (higher than 8 mg L^{-1} for air purging and less than 1 mg L^{-1} for nitrogen gas purging).

To determine the degradation mechanism of HANs, the molar absorptivity (ε), quantum yield (Φ), observed degradation rate constants ($k_{obs,HANs}$), and rate constants of $OH^\bullet$ with HANs ($k_{OH\bullet/HANs}$) were determined. Moreover, fluence-based degradation rate constants (k_f) were calculated for direct comparisons among degradation rate constants obtained with different photoreactors (Xiao et al., 2014). Details for these equations can be found in APPENDIX B (Text B1).

4.2.3 Analytical methods

The concentration of HANs was analyzed by a gas chromatography with electron capture detector (GC-ECD, Agilent 4890D, USA). The analysis method was modified from U.S.EPA method 551.1 (U.S.EPA., 1995). The degradation

intermediates of each HAN during VUV were identified by a GC/mass spectrometer (GC/MS, Agilent 7890B, USA). More details on GC-ECD and GC/MS conditions were found in APPENDIX A, respectively. The concentration of MB and molar absorptivity of HANs were determined using a spectrophotometer (HACH, DR6000, USA) at 664 nm, and 200 to 400 nm, respectively. The molar absorptivity of HANs at (100 μg L^{-1}) at wavelength 254 nm was determined for quantum yield calculation (APPENDIX B, Figure B.1). The concentration of H_2O_2 was determined by the titanium oxalate method and measured at 390 nm using a spectrophotometer (Brandhuber & Korshin, 2009).

4.3 Results and discussion

4.3.1 Competitive effect among HANs under VUV

Figure 4.1 presents degradation of each HAN in the single and mixed solutions by VUV. The error bars represent standard deviation. The removal of each HAN in the mixed solution was slightly less than that in the single solution, suggesting the competitive effect among HANs. The paired *t*-test showed that the results from mixed and single compound were statistically significant difference for MCAN, DCAN and TCAN (the *p*-value of 0.0041, 0.0009, and 0.0002, respectively, which is <0.05). Degradation of DBAN was completed (concentration below the detection limit) within 15 min in both single and mixed solution. The degradation rate constants were determined based on initial degradation rates (during the first 5-30 min) because a good linear relationship (ln C/C_0 vs time) was not observed for the overall degradation kinetics. The pseudo first order rate law has been proposed for the degradation of HANs under VUV since the steady-state concentration of OH$^{\bullet}$ is assumed to be constant with respect to contaminant concentrations (Jo, Dietrich, & Tanko, 2011; Xiao et al., 2014).

When comparing among HANs in the single solutions under VUV, the order of degradation rate constants was DBAN>TCAN>DCAN>MCAN (APPENDIX B, Table B.1). In the mixed solution, the order of degradation rate constants was similar to individual compounds with the rate constant values less than those of single solutes by 1.7, 1.3, and 1.4 times for TCAN, DCAN, and MCAN, respectively. The degradation rate constants of DBAN in single and mixed solutions were not significantly different (*p* = 0.1932). Among chlorinated HANs in the mixed solution, TCAN exhibited the highest degradation rate. HANs with higher the number of chlorine

atoms are less stable to photodegradation due to more electron withdrawing effect (Fang, Ling, & Shang, 2013). This is in agreement with a previous study, which found that the compound with less degree of halogen was resistant to solar photolysis (Chen et al., 2010). Brominated HAN (DBAN) was more susceptible to photodegradation than chlorinated HANs. This could be described by the bond-dissociation energy of halogen-bound carbon. The bond strength of C−Br (280 kJ mol^{-1}) is weaker than C−Cl (397 kJ mol^{-1}) (Xiao et al., 2014). Therefore, brominated HAN is easier for dissociation. This result was similar to previous studies that reported more rapid degradation of brominated HANs and THMs compared to corresponding chlorinated DBPs (Chen et al., 2010; Hansen et al., 2013).
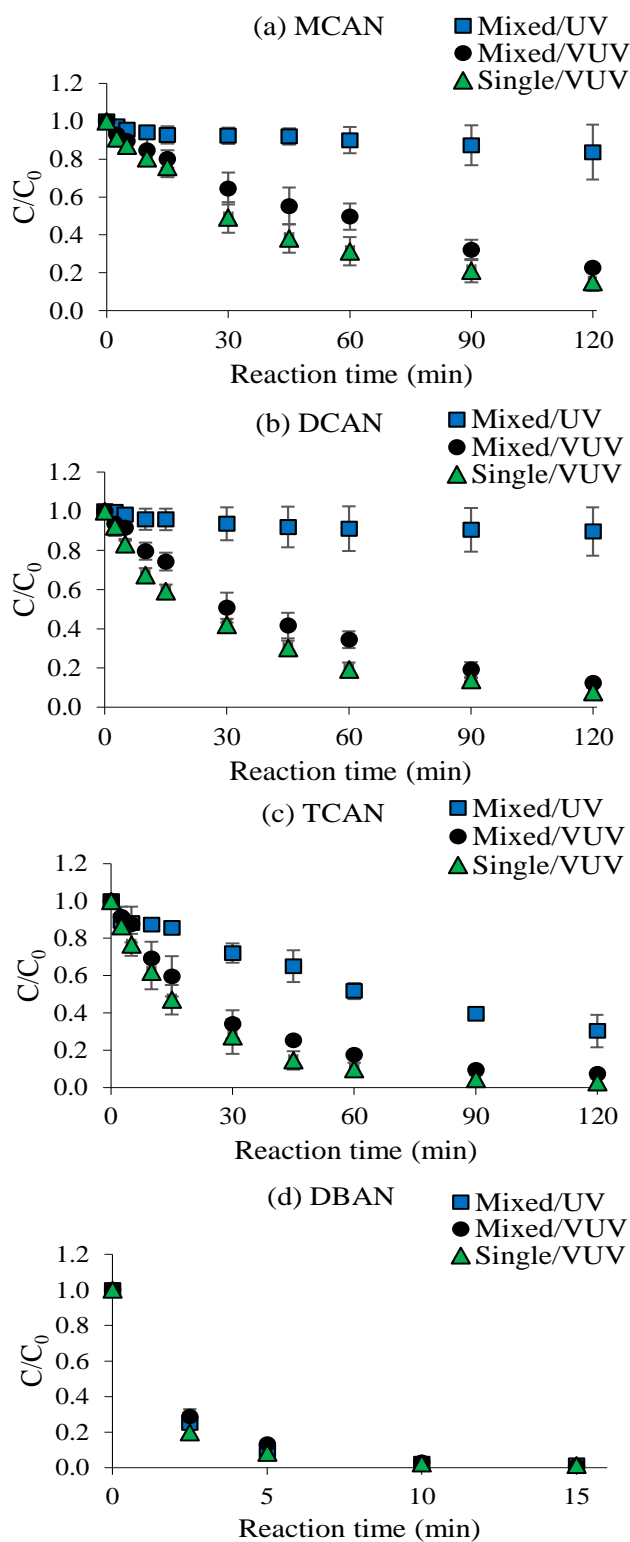
Figure 4.1 Concentration of each HAN at different reaction times (C) normalized by initial concentration (C_0) in the single and mixed HANs solutions under VUV and UV treatment: (a) MCAN, (b) DCAN, (c) TCAN, and (d) DBAN

4.3.2 Effect of gas purging under VUV

Effects of air and nitrogen gas purging on the degradation of mixed HANs under VUV are shown in Figure 4.2. All HANs were completely removed within 15 min under nitrogen purging while the removal of MCAN, DCAN, TCAN, and DBAN were 19, 28, 62 and 97% under aerated condition at 15 min. The pseudo first order degradation rate constants of HANs under nitrogen-saturated conditions were higher than those of under aerated solutions (APPENDIX B, Table B.1) Oxygen (O_2) can have either positive or negative effect on contaminant degradation. The presence of O_2 under VUV irradiation could enhance the degradation of contaminant due to the in situ formation of H_2O_2 or ozone (O_3) (Zoschke, Börnick, & Worch, 2014). In contrast, under nitrogen purging, the removal rate constants of HANs was much higher than that of the aerated condition by 34.4, 34.9, 10.1, and 3.8 times for MCAN, DCAN, TCAN, and DBAN, respectively. The $H^\bullet$ (formed during H_2O homolysis by VUV) could contribute to degradation of HANs. Under the presence of DO, the $H^\bullet$ combines with O_2 and forms less reactive oxidizing species ($HO_2^\bullet/O_2^{\bullet-}$) (Arany et al., 2013). Thus, less HANs degradation occurred with air purging condition. In addition, O_2, O_3 and H_2O_2 may cause interference with contaminants degradation by absorb or compete the photon available for direct photolysis of the contaminants (Oppenländer, 2003; Sharpless & Linden, 2003). This effect was more pronounce for the compound with less value of UV molar absorptivity. In this case, MCAN and DCAN have molar absorptivity at 254 nm of 4615 and 5495 M^{-1} cm^{-1}, respectively, which are about twice less than TCAN (10145 M^{-1} cm^{-1}).
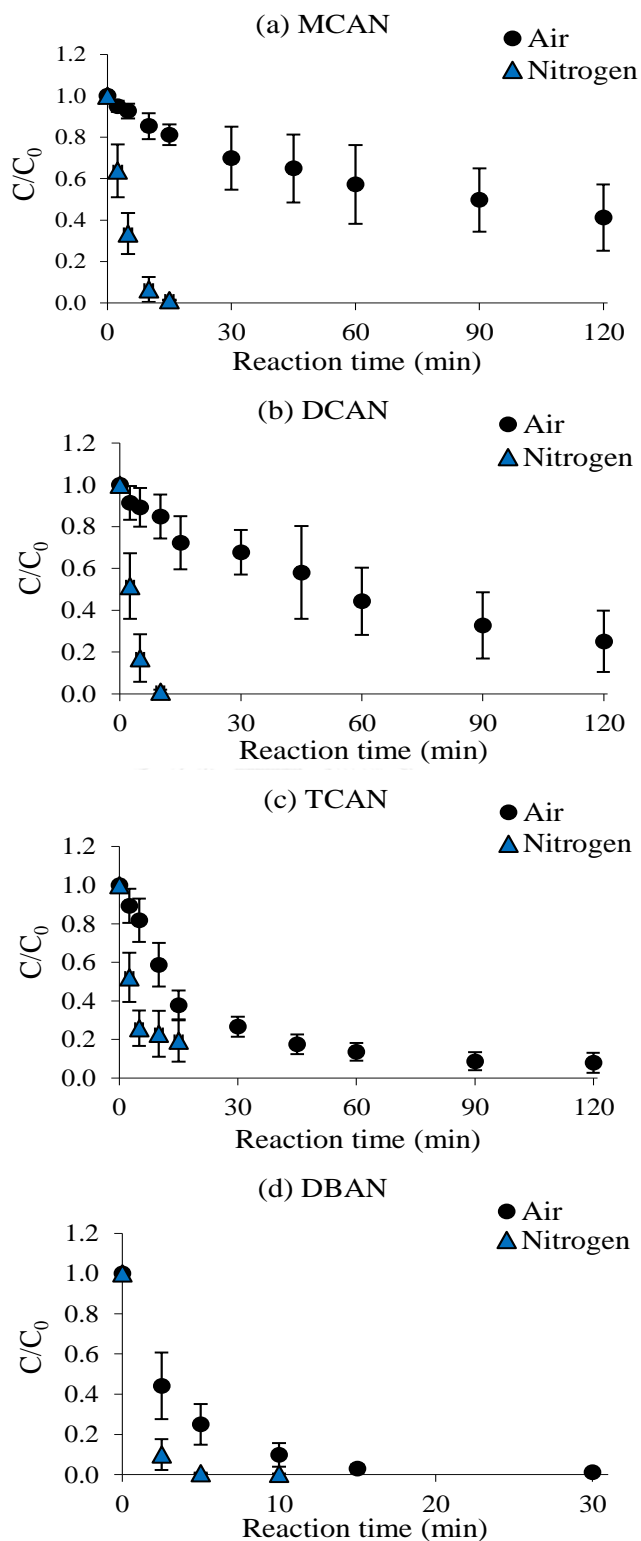
Figure 4.2 Concentrations of HANs in the mixed solution at different VUV irradiation time (C) normalized by initial concentration (C_0) under air and nitrogen purging: (a) MCAN, (b) DCAN, (c) TCAN, and (d) DBAN

4.3.3 Effect of light source

The degradation of mixed HANs solution under VUV was compared with conventional UV (Figure 4.1). The results reveal that VUV degraded HANs more effectively than UV process. The degradation rate constants of HANs under VUV were higher than that of UV by 6.0, 7.0, 4.6 and 1.6 times for MCAN, DCAN, TCAN, and DBAN, respectively (APPENDIX B, Table B.1). The removal rate of mixed HANs obtained by VUV and UV was in the same order of DBAN>TCAN>DCAN>MCAN. Under VUV, the degradation of HANs was associated with direct photolysis by 185+254 nm, and indirect photolysis by OH$^\bullet$. While under UV, HANs can be degraded only by direct photolysis of 254 nm. The highest removal rate under VUV and UV was observed for DBAN indicating that brominated HAN tends to be degraded by direct photolysis. The degradation efficiency under UV at 254 nm could be described by the molar absorptivity and quantum yield (Table 4.1). As the molar absorptivity and the quantum yield of DBAN were high, its degradation was subject mainly to photon adsorption at 254 nm. For chlorinated HANs, VUV provided more effective degradation than UV. This suggests that direct photolysis at 185 nm and/or indirect photolysis by OH$^\bullet$ were the main degradation mechanisms of these compounds. To determine the major degradation mechanism of each HAN species, the percentage of degradation mechanisms (185 nm, 254 nm, OH$^\bullet$) was calculated and discussed in the next section.
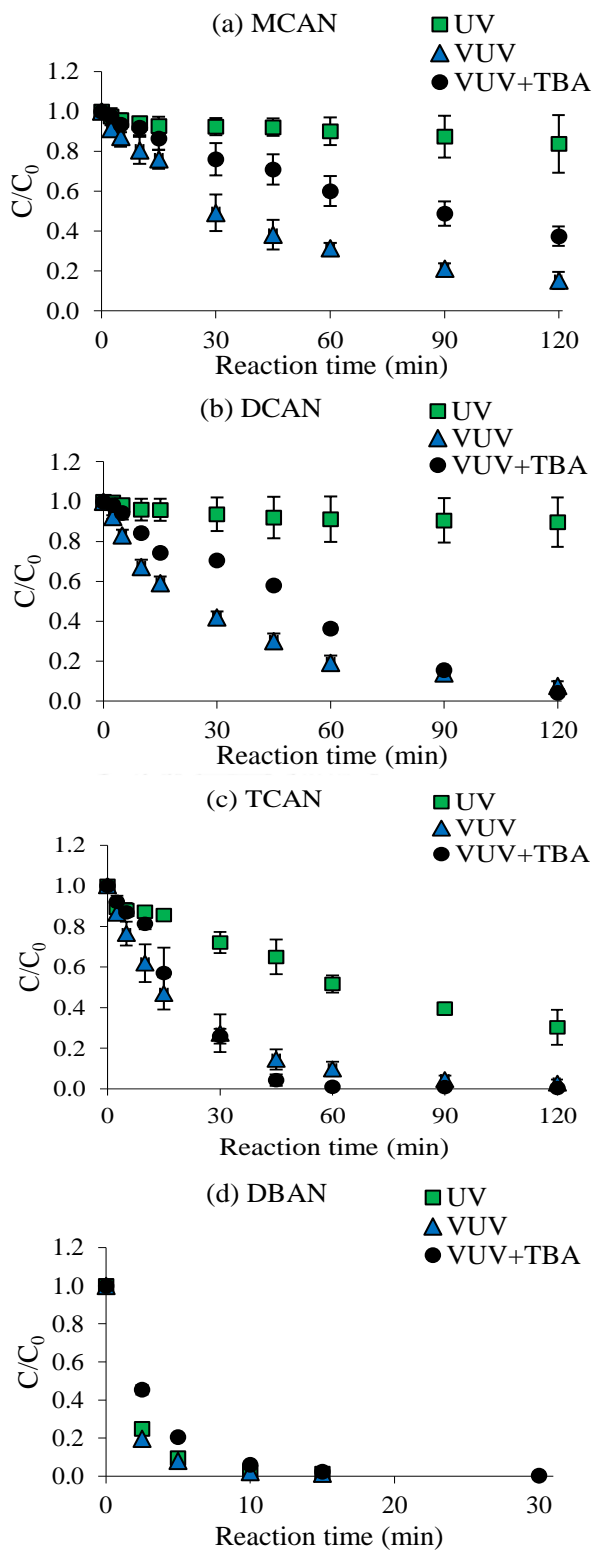
Figure 4.3 Concentration of single-HANs at different reaction times (C) normalized by initial concentration (C_0) under VUV and UV with and without the addition of 20 mM TBA: (a) MCAN, (b) DCAN, (c) TCAN, and (d) DBAN

4.3.4 Determination of degradation mechanisms

Figure 4.3 shows the degradation of each HAN under UV and VUV with and without the addition of TBA (OH• scavenger). Under UV, the concentration of OH• was relatively low and its affect was negligible (Kutschera, Börnick, & Worch, 2009). Therefore, the addition of TBA into UV system can be ignored. If the degradation of target compounds by VUV in the presence of TBA is much lower than that in the absence of TBA, the dominant degradation mechanism is by OH• (Kutschera, Börnick, & Worch, 2009). As shown in Figure 4.3, the reduction of all chlorinated HANs under UV was relatively low, suggesting that UV is not a significant degradation mechanism for chlorinated HANs. Under VUV, the removal rate constants of single MCAN, DCAN, TCAN, and DBAN were higher than those of under VUV with TBA by about, 2.1, 1.0, 1.1, and 1.1 times respectively (APPENDIX B, Table B.1). This indicates that OH• had more impact on the degradation of MCAN than other HANs.

To determine the major degradation mechanism for each HAN, the percentage of the rate constants associated with direct photolysis by 254 nm and 185 nm and oxidation by OH• were calculated and compared (Figure 4.4). Each species of HANs has different sensitivity towards direct and indirect photolysis. OH• played an important role for the degradation of MCAN due to its low light absorption. Direct photolysis at 185 nm was the major degradation mechanism for DCAN and TCAN removal. This might be due to the strength of C−Cl bond (397 kJ mol^{-1}) which requires high energy to split the bond (Xiao et al., 2014). DCAN and TCAN molecules have more C-Cl bonds than MCAN in which they have more probability to absorb photon at 185 nm. Direct photolysis at 254 nm was a dominant reaction for the degradation of DBAN because it has the highest quantum yield. Another possible reason is related to the low strength of C−Br bond which requires less dissociation energy as mentioned in Section 4.4.1. The result here is similar to a previous study which reported that UV photolysis at 254 nm was a dominant mechanism for the removal of brominated HAAs (Jo, Dietrich, & Tanko, 2011).

Table 4.1 Molar absorptivity (ε) at 254 nm, quantum yield (Φ) at 254 nm, time-based direct photolysis rate constants for 254 nm (k_{d_254}) and 185 nm (k_{d_185}), fluence-based direct photolysis rate constants for 254 nm (k_{f_254}) and 185 nm (k_{f_185}), indirect photolysis rate constants ($k_{i\_OH\bullet}$), and second order rate constants ($k_{OH\bullet/HANs}$) of HANs

HANs	ε at 254 nm	Φ at 254 nm	k_{d_254}	k_{f_254}	k_{d_185}	k_{f_185}	$k_{i\_OH^\bullet}$	$k_{OH^\bullet/HANs}$
	$M^{-1} cm^{-1}$	$\times10^{-3}$ mol E^{-1}	$\times10^{-2}$ min^{-1}	$\times10^{-4}$ cm^2 mJ^{-1}	$\times10^{-2}$ min^{-1}	$\times10^{-4}$ cm^2 mJ^{-1}	$\times10^{-2}$ min^{-1}	$\times10^9$ M^{-1} s^{-1}
MCAN	4615	0.20	0.16	0.05	0.66	1.36	0.91	1.35
DCAN	5495	0.38	0.12	0.03	2.09	4.34	0.10	0.16
TCAN	10145	0.58	1.02	0.29	3.10	6.45	0.25	0.37
DBAN	10000	27.96	33.10	9.44	-*	-*	1.88	2.80

*k_d and k_f at 185 nm could not be observed for DBAN due to the overlapping between k_{d_185} and k_{d_254}.
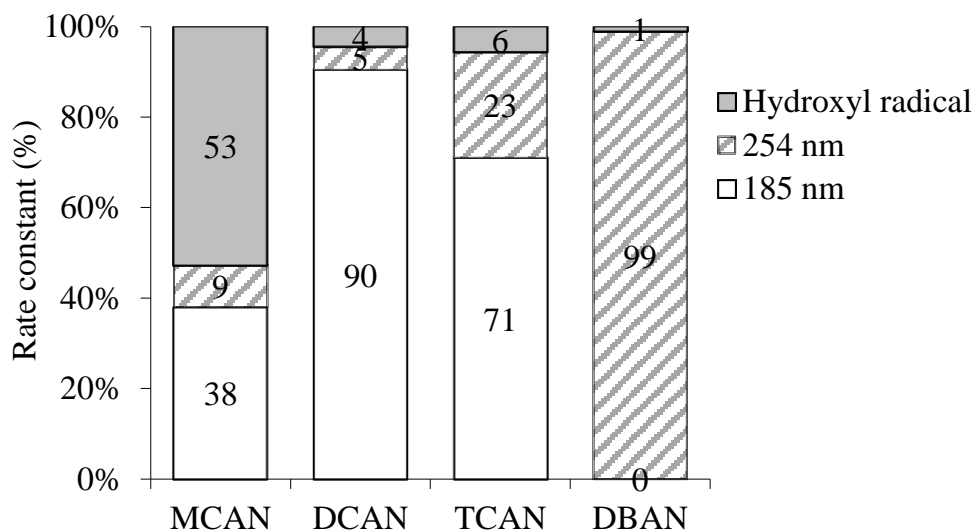
Figure 4.4 The percentage of rate constants of single HANs degraded by different mechanisms

To study the sensitivity of each HAN with OH$^{\bullet}$, the competition kinetics were determined by calculating the second order rate constants between HANs and a probe compound of OH$^{\bullet}$ ($k_{OH^{\bullet}/HANs}$). The $k_{OH^{\bullet}/HANs}$ in this study was range from 0.16 to 2.80×10^9 M^{-1} s^{-1} (Table 4.1). There is a previous study reported the second order rate constants of DBPs with OH$^{\bullet}$ (produced by pulse radiolysis system). For example, the $k_{OH^{\bullet}/THMs}$, $k_{OH^{\bullet}/HNMs}$, and $k_{OH^{\bullet}/TCAN}$ were found in the range of 10^7 to 10^8 M^{-1} s^{-1} (Mezyk et al., 2006). Xiao and co-workers (2015) reported $k_{OH^{\bullet}}$ of I-THMs such as CHCl$_2$I and CH$_3$I under UV/H$_2$O$_2$ at 8×10^9 and 8.9×10^9 M^{-1} s^{-1}, respectively. The results obtained in this work show that HANs can react with OH$^{\bullet}$ as well as other DBPs. VUV can be easily retrofitted in existing UV disinfection or with chlorination system. This also adds the benefit for not only disinfection but also remove other compounds such as taste and odor (Wang, Bolton, Andrews, & Hofmann, 2015). For taste and odor removal, the medium pressure UV (Wang, Bolton, Andrews, & Hofmann, 2015) and VUV doses (Kutschera, Börnick, & Worch, 2009) required were 2000 mJ cm^{-2} (7.2 s exposure time) and 4000 mJ cm^{-2} (30 s exposure time), respectively. In this study, the VUV dose required for DBAN removal was 5980 mJ cm^{-2} (15 min exposure time). Although, the exposure time for HANs removal was longer than that of taste and odor, this could be

reduced by adding number of lamps to increasing VUV intensity. Therefore, VUV process which generated the OH$^{\bullet}$ could be a possible technique for the treatment of HANs. Also more detail study under pilot or full scale is needed

4.3.5 Intermediates formation

The photodegradation intermediates of each HAN in the single solution under VUV were determined by GC/MS (APPENDIX B, Table B.2). The mass spectra of intermediates are presented in (APPENDIX B, Figure B.2-B.13). From GC/MS results, the degradation pathways of each HAN are proposed (Figure 4.5). There were two intermediates generated from dechlorination, methylation, and polymerization reaction of MCAN degraded under VUV. Photodegradation of DCAN under VUV led to the formation of MCAN, 2-chloropropionitrile, and dichloroacetamide (DCAcAm) as intermediates (APPENDIX B, Table B.2). Dechlorination of DCAN (detachment of Cl atom) lead to the formation of MCAN (Figure 4.5). For sample without VUV irradiation, DCAcAm was also detected. This indicates that the decomposition of DCAN could be from hydrolysis reaction (Reckhow et al., 2001). Based on a previous study, DCAcAm could be further hydrolysed or react with free chlorine to form dichloroacetic acid (DCAA) (Reckhow et al., 2001). However, no DCAA was found in this study due to the absence of free chlorine. In addition, as VUV irradiation time increased, the peak area of the DCAcAm also decreased suggesting that DCAcAm might be mineralized by direct photolysis or oxidized by OH$^{\bullet}$.

For TCAN degradation, DCAN and 2,2,2-trichloroacetamide (TCAcAm) were detected as intermediates (APPENDIX B, Table B.2). The formation of DCAN was due to the C−Cl bond cleavage and hydrogen atom from water molecules was added (Figure 4.5). Also, MCAN was expected to be observed during TCAN degradation since MCAN was found as intermediates during DCAN degradation. However, the peak of MCAN was not detected. TCAcAm was identified in a control sample, suggesting that it was an intermediate generated from the addition of water molecules into TCAN molecule. After 60 min of reaction time, the peak area of TCAcAm was elevated and then was not detected after 120 min of irradiation. This implies that TCAcAm was an intermediate from TCAN treated by VUV and it could be completely degraded by VUV.

The degradation of DBAN resulted in the formation of five intermediates (APPENDIX B, Table B.2). When the debromination reaction took place, bromine atom was removed and substituted by hydrogen atom, leading to the formation of MBAN. MBAN was detected in the sample prior to irradiation due to the hydrolysis of DBAN. One bromine atom of MBAN was then removed and replaced by a methyl group (CH_3) via methylation reaction, resulting in the formation of 2,2-dimethylpropanenitrile (Figure 4.5). Methylation and hydroxylation of MBAN molecules formed 1-bromo-2-methyl-2-butanol which was further transformed to 1-bromo-2-methyl-2-propanol via dehydrogenation and demethylation. Fumaronitrile was also detected as a possible intermediate of DBAN. It could be form via a polymerization of two MBAN monomer. The majority of the intermediates from HANs degradation by VUV were from the replacement of halogen atom with hydrogen atom. The loss of halogen seems to be the first degradation step of HANs which is similar to HHMs degradation pathway under UV photolysis (J.-Y. Fang, Ling, & Shang, 2013). The photo-cleavage of the bond depends on the bond energy and photon energy in the system. UV light photons at 185 nm and 254 nm have energy of 647 kJ mol^{-1} and 471 kJ mol^{-1}, respectively, which are higher than the bond energy of C−Cl (397 kJ mol^{-1}) and C−Br (280 kJ mol^{-1}) (Xiao et al., 2014). As a result, photon adsorption at such wavelengths can easily split the C−X bond. The bond energy of C≡N (866 kJ mol^{-1}) (De, 2003) was higher than the photon energy of the wavelengths used, making it difficult to breakdown.
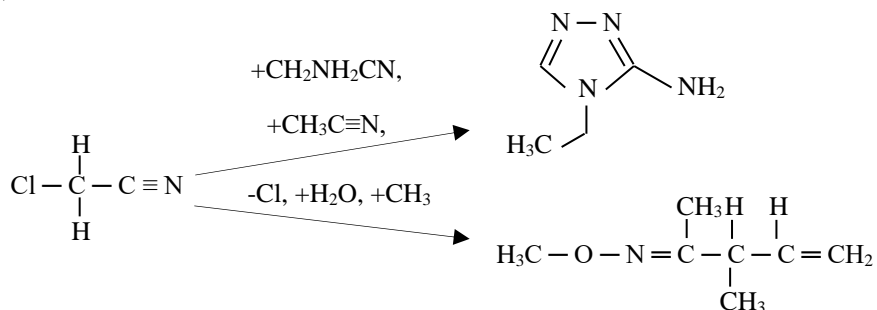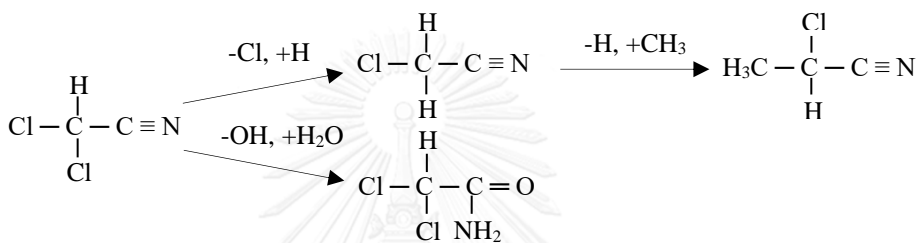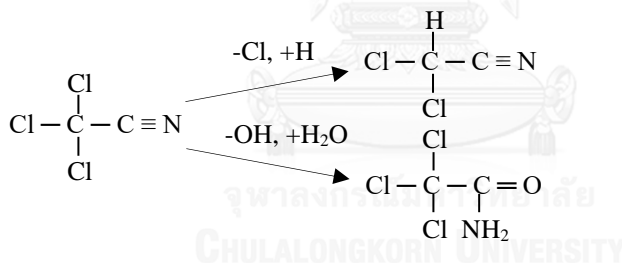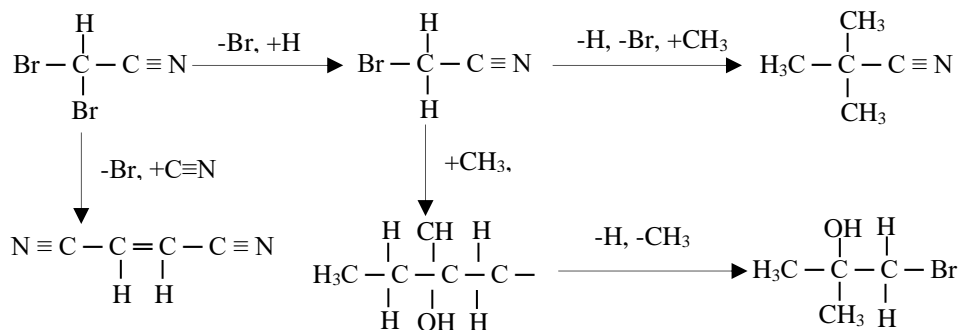
Figure 4.5 Proposed degradation intermediates of each HAN under VUV

4. 4 Summary

HANs were degraded by VUV better than UV. VUV irradiation was able to degrade HANs individually and all together. Competitive degradation was observed for mixed HANs (except for DBAN), leading to lower removal of each HAN compared to single HAN. The degradation rate constants of HANs followed pseudo first order reaction. The photodecomposition rate of HANs in the presence of DO was much lower than in the presence of nitrogen. The order of degradation efficiency by VUV and UV was similar (DBAN>TCAN>DCAN>MCAN). The efficiency of direct photolysis by UV corresponded to the molar absorptivity and the quantum yield of the compounds. Under UV and VUV, DBAN was completely degraded within 30 min suggesting that DBAN is more susceptible to direct photolysis at 254 nm. MCAN was degraded mainly by indirect photo-initiated by OH$^{\bullet}$. DCAN and TCAN were degraded by direct photolysis at 185 nm. The formation of intermediates from the degradation of single HANs under VUV was due to the substitution, addition, and polymerization reaction. VUV not only can degrade HANs but also can remove their intermediates from the system. VUV-based-AOP is a potential treatment technology for the removal of HANs in water. In practice, the other water constituents such as NOM, alkalinity, and turbidity could affect the removal of HANs by VUV. Future research should be conducted on the removal and mineralization of HANs by VUV for different water matrices. Moreover, the toxicity of intermediates from photodegradation of HANs should be evaluated.

CHAPTER 5

REDUCTION OF DON AND HANFP BY VUV, VUV/H$_2$O$_2$, UV, AND UV/H$_2$O$_2$

5.1 Introduction

HANs are an emerging group of N-DBPs. HANs have toxicity about two orders of magnitude higher than regulated HAAs (Muellner et al., 2007). During water disinfection, HANs can be formed via the reaction between disinfectant (e.g. chlorine and chloramine) and NOM. Organic nitrogen portion of NOM (measured as DON) is known to be a precursor of HANs as well as other N-DBPs such as NDMA, HNMs, and HAcAms (Chu, Gao, Deng, & Krasner, 2010; Lee, Westerhoff, & Croué, 2007).

The presence of DON raised a concern of N-DBPs in both drinking water as well as reclaimed wastewater. This is because drinking water source can be contaminated by treated wastewater effluent or increasing of water reuse from wastewater reclamation. In surface water, DON concentration ranges 0.07 to 0.62 mg-N L^{-1} with a median value of 0.3 mg-N L^{-1} (Chu et al., 2014; Krasner, Mitch, Westerhoff, & Dotson, 2012; Xu et al., 2011). For secondary wastewater effluent, DON concentration ranges 0.30 to 3.33 mg-N L^{-1} (Chen, Kim, & Westerhoff, 2011; Huang, Wu, Hu, & Mitch, 2012; Pehlivanoglu-Mantas & Sedlak, 2008; Simsek et al., 2013).

To reduce N-DBPs formation, one of the approaches is to remove the precursors (i.e. DON) before chlorination. Since N-DBPs precursors are likely hydrophilic (Westerhoff & Mash, 2002), conventional water treatment processes include coagulation, flocculation and filtration have been reported for their low DON removal efficiencies (Chu, Gao, & Deng, 2010; Chu et al., 2012). Moreover, DON had low adsorption capacities onto coagulants, lime (for softening) and activated carbon (Chen, Chen, & Wang, 2011).

UV-based AOPs, are promising technologies that destroy various types of trace organic contaminants as well as N-DBPs precursors for drinking water and reclaimed water. Previous literatures reported the application of UV/H$_2$O$_2$ for the reduction of DON. In drinking water, DON can be removed by 12 to 35% under UV dose in a range of 30 to 585 mJ cm^{-2} and 1 to 20 mg L^{-1} H$_2$O$_2$ addition (Chu et al., 2014). For secondary wastewater effluent, the reduction of DON was 20 to 30% under UV fluence of 7200

mJ cm^{-2} and 50 to 100 mg L^{-1} H$_2$O$_2$ addition (Qi & Jiangyong, 2016). UV/H$_2$O$_2$ systems effectively reduced various types of N-DBPs formation such as HAcAms (Chu et al., 2014) and HNMs (Yimeng et al., 2017) in drinking water and NDMA (Qi & Jiangyong, 2016) in reclaimed water. At UV fluence of 585 mJ cm^{-2} and H$_2$O$_2$ of 10 mg L^{-1} (typical level used in drinking water plant to remove emerging contaminants), 78 to 92% and 52 to 65% reduction of HAcAms and HNMs formation were achieved, respectively (Chu et al., 2014).

Recently, VUV, one of UV-based AOPs, has received attention among researchers because its ability to generate OH$^{\bullet}$ in-situ from water homolysis at a wavelength of below 190 nm (Gonzalez, Oliveros, Wörner, & Braun, 2004). VUV have been studied for degradation of various contaminants such as antibiotics (Li et al., 2017; Yao, Pei, Wang, & Fu, 2017), biocide (Yuval et al., 2017), pesticide (Bagheri & Mohseni, 2015; Moussavi, Hossaini, Jafari, & Farokhi, 2014), methylene blue (Li et al., 2016), N-DBPs (Kiattisaksiri, Khan, Punyapalakul, & Ratpukdi, 2016), NOM (Buchanan, Roddick, & Porter, 2006; Imoberdorf & Mohseni, 2014; Ratpukdi, Siripattanakul, & Khan, 2010) as well as formation of regulated C-DBPs (THMs and HAAs) (Buchanan, Roddick, & Porter, 2006; Imoberdorf & Mohseni, 2014). To enhance VUV degradation performance, H$_2$O$_2$ was added to generate more OH$^{\bullet}$. A previous study reported a synergetic effect of VUV/H$_2$O$_2$ (15 mg L^{-1}); removal of NOM by VUV/H$_2$O$_2$ and VUV alone was 70 and 50%, respectively (Imoberdorf & Mohseni, 2014). Another factor affecting DBP formation is characteristics of precursors. Like other AOPs, change of precursor characteristics occur when they oxidized by VUV. The oxidation of NOM transformed HPO large molecular size NOM to HPI smaller molecular size NOM, resulting in less THMs and HAAs formation (Lamsal, Walsh, & Gagnon, 2011; Sarathy & Mohseni, 2007). Chu and co-workers (2014) reported that HAcAms formation after UV/H$_2$O$_2$ was solely from HPI fraction.

VUV is a potential water treatment process. Up to date, application of VUV for DON removal associated with HANFP has never been investigated. In addition, a link between characteristics of HANs precursor to its formation after VUV treatment has never been explored. The objective of this work was to investigate the feasibility of using VUV for the removal of DON in water in comparison with UV. Also the effect of H$_2$O$_2$ addition to enhance the reduction HANFP was determined. Dissolved organic

characteristics (i.e. DON, DOC, UV_{254}, HPO and HPI fractions, and FEEM) upon VUV and UV treatment were also examined to provide a better understanding on HANFP.

5.2 Materials and Methods

5.2.1 Water samples

Water samples were collected from two different sources including (1) surface water (SW) and (2) secondary treated wastewater effluent (WW). SW samples were collected after coagulation, sedimentation and filtration of Kota water treatment plant, Khon Kaen Municipality, Thailand. The raw water source comes from the Nampong River. WW samples were collected at effluent of aerated lagoon system of Bueng Thungsang wastewater treatment plant of Khon Kaen Municipality, Thailand. Sampling date for SW and WW samples was November 24, 2016, and February 13, 2017, respectively. The WW sample was coagulated with alum (20 mg L^{-1} as Al^{3+}) to remove particle before VUV and UV treatments. The samples were stored at $4^{o}C$ prior to treatment. After treatment in a photoreactor, all samples were filtered through a 0.45 µm pore-size cellulose acetate membrane (Filtrex, India) before analysis and characterization. The characteristics of water samples are presented in Table 5.1.

5.2.2 Experimental procedure

The experimental setup is described in Chapter 3. Photodegradation experiments were conducted using 4 systems including VUV, VUV/H_2O_2, UV and UV/H_2O_2. The volume of water used in each experimental run was 6 L. The H_2O_2 (>30% w/v, Fisher, UK) was added into the reaction at doses ranging from 5 to 20 mg L^{-1} for SW samples and 10 to 50 mg L^{-1} for WW samples. The initial concentration of H_2O_2 applied for treating WW samples was higher than that of SW samples due to higher DOC and DON concentrations. Before the addition, the concentration of H_2O_2 was standardized using a titanium oxalate method (Brandhuber & Korshin, 2009). During the irradiation, the sample was mixed by a paddle mixer (400 rpm). The experiment was operated for 60 min at $25\pm1^{o}C$. Approximately 200 mL of the water sample were collected at different reaction time.

Table 5.1 Characteristics of water samples

Parameters	Unit	SW[a]	WW[b]	WW[c]
pH	-	7.03 ± 0.07	7.75 ± 0.05	7.07 ± 0.02
UV_{254}	cm^{-1}	0.082 ± 0.003	0.248 ± 0.007	0.096 ± 0.005
UVT_{254}*	%	82 ± 0.004	56 ± 0.141	80 ± 0.004
DOC	$mg\text{-}C\ L^{-1}$	3.43 ± 0.13	7.52 ± 0.16	5.85 ± 0.14
SUVA	$L\ mg\text{-}C^{-1}\ m^{-1}$	2.40 ± 0.16	3.30 ± 0.16	1.64 ± 0.11
DON	$mg\text{-}N\ L^{-1}$	0.355 ± 0.02	1.448 ± 0.10	1.425 ± 0.09
TDN	$mg\text{-}N\ L^{-1}$	0.578 ± 0.03	16.775 ± 0.06	16.377 ± 0.36
$NH_3\text{-}N$	$mg\text{-}N\ L^{-1}$	0.019 ± 0.004	15.316 ± 0.04	14.897 ± 0.39
$NO_3\text{-}N$	$mg\text{-}N\ L^{-1}$	0.203 ± 0.007	0.008 ± 0.001	0.01 ± 0.005
$NO_2\text{-}N$	$mg\text{-}N\ L^{-1}$	0.001 ± 0.001	0.003 ± 0.00	0.003 ± 0.002

Remark:

* UVT_{254} is ultraviolet transmittance at 254 nm

[a] Surface water sample after filtration from Kota water treatment plant (n=16)

[b] Secondary treated wastewater effluent at a sedimentation pond of Bueng Thungsang wastewater treatment plant (n=2)

[c] Secondary treated wastewater effluent after coagulation with alum (20 mg L^{-1} as Al^{3+}) (n=16)

After irradiation, HANs and THMs formation potential tests were conducted with excess free chlorine to ensure that chlorine residual could be detected after 24 hr contact time. A stock solution of free chlorine was prepared from a sodium hypochlorite solution (available chlorine 5-6% w/w, Haiter, Thailand). The concentration of the free chlorine stock solution was standardized using the iodometric method (APHA, 2012). The chlorine dosages for each water samples were calculated based on DOC and NH_3-N concentrations as shown in Equation (5.1) (Dotson, Westerhoff, & Krasner, 2009). The chlorination experiment was carried out in 40 mL of water samples buffered at pH 7 using 10 mM phosphate buffer. Samples were incubated under head-space free amber glass bottles at $20 \pm 1^{\circ}C$ in the dark. To stop the reaction of free chlorine after the formation potential tests, ascorbic acid was added immediately at a concentration twice higher than the initial chlorine dosage (Chu et al.,

2012). For water samples treated with VUV/UV+H_2O_2, chlorination test and H_2O_2 quenching was conducted in a single step (immediately after sampling). Additional free chlorine (1 mg-H_2O_2 L^{-1} requires 2.09 mg-Cl_2 L^{-1}) was added to remove H_2O_2 residual (Dotson, Keen, Metz, & Linden, 2010). The amount of chlorine residual and H_2O_2 residual was measured by DPD method (*N*,*N*-diethyl-*p*-phenylenediamine; DPD powder pillows, HACH, USA) (Dotson, Keen, Metz, & Linden, 2010) and titanium oxalate method (Brandhuber & Korshin, 2009), respectively (APPENDIX A). For all chlorinated water samples, the chlorine residual after 24 hr chlorination test was in the range of 4 to 6 mg L^{-1}. The H_2O_2 residual of each batch test was different and results are shown in APPENDIX C (Figure C.1-C.12).

$$\text{Chlorine dose (mg } L^{-1})$$
$$= \quad 3 \times \text{DOC (mg-C } L^{-1}) + 8 \text{ NH}_3\text{-N (mg-N } L^{-1}) + 10 \text{ (mg } L^{-1}) \text{ Cl}_2 \qquad (5.1)$$

Water samples before and after irradiation were fractionated into two fractions: HPO and HPI. A solid phase extraction method using a bondelute®ENV cartridge (Varian, Inc., CA, USA) was used for fractionation (Ratpukdi, Rice, Chilom, & Khan, 2008). Before use, the cartridge was cleaned with 10 mL of methanol (MeOH, HPLC grade, RCI Labscan, Thailand) followed by 1.5 L of deionized (DI) water. The water sample was adjusted to pH 2.5using concentrated sulfuric acid (H_2SO_4, 98%, RCI Labscan, Thailand) and then drawn through the cartridge by a vacuum pump at 20 mm Hg. The organic fraction retained in the cartridge is HPO while non retained fraction is considered as HPI. The HPO fraction was eluted with 0.1 N sodium hydroxide (NaOH, QRëC, New Zealand).

5.2.3 Analytical methods of HANs

Extraction and analysis of HANs were modified from the U.S. EPA method 551.1 (U.S.EPA., 1995). Twenty-five milliliters of the water sample were extracted by 2.5 mL of methyl-*t*-butyl ether (MTBE, HPLC grade, RCI Labscan, Thailand) as the extraction solvent and 5 g of sodium sulfate (Na_2SO_4, Carlo Erba, France) as the extraction salt. One microliter of MTBE extract was analyzed by GC-ECD. More details on HANs extraction and analysis are in APPENDIX A.

5.2.4 Characterizations of NOM and DON

UV_{254} was determined using a UV-visible spectrophotometer (DR2000, Hack, USA). DOC and total dissolved nitrogen (TDN) concentration were measured by TOC/TN analyzer (multi N/C 2100, Analytik Jena, Germany). DON concentration was calculated based on the difference of TDN and dissolved inorganic nitrogen (DIN) (i.e. ammonia (NH_3-N), nitrate (NO_3-N), and nitrite (NO_2-N)), as shown in Equation (5.2). The concentrations of NH_3-N, NO_3-N, and NO_2-N were determined by the phenate, sponge cadmium reduction, and colorimetric methods, respectively (APHA, 2012; Jones, 1984). Details on DIN analysis are in APPENDIX A.

$$DON \ (mg \ L^{-1}) = TDN - (NO_3\text{-}N) - (NO_2\text{-}N) - (NH_3\text{-}N) \qquad (5.2)$$

Where,   TDN is concentration of total dissolved nitrogen (mg N-L^{-1}),

            NO_3-N is concentration of nitrate-nitrogen (mg N-L^{-1}),

            NO_2-N is concentration of nitrite-nitrogen (mg N-L^{-1}),

            NH_3-N is concentration of ammonia-nitrogen (mg N-L^{-1}).

Three-dimension fluorescence excitation-emission matrix (FEEM) was analyzed using a spectrofluorometer (FP-8200, JASCO, Japan). The excitation (Ex) and emission (Em) spectra were measured at wavelengths from 220 to 600 nm with 5 nm intervals and scanning speed at 1200 nm min^{-1}.

5.3 Results and discussion

5.3.1 DOC and DON removal

Figure 5.1 shows normalized concentrations (C/C_0) of DOC and DON of SW samples treated by VUV and UV, respectively. Average DOC and DON of SW samples were 3.42 mg-C L^{-1} and 0.355 mg-N L^{-1}, respectively (Table 5.1). DOC removal increased gradually with reaction time (Figure 5.1 (a) and (b)). At 60 min (VUV dose of 24 J cm^{-2}), DOC removal was approximately 21%. Adding H_2O_2 at 5, 10, and 20 mg L^{-1} (hereafter referred to as VUV/H5, VUV/H10, and VUV/H20) improved DOC mineralization at 60 min to 32, 37, and 51%, respectively (Figure 5.2

(a)). For UV treatment, the reduction of DOC was only 8% at 60 min of irradiation time (UV dosage of 21 J cm^{-2}). The addition of H$_2$O$_2$ at 5, 10, and 20 mg L^{-1} (hereafter referred to as UV/H5, UV/H10, and UV/H20) enhanced the removal efficiency of DOC to 23, 30, and 45%, respectively. For VUV and UV alone, VUV provided higher DOC removal than UV (21% vs 8% at 60 min). This is attributed to the direct photolysis of 185 nm and OH$^•$ generated from VUV while UV oxidized DOC by only 254 nm direct photolysis. Efficiencies of DOC reduction by VUV/H$_2$O$_2$ were slightly better than those of UV/H$_2$O$_2$ as H$_2$O$_2$ concentration increased (6 to 9% difference). This suggests that under VUV or UV with the presence of H$_2$O$_2$, enhanced DOC mineralization was mainly due to oxidation by OH$^•$ which was generated from H$_2$O$_2$ addition (Imoberdorf & Mohseni, 2011).

The reduction of DON under VUV and UV with time is presented in Figure 5.1 (c) and (d), respectively. The results showed that 15% of DON was removed under VUV alone at 60 min (VUV dose of 24 J cm^{-2}). With the addition of H$_2$O$_2$, the removal efficiencies of DON under VUV/H5, VUV/H10, and VUV/H20 systems were 16, 21, and 31%, respectively (Figure 5.2 (b)). Under UV, UV/H5, UV/H10, and UV/H20 systems, the reduction of DON was 10, 13, 17, and 26%, respectively (Figure 5.2 (b)).
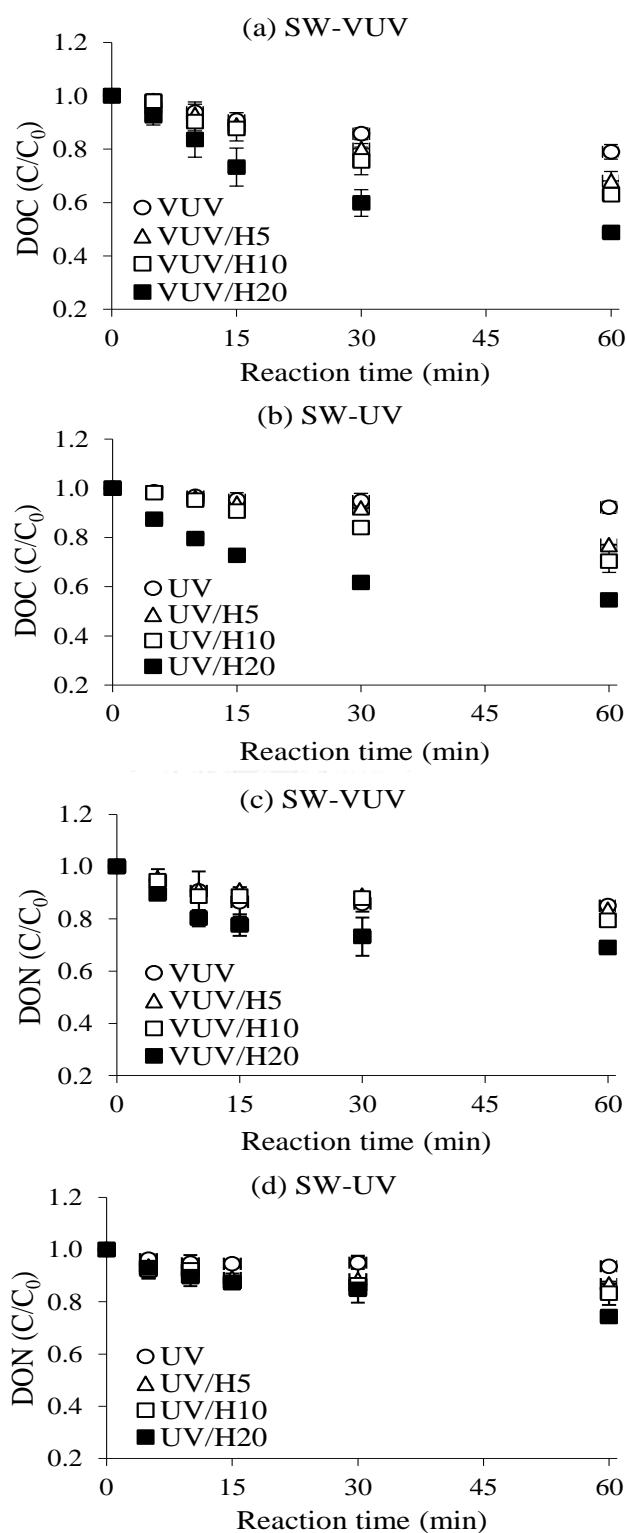
Figure 5.1 Normalized DOC and DON concentrations of SW samples treated by VUV and UV: (a) DOC-VUV, (b) DOC-UV, (c) DON-VUV, and (d) DON-UV (H5, H10, and H20 represent H_2O_2 concentration at 5, 10, and 20 mg L^{-1}, respectively)

Comparing among the treatment systems, the DOC and DON reduction was in the following order: VUV/H20 > UV/H20 > VUV/H10 > UV/H10 > VUV/H5 > UV/H5 > VUV > UV. However, the removal efficiencies of DON were less than those of DOC at the same H_2O_2 concentration (except for UV alone). This is because DON is associated with 10% of DOC in the forms of amino acid or protein bound in the center of complex organic molecules (Chen, Chen, & Wang, 2011; Dignac et al., 2000) . Therefore, it is more difficult to mineralize organic nitrogen molecules than organic carbon molecules.
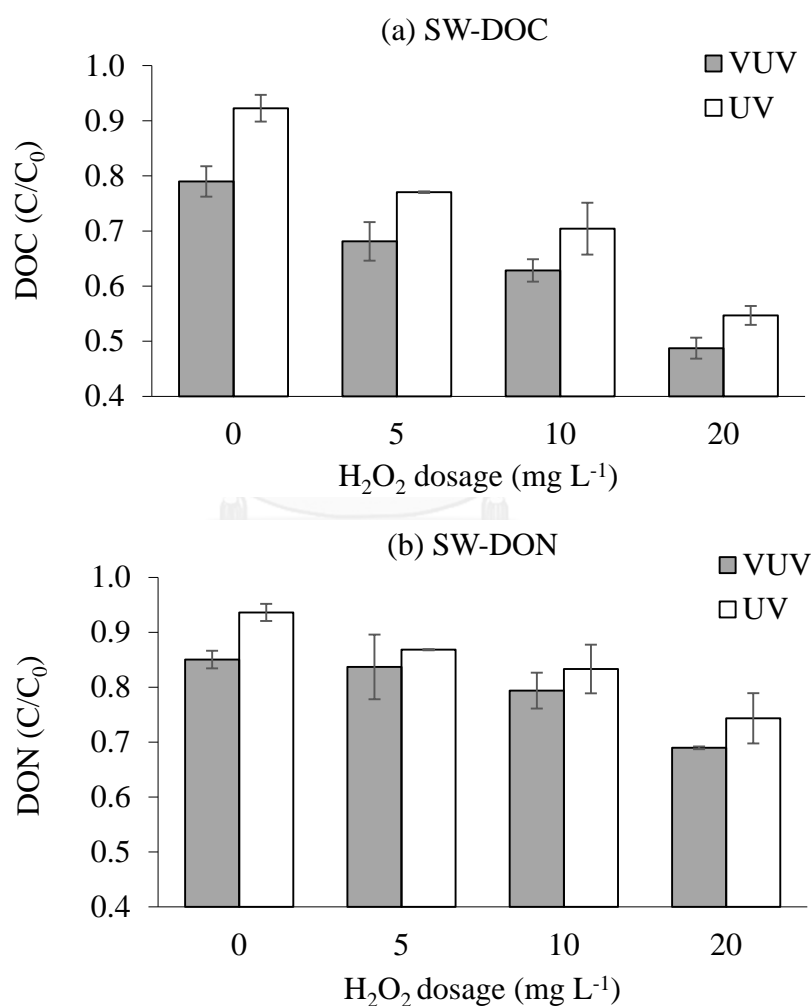
Figure 5.2 Effect of H_2O_2 dosage on removal of DOC and DON of SW samples treated for 60 min by VUV and UV: (a) DOC and (b) DON

Figure 5.3 illustrates the normalized concentrations of DOC and DON of WW samples under VUV and UV. Average concentrations of DOC and DON in WW samples were 5.85 mg-C L^{-1} and 1.425 mg-N L^{-1}, respectively (Table 5.1). DOC concentration decreased steadily with reaction time (Figure 5.3 (a), (b)).

For the VUV system, the removal of DOC of WW samples was 11% at 60 min (Figure 5.4 (a)). The addition of H_2O_2 (10, 20, and 50 mg L^{-1}) to the VUV system (hereafter referred to as VUV/H10, VUV/H20, and VUV/H50), was found to increase DOC removal to 38, 47 and 57%, respectively. The UV system showed a similar trend of DOC reduction with slightly less removal efficiencies (Figure 5.4 (a)). The reduction of DON was 7% under VUV at 60 min (Figure 5.4 (b)). The removal of DON was elevated when H_2O_2 was added. VUV with 50 mg L^{-1} H_2O_2 (VUV/H50) provided the highest DON removal at 40%. Under VUV/H10 and VUV/H20, the reduction of DON was 20 and 29%, respectively. For UV treatment, there was a limited change in DON reduction (Figure 5.4 (b)). Only 4% of DON was reduced after treatment with UV (60 min). The reduction of DON under UV/H10, UV/H20, and UV/H50 was 13, 25, and 31%, respectively. This finding was consistent with a previous study which reported that DON was reduced by 20 to 30% when adding 50 to 100 mg L^{-1} H_2O_2 in the UV system (Qi & Jiangyong, 2016).

Interestingly, DOC decreased steadily with time while DON reduction mostly occurred during the first 15 to 30 min of reaction time. The trend of DON reduction was analogous to the reduction of UV_{254} (mainly during the 15-30 min of reaction time) (APPENDIX C, Figure C.13-C.16). This because UV_{254} represents aromatic carbon structures which have high electron density and therefore are preferably attacked by $OH^{•}$. Nitrogen bound with aromatic structures was then liberated and oxidized. In the later period of reaction time, the degradation of DON was minimal. This suggests that the nitrogen intermediate degradation products were not mineralized due to their persistence to oxidation by $OH^{•}$ or photolysis. Chen and co-workers (Chen, Chen, & Wang, 2011) reported the DON removal of selected organic compounds and found that compounds with imidazole ring (histamine) were more susceptible to oxidation by $OH^{•}$ than triazine ring (atrazine) or C-N single bond (triethanolamine) compounds.
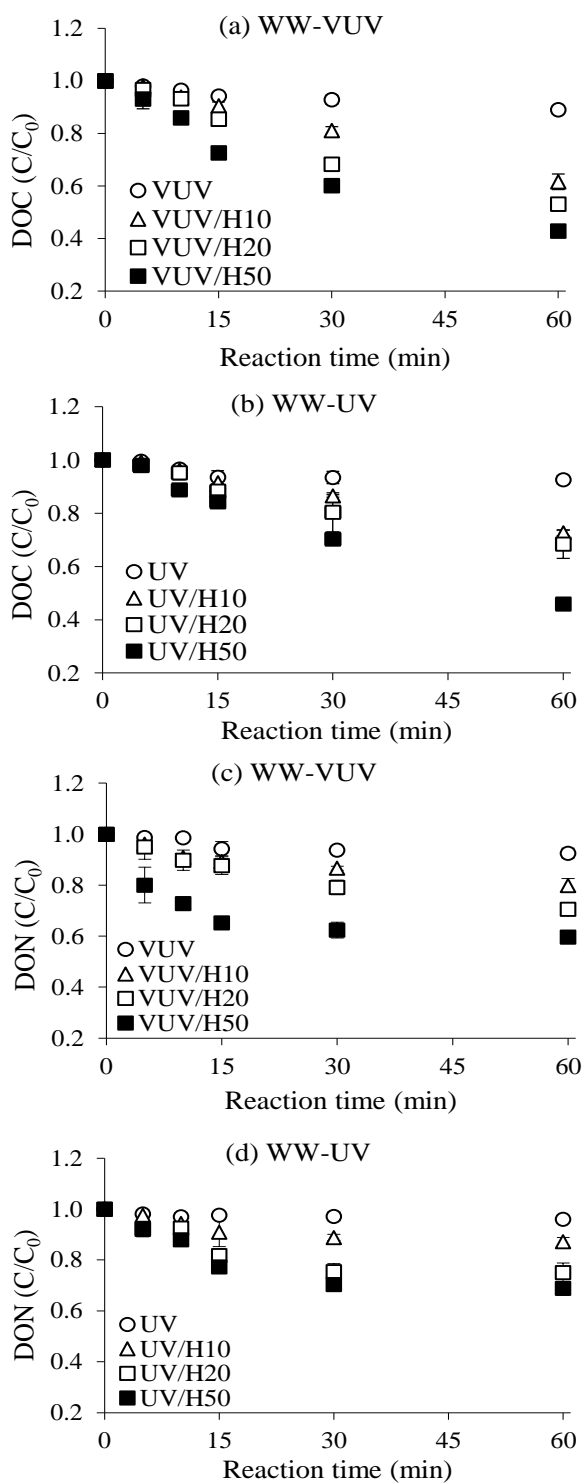
Figure 5.3 Normalized DOC and DON concentrations of WW samples treated by
VUV and UV: (a) DOC-VUV, (b) DOC-UV, (c) DON-VUV, and (d) DON-UV
(H10, H20, and H50 represent H_2O_2 concentration at 10, 20, and 50 mg L^{-1},
respectively)
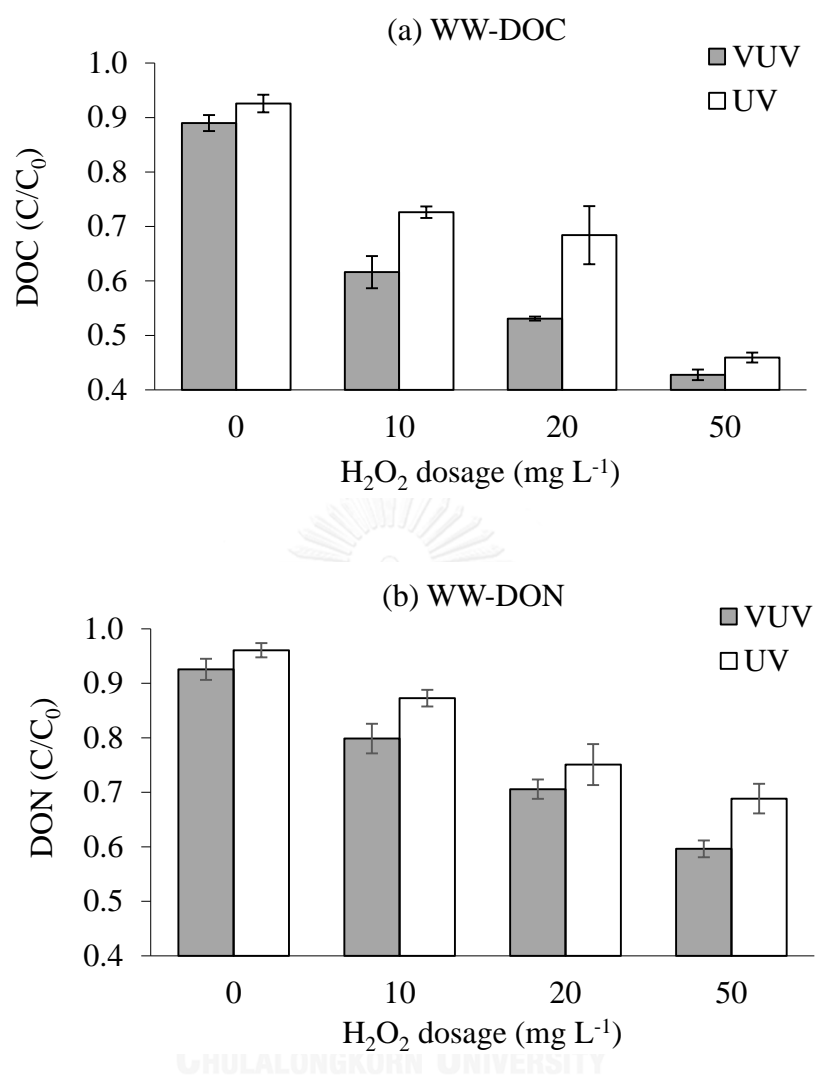
Figure 5.4 Effect of H_2O_2 dosage on removal of DOC and DON of WW samples treated for 60 min of VUV and UV: (a) DOC and (b) DON

5.3.2 Fraction

Figure 5.5 presents observed changes in HPI and HPO fractions of SW samples treated by VUV and UV alone and with H_2O_2. The concentrations of HPI and HPO fractions were measured in term of DOC values. For SW samples, the concentrations of HPI and HPO were 1.86 and 1.58 mg-C L^{-1}, respectively. After treatment by 10 min of VUV and UV, the HPI and HPO only slightly changed, except VUV and UV with H_2O_2 of 20 mg L^{-1}. This indicates that during the first period of reaction time (10 min), reaction of organic molecules and oxidants (photon or $OH^{\bullet}$) was not sufficient to change the polarity of organic carbon. However, at the end of the reaction (60 min), substantial reduction of both fractions was observed. At 60 min of VUV irradiation, the reduction of HPI and HPO increased to 24 and 18%, respectively. The addition of H_2O_2 into the VUV or UV systems enhanced the degradation efficiencies of the HPI and HPO fractions (Figure 5.5 (a) and (b)). At 60 min of VUV with 20 mg L^{-1} H_2O_2, 77% of HPO and 36% of HPI were removed, respectively. For UV, at the same H_2O_2 dosage, HPO and HPI removal was 77% and 21%, respectively. The reduction of HPO fraction was more than that of HPI. This is likely because HPO molecules were easily broken down and transformed to HPI under oxidation reaction and only some parts of HPI were mineralized.

จุฬาลงกรณ์มหาวิทยาลัย
CHULALONGKORN UNIVERSITY
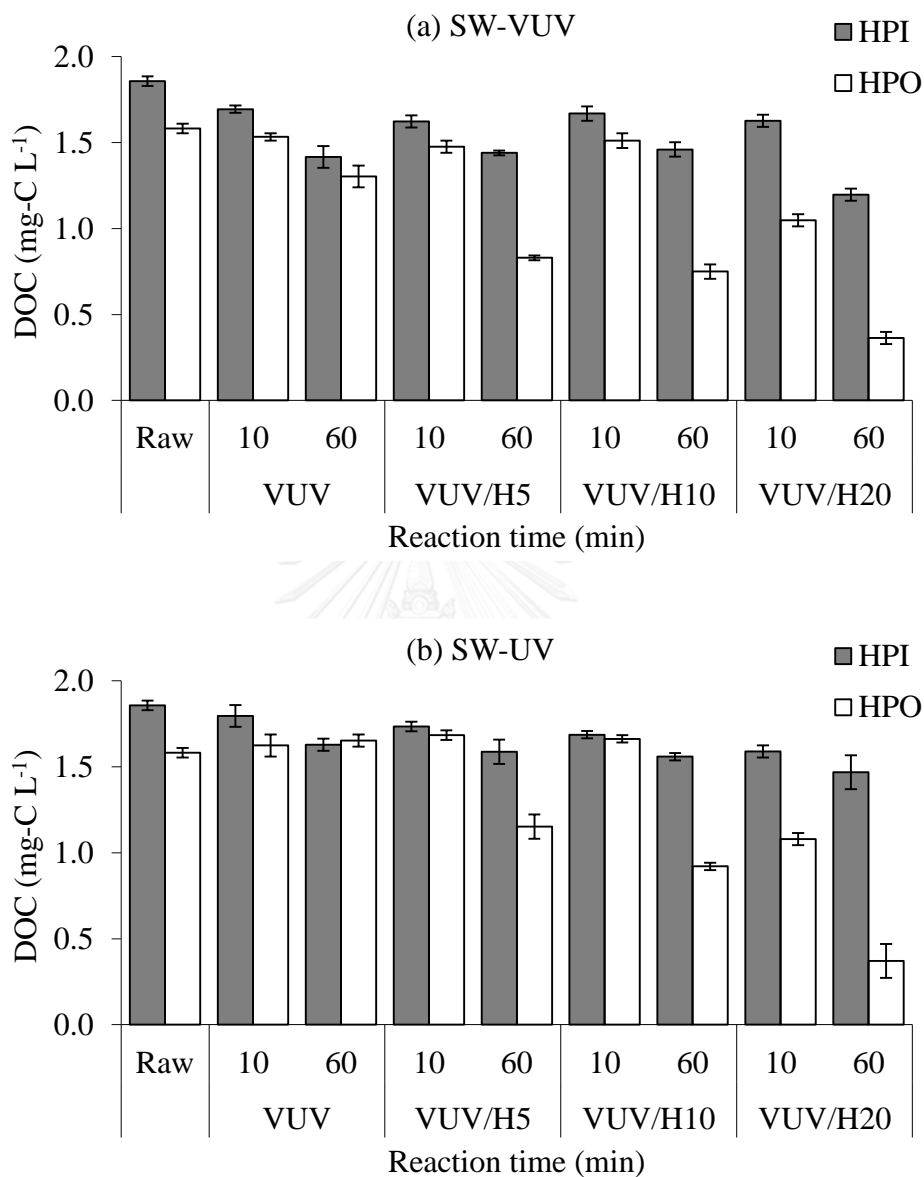
Figure 5.5 Fractions of SW samples after treatment by (a) VUV and (b) UV
(H5, H10, and H20 represent H_2O_2 concentration at 5, 10, and 20 mg L^{-1},
respectively)

Figure 5.6 illustrates the changes in HPI and HPO fractions of WW samples treated by VUV and UV alone and with 10 to 50 mg L^{-1} H_2O_2. Treatment with VUV and VUV/H_2O_2 at 10 min could not reduce HPO but reduced HPI by 14 to 31% (Figure 5.6 (a)). The results contrasted with UV and UV/H_2O_2 (10 and 20 mg L^{-1} H_2O_2) that very minimal reduction of HPI and HPO was observed after 10 min of irradiation time. This suggests that organic molecules in HPI fraction of WW were readily mineralized by VUV irradiation (185 nm). As observed with SW samples, the reduction of NOM fractions in WW samples increased with increases in reaction times and H_2O_2 dosage. At 60 min of VUV and VUV/H_2O_2, HPI and HPO were eliminated by 18 to 41% and 2 to 80%, respectively. The highest removal of HPI (41%) and HPO (80%) was provided by the VUV with 50 mg L^{-1} H_2O_2 (VUV/H50) system.

For the UV and UV/H_2O_2 systems, the reduction of HPI and HPO under UV/H_2O_2 at 60 min was in the range of 5 to 50% and 8 to 62%, respectively (Figure 5.6 (b)). Overall, both HPO than HPI fractions were removed and the addition of H_2O_2 elevated the removal efficiency of all systems suggesting that DOC in WW samples was converted to more hydrophilic characteristics as reaction time and OH$^{\bullet}$ increased.
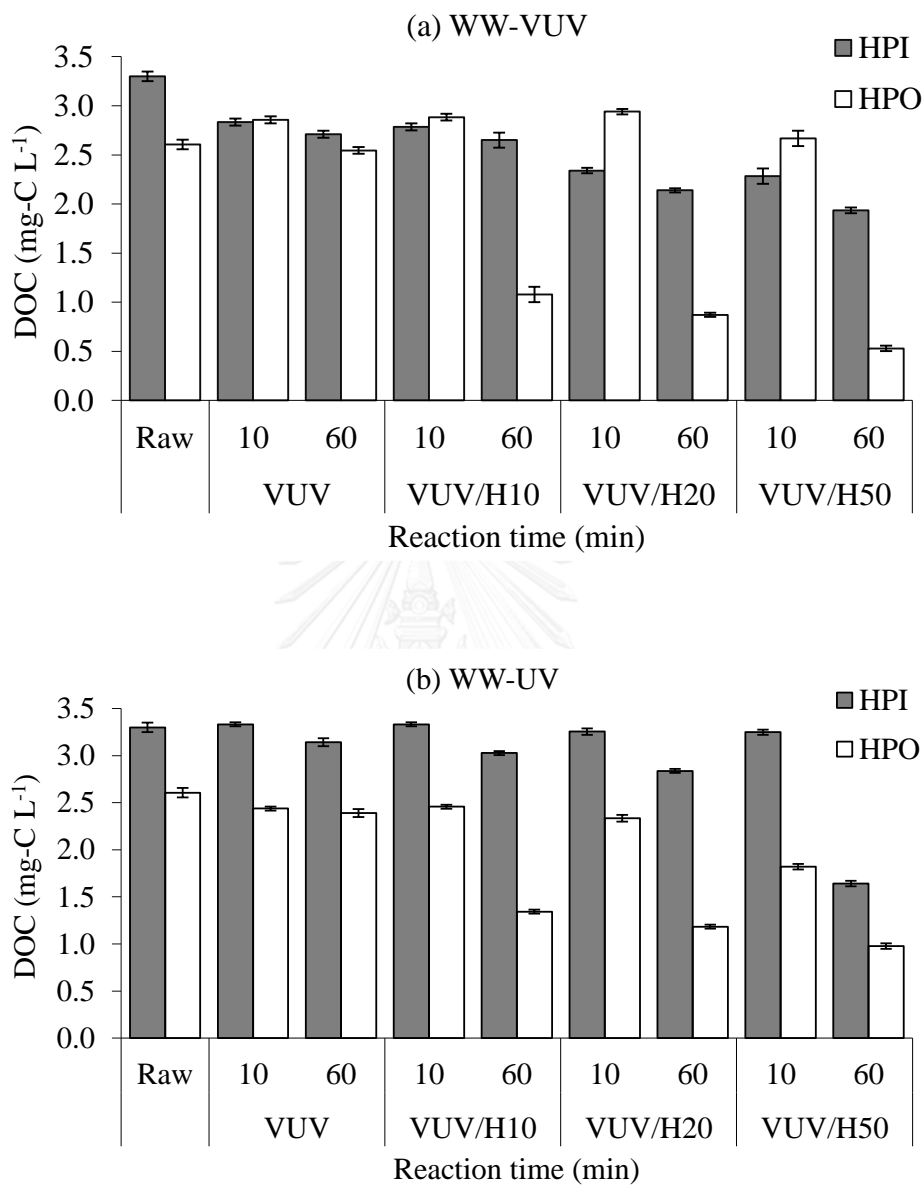
Figure 5.6 Fractions of WW samples treated by (a) VUV and (b) UV
(H10, H20, and H50 represent H_2O_2 concentration at 10, 20, and 50 mg L^{-1},
respectively)

5.3.3   FEEM

Figure 5.7 presents 3-D FEEM contours of raw water of SW and WW samples before and after treatment with VUV and UV. The FEEM contours of SW and WW samples treated with VUV/H_2O_2 and UV/H_2O_2 are in APPENDIX C (Figure C.21-C.24). The peak intensities of all samples are in APPENDIX C, (Table C.1-C.4). Locations of FEEM peaks were identified based on the study of Chen and co-workers (Chen, Westerhoff, Leenheer, & Booksh, 2003) . Three major fluorescent peaks were identified for both SW and WW samples including aromatic protein (Peak A), tryptophan and protein-like (Peak B), and humic acid-like compound (Peak C).

There are two main peaks detected in SW samples, peaks B and C which occurred at the excitation/emission wavelengths (Ex/Em) of 295/340 and 270/420 nm, respectively (Figure 5.7 (a)). The intensity of peaks B and C in a raw water sample was 2.10 and 4.21 QSU, respectively. Peak C was a dominant peak indicating that humic acid-like compounds (released from organic matter degradation) were a major component of NOM in SW samples. Greater reduction of peak C intensity was observed under the VUV/H_2O_2 system. At 20 mg L^{-1} H_2O_2, the intensity of pack C disappeared (Figure 5.8 (a)). This was also the case for UV/H20 (Figure 5.8 (b)), suggesting the mineralization of humic acid-like compounds was mainly due to the oxidation by OH$^\bullet$ or photolysis at 185 nm rather than photolysis by 254 nm. The removal of peak B was 51 and 15% by VUV (Figure 5.8 (a)) and UV (Figure 5.8 (b)), respectively. Addition of 20 mg L^{-1} H_2O_2 into the UV and VUV systems could eliminate the intensity of peak B by 83 and 100%, respectively. This implies that tryptophan and protein-like compounds were preferably degraded by OH$^\bullet$.
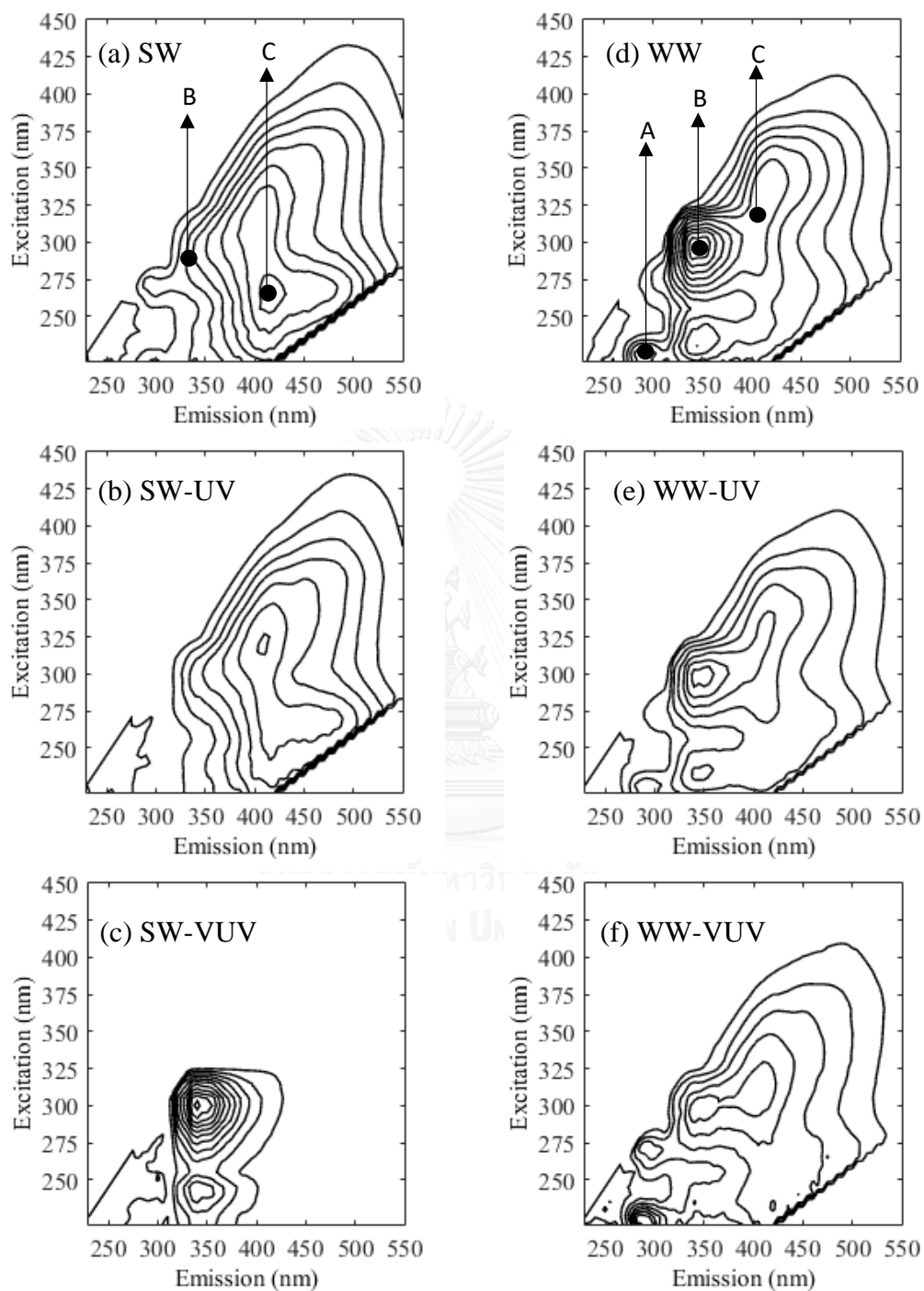
Figure 5.7 FEEM of SW and WW samples treated by VUV and UV at 60 min

For WW samples, there are three major peaks: A, B, and C at the Ex/Em of 220/295, 290/340, and 315/405 nm, respectively (Figure 5.7 (d)). The intensities of peaks A, B, and C in WW samples were 5.54, 14.05, and 9.08 QSU, respectively. The intensities of peaks B and C in WW samples were 7 and 2 times greater than those of surface water, suggesting high level of tryptophan and humic acid-like substances in wastewater effluent. Peak B was the highest peak indicating the dominance of tryptophan and protein-like compounds in wastewater effluent with high DON levels. The removal of tryptophan and protein increased with the dose of H_2O_2, 60, 61, 63 and 98% for VUV, VUV/H10, VUV/H20, and VUV/H50, respectively (Figure 5.8 (c)). The efficiency of UV was slightly less than VUV (~10%), suggesting that tryptophan and protein groups were eliminated less by UV.

Interestingly, substantially reduction (91 to 99%) of peak B intensity was observed when adding H_2O_2 at 10 to 50 mg L^{-1} into the UV system (Figure 5.8 (d)). This infers that tryptophan and protein-like compounds were susceptible to OH$^•$. Since tryptophan-like compounds have hydrophobic characteristics (Su et al., 2016), higher reduction in tryptophan associated peak intensity can be tied to the decrease of HPO fraction as described in the previous subsection (Figure 5.6).

For aromatic proteins (peak A) and humic acid like substances (peak C), the reduction of peak intensities was somewhat similar. The removal of peak A by UV and VUV was 55 and 75%, respectively. For peak C, the reduction of peak intensities by UV (42%) was much less than that by VUV (88%) (Figure 5.8 (c, d). Similar to tryptophan like substances (peak B), the reduction of aromatic protein (97 to 100%) and humic acid (96 to 99%) were greater when adding H_2O_2 into VUV system. UV/H_2O_2 also effectively removed aromatic proteins and humic acid like substances by 55 to 94% and 96 to 99%, respectively. The efficiencies of VUV/H_2O_2 (Peak A: 97 to 100% and Peak C: 96 to 99%) and UV/H_2O_2 (Peak A: 92 to 94% and Peak C: 94 to 98%) for the reduction of two peak intensities were not different, implying that aromatic proteins, and humic-like substances were favorably degraded by OH$^•$ and VUV light at 185 nm.
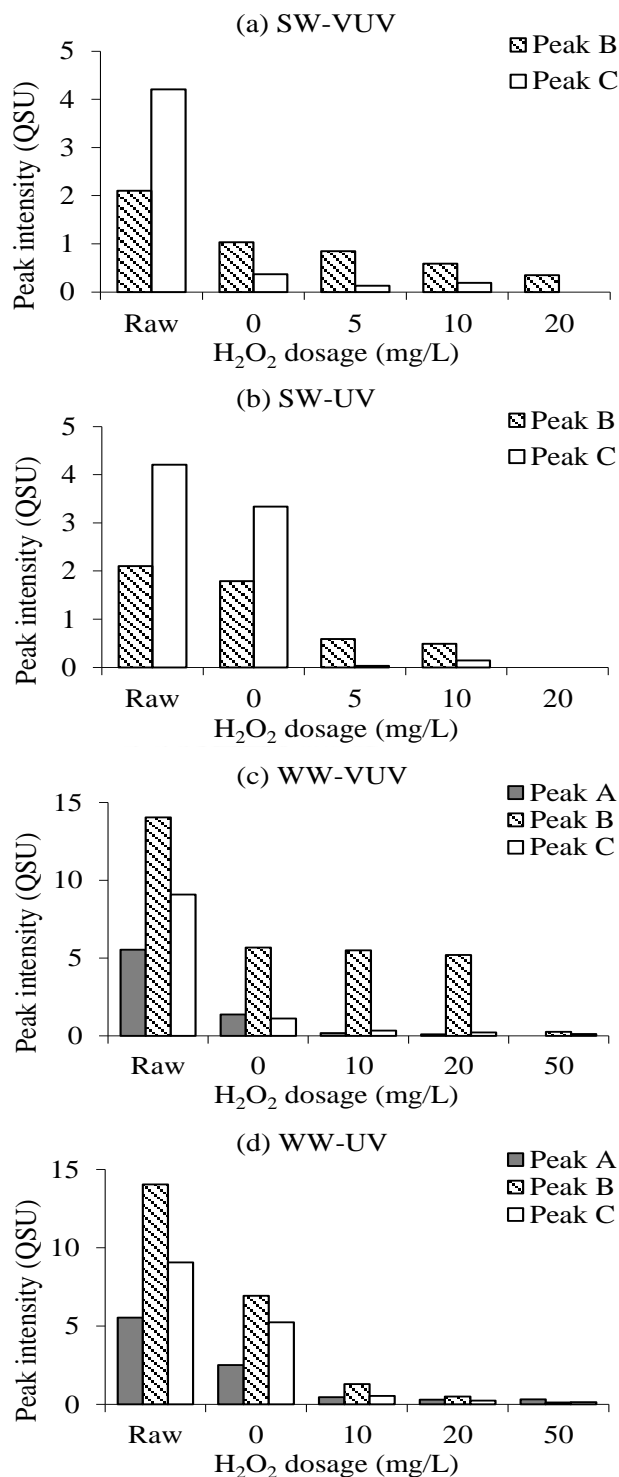
Figure 5.8 Effect of H₂O₂ dosage on removal of organic compounds associated with FEEM peaks of SW and WW samples treated for 60 min: (a) SW-VUV, (b) SW-UV, (c) WW-VUV, and (d) WW-UV. (Peak A = aromatic proteins, Peak B = tryptophan-like substances, and Peak C = humic acid-like substances)

5.3.4 HANs formation potential (HANFP)

Figure 5.9 presents the normalized HANFP (C/C_0) of SW samples treated by VUV and UV, respectively. The irradiated samples at 10, 30, and 60 min were selected for the chlorination test. The HANFP of SW samples was 4.17 ± 0.20 µg L^{-1}. In this study, TCAN and DCAN were two HANs species detected after chlorination for 24 hr. DCAN was the dominant species (3.81 ± 0.19 µg L^{-1}) while TCAN (0.37 ± 0.03 µg L^{-1}) accounted for 9% of total HANFP. The HANFP after treatment with VUV increased by 6% at 10 min and then decreased by 18% at 60 min (Figure 5.9 (a)). Under VUV with 5 to 20 mg L^{-1} H$_2$O$_2$, the HANFP also increased in the range of 5 to 11% at 10 min and then decreased by 34 to 54% at 60 min, respectively. More H$_2$O$_2$ addition results in more reduction of HANFP under VUV irradiation at 60 min (Figure 5.9 (a)). Little change in HANFP reduction was observed under the UV irradiation (Figure 5.9 (b)). Similar to the VUV system, the addition of H$_2$O$_2$ into the UV system enhanced the HANFP by 4 to 9% at 10 min and then decreased by 17 to 41% at 60 min. The HANFP at 60 min of VUV and VUV/H$_2$O$_2$ (5, 10, and 20 mg L^{-1}) were less than those of UV and UV+H$_2$O$_2$ by 1.2 to 1.4 times. This suggested that VUV was more effective on HANFP reduction than UV due to more OH$^\bullet$ generated under VUV system. The treatment by VUV/H$_2$O$_2$ exhibited the highest HANFP reduction (Figure 5.9 (a)). This is because VUV/H$_2$O$_2$ could decrease more hydrophobic (Figure 5.5 (a), Figure 5.8 (a)) and aromatic constituents in water (UV$_{254}$ reduction, APPENDIX C, Figure C.13-C.16) and more HANs precursor (DON reduction, Figure 5.2).

Figure 5.9 (c) and (d) represents HANs yields of SW samples treated by VUV and UV, respectively. HANs yields (µg mg-N^{-1}) are normalized HANFP (µg L^{-1}) with the DON concentration (mg-N L^{-1}). An average HANs yield of untreated SW samples was 11.52 ± 0.56 µg mg-N^{-1}. At the beginning of VUV and VUV/H$_2$O$_2$ experiments, HANs yield increased by 14 to 28% due to the HANFP increase (Figure 5.9 (a)) while DON slightly decreased (Figures 5.1 and 5.2). At 60 min of reaction time, the reduction of HANs yield was 4% and elevated to 21 to 33% with H$_2$O$_2$ of 5 to 20 mg L^{-1} (Figure 5.9 (c)). The reduction of HANs yield increased with times and H$_2$O$_2$ dosage. UV treatment could not reduce the HANFP yield (Figure 5.9 (b)), while 5 to 21% of the yield were removed by UV/H$_2$O$_2$ (Figure 5.9 (d)). The efficiency of VUV/H$_2$O$_2$ for the reduction of HANs yield was 1.6 to 4.3 times greater than UV/H$_2$O$_2$.

Overall, HANs yield increased at the beginning and then decreased over time. This could be because some organic nitrogen was degraded to form intermediate precursors of HANs at the beginning of the reaction (first 10 min). As the reaction time progressed, these intermediates were degraded and consequently reduced HANFP. This phenomenon was also observed in previous studies that investigated the removal of THMs by VUV (Buchanan, Roddick, & Porter, 2006; Imoberdorf & Mohseni, 2014) or UV+H_2O_2 (Dotson, Keen, Metz, & Linden, 2010) . Buchanan and co-workers (2006) reported increasing of THMFP below a VUV dose of 40 J cm^{-2} and decreasing as more VUV doses of 40 to 240 J cm^{-2} (more irradiation time) was applied. Increasing of THMFP at VUV doses of 1 to 3 J cm^{-2} and decreasing at higher doses were reported (Imoberdorf & Mohseni, 2014).

Figure 5.10 illustrates the normalized HANFP (C/C_0) and HANFP yields of WW samples treated by VUV and UV. The HANFP of WW sample (before AOPs treatments) was 6.38 ± 0.13 µg L^{-1} consisting of 5.64 ± 0.16 µg L^{-1} of DCANFP and 0.74 ± 0.09 µg L^{-1} of TCANFP. The HANFP of WW samples was 1.5 times higher than that of SW samples due to higher DOC and DON concentrations in WW samples. The HANs yield of WW samples was 4.34 ± 0.14 µg mg-N^{-1}, which was 3 times lower than that of SW samples. This implies that organic constituents in WW were less reactive to chlorine compared to SW sample. Krasner and co-workers (2005) compared the reactivity of NOM in drinking water and wastewater effluent with chlorine and found that wastewater effluent had lower THM yields due to lower SUVA values. As observed with SW samples, the HANFP and HANs yield of WW samples tended to increase and then gradually decreased with time. At the initial stage of the experiment (10 min), the HANFP and HANs yields increased by 2% for VUV and 7 to 16% for VUV/H_2O_2 (Figure 5.10 (a) and (c)). At 60 min, HANFP and HANs yield in the VUV/H_2O_2 system decreased by 30 to 73%, and 12 to 54%, respectively. HANFP decreased at high VUV dose (24 J cm^{-2}) and H_2O_2 dose (50 mg L^{-1}) due to increase of $OH^\bullet$ and degradation of HANs precursors.
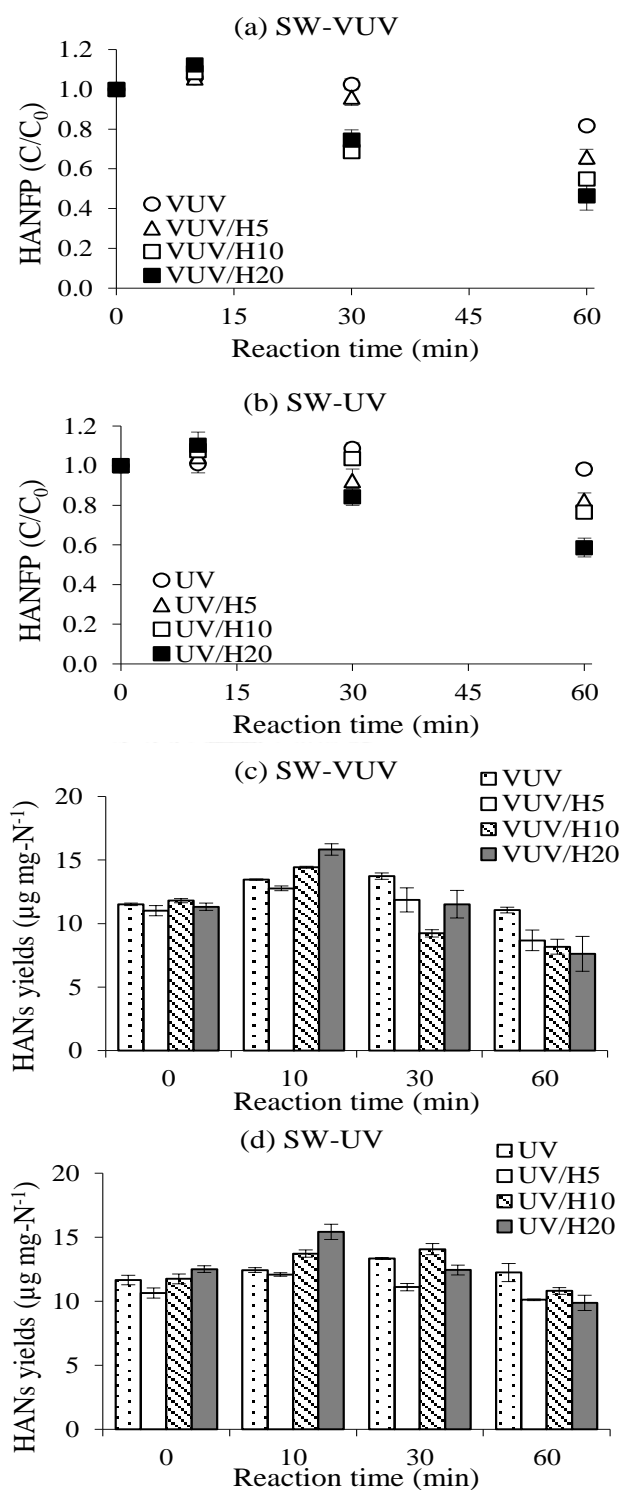
Figure 5.9 Normalized HANFP and HANs yields of SW samples treated by VUV and UV without and with H_2O_2 addition: (a) HANFP-VUV, (b) HANFP-UV, (c) HANs yields-VUV, and (d) HANs yields-UV
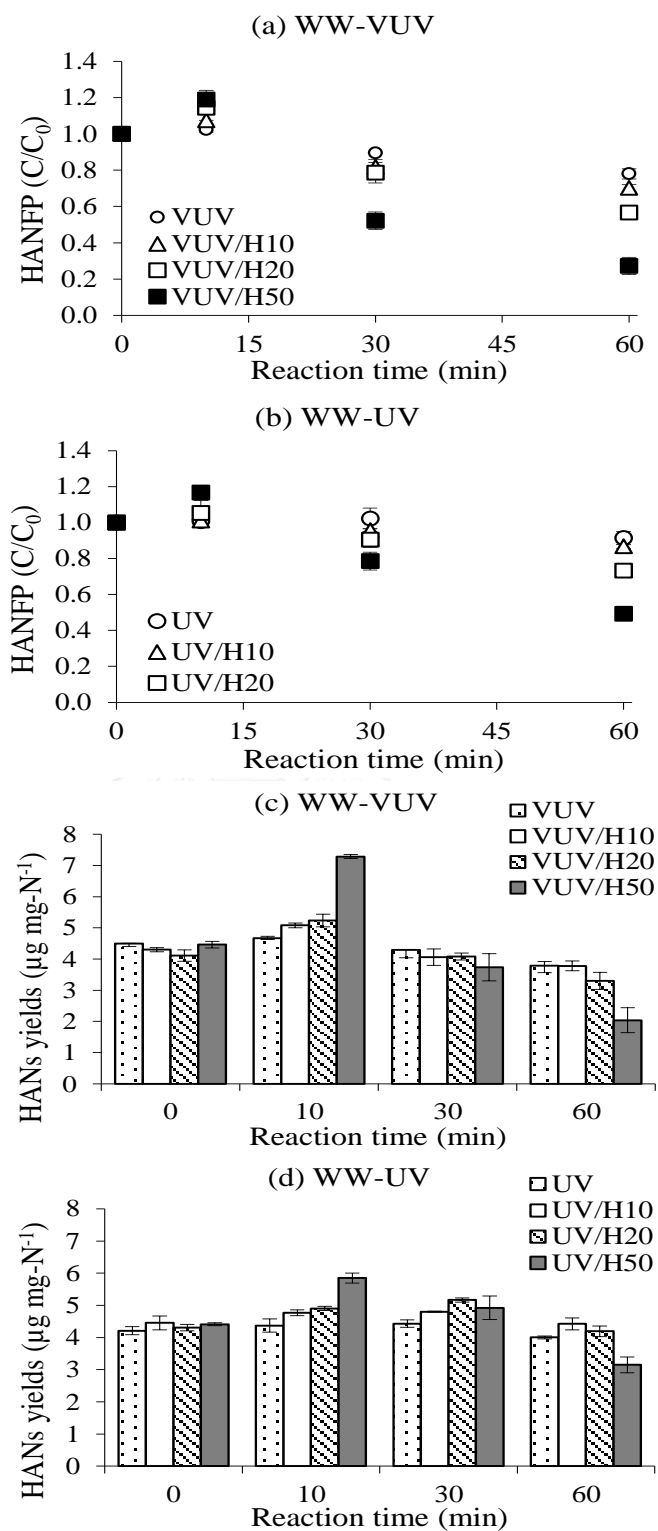
Figure 5.10 Normalized HANFP and HANs yields of WW samples: (a) HANFP-VUV, (b) HANFP-UV, (c) HANs yields-VUV, and (d) HANs yields-UV

For the UV system, the removal of HANFP (Figure 5.10 (b)) and HANs yield (Figure 5.10 (d)) show similar trends with the VUV systems. After 60 min of UV irradiation, the HANFP decreased by 8% because UV photolysis did not effectively reduce DOC and DON (Figure 5.3). The efficiency of UV was enhanced when adding H_2O_2. Under UV with 50 mg L^{-1} H_2O_2 (UV/H50), the removal of HANFP and HANs yield were 51 and 29%, respectively. This suggests that the decreases in HANFP and HANs yields was due to the formation of $OH^{\bullet}$ by UV activated H_2O_2, not by the UV photolysis. Comparing with VUV at the same H_2O_2 dosage, removal of HANFP by the UV system was less for H_2O_2 doses of 10, 20 and 50 mg L^{-1} by 2.2, 1.6, and 1.4 times, respectively.

Interestingly, the greater HANFP at the initial time was observed at the higher H_2O_2 concentration (i.e. VUV/H50). This might be due to some organic nitrogen was degraded to form intermediate of HANs precursor at the beginning of the experiment (Qi & Jiangyong, 2016). Another possible reason is the scavenging effect of $OH^{\bullet}$ by H_2O_2 could occur at the beginning when adding high amounts of H_2O_2, as shown in Equation (5.3) and (5.4) (Chu et al., 2014) .

$$OH^{\bullet} + H_2O_2 \quad \rightarrow \quad H_2O + OOH^{\bullet} \tag{5.3}$$
$$OH^{\bullet} + OOH^{\bullet} \quad \rightarrow \quad H_2O + O_2 \tag{5.4}$$

At longer reaction time, HANFP and HANs yield decreased due to the oxidation of HANs and HANs precursor by $OH^{\bullet}$. Since H_2O_2 activated VUV and UV did not show greater reduction in DON, higher reduction in HANFP and HANs yield were attributed to changes of precursor structures rather than mineralization. Based on the fractionation results, more reduction occurred for the HPO fraction as H_2O_2 dose increased (Figures 5.5 and 5.6). This trend is analogous to the reduction HANFP (Figures 5.9 and 5.10). Relationship between FEEM intensity and HANFP was also observed. The intensity of tryptophan-like substances (Peak B) correlated well with HANFP. For SW, the correlation coefficients (R^2) of the VUV and UV systems were 0.962 and 0.953, respectively (APPENDIX C, Figure C.25-C.28, Table C.5). This is because tryptophan-like peak represents amino acids or protein components which is nitrogen rich and therefore could be the precursor of HANs (Bond, Templeton, &

Graham, 2012; Jia, Wu, & Duan, 2016; Yang, Fan, Shang, & Zhao, 2010). The intensities of other FEEM peaks including aromatic proteins (Peak A) and humic-like substances (Peak C) had weak correlations with HANFP. Those organic constituents might not be HANs precursors. For WW, similar correlations were also found but not as strong as SW. This could be because the composition of organic in secondary treated wastewater effluent which is made up of more soluble microbial products was different from that of surface water (Huang et al., 2016; Liu & Li, 2015)) .

5.4   Summary

VUV exhibits a greater performance than UV process on the reduction of DOC, DON, UV_{254}, HPI and HPO fractions, FEEM, and HANFP. The efficiency of VUV could be elevated by the addition of H_2O_2. VUV/H_2O_2 (24 J cm^{-2}) treatment effectively removed DOC up to 51% for SW samples (20 mg L^{-1} H_2O_2) and 57% for WW samples (50 mg L^{-1} H_2O_2). The removal of DON by VUV/H_2O_2 was 31 and 40% for SW and WW samples, respectively. HPO fraction was more preferentially removed than HPI fraction in both SW and WW samples. VUV/H_2O_2 and UV/H_2O_2 exhibited more reduction in organic matter structures (aromatic proteins, and humic acid-like and tryptophan-like compounds) compared to VUV and UV alone, suggesting that fluorescent components were favorably removed by OH$^{\bullet}$ and VUV at 185 nm. Strong correlations between tryptophan-like compounds and HANFP were found. HANFP increased slightly at the initial reaction time (10 min), and then decreased at the end of treatment (60 min). Addition of H_2O_2 into VUV at 20 mg L^{-1} for SW samples and 50 mg L^{-1} for WW samples provided lower HANFP than UV/H_2O_2 at the dosages of H_2O_2. The VUV/H_2O_2 system is suitable for controlling of HANs precursors and HANs formation in drinking water and reclaimed wastewater.

CHAPTER 6
CONCLUSIONS AND RECOMMENDATIONS FOR FUTURE WORK

6.1   Conclusions

HANs, one group of N-DBPs, are potential human carcinogens and has been shown to be more toxic than the regulated DBPs (THMs and HAAs). The formation of HANs is tied to the reaction between chlorine and DON in water. This research investigated two major approaches for controlling of HANs: (1) degradation of HANs directly after formation and (2) reduction of HANs precursors (DON) before chlorination. The results obtained from experiments corresponding to the two approaches are concluded in subsections 6.1.1 and 6.1.2.

6.1.1   Part 1: Degradation of HANs by VUV and UV

This part gives a better understanding on HANs removal efficiency and removal mechanisms by VUV and UV. The results can be concluded as follow:

(1)   The efficiency of VUV for removing four species of HANs was better than UV by 1.6 to 7.0 times.

(2)   The degradation efficiency of mixed HANs was slightly lower than that of single HANs by 1.4 to 1.7 times (except for DBAN), suggesting a competitive effect among HANs species.

(3)   The photodecomposition rate of HANs in the presence of DO was much lower than that in the presence of nitrogen. The removal rate of mixed HANs obtained by VUV and UV was in the same order of DBAN > TCAN > DCAN > MCAN.

(4)   Brominated HANs species (DBAN) had the highest removal rate under VUV as well as UV, due to the weaker bond dissociation energy of C-Br bond compared to C-Cl bond. Among chlorinated HANs, TCAN had the highest degradation rate due to higher number of Cl atoms making it more susceptible to photolysis.

(5) Degradation mechanism of HANs species was different depending on properties of the compounds such as molar absorptivity, bond dissociation energy, and quantum yield.

- Direct photolysis at 254 nm was a major mechanism of DBAN removal. This is because DBAN has high molar absorptivity and quantum yield at 254 nm.

- Direct photolysis at 185 nm was the dominant mechanism for DCAN and TCAN degradation due to the strength of C-Cl bond which requires high energy to split it.

- Indirect photolysis by OH$^{\bullet}$ was the main mechanism for MCAN reduction due to its low light absorption.

(6) The formation of intermediates from the degradation of single HANs under VUV was due to the substitution, addition, and polymerization reaction. VUV not only can degrade HANs but also can remove their intermediates from the system. This could be observed by the reduction of intermediates mass spectra with increase reaction time.

6.1.2 Part 2: Reduction of DON and HANFP by VUV, VUV/H_2O_2, UV, and UV/H_2O_2

VUV, VUV/H_2O_2, UV, and UV/H_2O_2were employed to reduce the concentration of DON or changes in DON characteristics. This part of the research aimed to minimize the formation of HANs upon chlorination. The results from this part can be concluded as follows:

(1) VUV provided greater efficiency for reducing of all parameters (i.e. DON, DOC, UV$_{254}$, HPI and HPO fractions, and FEEM intensities) than UV process.

(2) The addition of H_2O_2 into VUV system elevated the reduction of all parameters as well as UV system. Increases in H_2O_2 concentration improved the removal efficiency.

(3) The best treatment method for reducing all parameters was VUV/H_2O_2 at VUV fluence of 24 J cm^{-2} and H_2O_2 dose of 20 and 50 mg L^{-1} for SW and WW samples, respectively. The performances of VUV/H_2O_2 (20 mg L^{-1} H_2O_2 for SW samples and 50 mg L^{-1} H_2O_2 for WW samples) are as follows:

- DON was removed by 31 and 40% for SW and WW samples, respectively.

- DOC in surface water and secondary treated wastewater effluent reduced by 51% and 57%, respectively.

- UV$_{254}$ was reduced by 90 and 88% for SW and WW samples, respectively.

- The reduction of HPO and HPI fractions in SW samples under VUV/H_2O_2 was 77% and 36%, respectively. For WW samples, HPO and HPI reduction was 80 and 41%, respectively. HPO fraction was more preferentially removed than HPI fraction. This might be because hydrophobic organic molecules were easy to degrade and transform into hydrophilic structures.

- VUV/H_2O_2 and UV/H_2O_2 exhibited more reduction in aromatic proteins, and humic acid-like and tryptophan-like compounds than bare VUV and UV systems, suggesting fluorescent components were favorably removed by OH$^•$ and VUV at 185 nm.

- Strong correlations between tryptophan-like compounds and HANFP were found for both SW and WW samples.

- The formation of total HANFP (DCAN+TCAN) increased slightly at 10 min, and then decreased at 60 min of reaction time. The VUV/H_2O_2 system (at the highest H_2O_2 dose applied in each type of samples) provided the lowest HANs formation. The VUV/H_2O_2 system is suitable for controlling of HANs precursor and HANs formation in drinking water and reclaimed wastewater.

This work demonstrated two approaches to control HANs by VUV: removal of HANs and reduction HANs precursor. Fundamental and important information such as

reactivity of HANs species with VUV and intermediate products was obtained for HAN removal as well as the link between surrogate parameters and HAN formation after VUV/UV+H_2O_2 treatments. The advantages of using VUV lamp instead of conventional UV lamp are VUV lamp is not only can kill pathogens in water (by 254 nm) but also can removed DBPs and DBPs precursor in water (by photolysis at 254 nm and 185 nm, and indirect photolysis by OH$^\bullet$).

6.2 Recommendations for future work

(1) Although VUV-based-AOP is a potential treatment technology for the removal of HANs in water. In practice, the other water constituents such as NOM, ionic species, alkalinity, and turbidity could affect the removal of HANs by VUV. Future research should be conducted on the removal and mineralization of HANs by VUV for different water matrices.

(2) The toxicity of intermediates from photodegradation of HANs by VUV should be evaluated.

(3) The formation of regulated DBPs such as THMs should also be observed. A correlation between THM formation and HAN formation should be determined.

(4) To better understand the HANs precursor, the formation of HANs from HPI and HPO fractions should be investigated. This helps in clarifying which fraction is the major precursor of HANs.

(5) Often oxidation process is followed by biological filtration to remove the degradation products generated. Combined VUV-based-AOP and biological filtration to reduce HAN precursors should be investigated.

(6) The electrical energy per order of contaminant removal (EE/O) VUV and UV with and without H_2O_2 should be estimated. The EE/O value can be useful to compare the energy efficiency of different treatment systems in order to study and the feasibility in full-scale application.

REFERENCES

Afzal, A., Kang, J., Choi, B.-M., & Lim, H.-J. (2016). Degradation and fate of N-nitrosamines in water by UV photolysis. *International Journal of Greenhouse Gas Control, 52*, 44-51.

APHA. (2012). Standard Methods for the Examination of Water and Wastewater, twenty-first ed. . Washington, DC: American Public Health Association.

Arany, E., Szabó, R. K., Apáti, L., Alapi, T., Ilisz, I., Mazellier, P., . . . Gajda-Schrantz, K. (2013). Degradation of naproxen by UV, VUV photolysis and their combination. *Journal of Hazardous Materials, 262*, 151-157.

Bagheri, M., & Mohseni, M. (2015). A study of enhanced performance of VUV/UV process for the degradation of micropollutants from contaminated water. *Journal of Hazardous Materials, 294*, 1-8.

Baytak, D., Sofuoglu, A., Inal, F., & Sofuoglu, S. C. (2008). Seasonal variation in drinking water concentrations of disinfection by-products in IZMIR and associated human health risks. *Science of The Total Environment, 407*(1), 286-296.

Bond, T., Goslan, E. H., Jefferson, B., Roddick, F., Fan, L., & Parsons, S. A. (2009). Chemical and biological oxidation of NOM surrogates and effect on HAA formation. *Water Research, 43*(10), 2615-2622.

Bond, T., Templeton, M. R., & Graham, N. (2012). Precursors of nitrogenous disinfection by-products in drinking water—A critical review and analysis. *Journal of Hazardous Materials, 235*, 1-16.

Brandhuber, P. J., & Korshin, G. (2009). *Methods for detection of residual hydrogen concentrations peroxide in advanced oxidation processes* (WRF-04-019). Retrieved from WateReuse Foundation, Alexandria, VA, USA:

Buchanan, W., Roddick, F., & Porter, N. (2006). Formation of hazardous by-products resulting from the irradiation of natural organic matter: Comparison between UV and VUV irradiation. *Chemosphere, 63*(7), 1130-1141.

Buchanan, W., Roddick, F., & Porter, N. (2008). Removal of VUV pre-treated natural organic matter by biologically activated carbon columns. *Water Research, 42*(13), 3335-3342.

Buchanan, W., Roddick, F., Porter, N., & Drikas, M. (2005). Fractionation of UV and VUV Pretreated Natural Organic Matter from Drinking Water. *Environmental Science & Technology, 39*(12), 4647-4654.

Chen, B., Kim, Y., & Westerhoff, P. (2011). Occurrence and treatment of wastewater-derived organic nitrogen. *Water Research, 45*(15), 4641-4650.

Chen, B., Lee, W., Westerhoff, P. K., Krasner, S. W., & Herckes, P. (2010). Solar photolysis kinetics of disinfection byproducts. *Water Research, 44*(11), 3401-3409.

Chen, B., & Westerhoff, P. (2010). Predicting disinfection by-product formation potential in water. *Water Research, 44*(13), 3755-3762.

Chen, H.-W., Chen, C.-Y., & Wang, G.-S. (2011). Performance evaluation of the UV/H2O2 process on selected nitrogenous organic compounds: Reductions of organic contents vs. corresponding C-, N-DBPs formations. *Chemosphere, 85*(4), 591-597.

Chen, W., Westerhoff, P., Leenheer, J. A., & Booksh, K. (2003). Fluorescence Excitation−Emission Matrix Regional Integration to Quantify Spectra for Dissolved Organic Matter. *Environmental Science & Technology, 37*(24), 5701-5710.

Chiang, P.-C., Chang, E. E., Chuang, C.-C., Liang, C.-H., & Huang, C.-P. (2010). Evaluating and elucidating the formation of nitrogen-contained disinfection by-products during pre-ozonation and chlorination. *Chemosphere, 80*(3), 327-333.

Chon, K., Lee, Y., Traber, J., & Von Gunten, U. (2013). Quantification and characterization of dissolved organic nitrogen in wastewater effluents by electrodialysis treatment followed by size-exclusion chromatography with nitrogen detection. *Water Research, 47*(14), 5381-5391.

Chu, W.-H., Gao, N.-Y., & Deng, Y. (2010). Formation of haloacetamides during chlorination of dissolved organic nitrogen aspartic acid. *Journal of Hazardous Materials, 173*(1), 82-86.

Chu, W.-H., Gao, N.-Y., Deng, Y., & Krasner, S. W. (2010). Precursors of Dichloroacetamide, an Emerging Nitrogenous DBP Formed during Chlorination or Chloramination. *Environmental Science & Technology, 44*(10), 3908-3912.

Chu, W., Gao, N., Krasner, S. W., Templeton, M. R., & Yin, D. (2012). Formation of halogenated C-, N-DBPs from chlor(am)ination and UV irradiation of tyrosine in drinking water. *Environmental Pollution, 161*, 8-14.

Chu, W., Gao, N., Yin, D., Krasner, S. W., & Mitch, W. A. (2014). Impact of UV/H_2O_2 pre-oxidation on the formation of haloacetamides and other nitrogenous disinfection byproducts during chlorination. *Environmental Science and Technology, 48*(20), 12190-12198.

De, A. K. (2003). *A Textbook of Inorganic Chemistry* (Ninth ed.): New Age International, New Delhi.

Dignac, M.-F., Ginestet, P., Rybacki, D., Bruchet, A., Urbain, V., & Scribe, P. (2000). Fate of wastewater organic pollution during activated sludge treatment: Nature of residual organic matter. *Water Research, 34*(17), 4185-4194.

Dobrović, S., Juretić, H., & Ružinski, N. (2007). Photodegradation of Natural Organic Matter in Water with UV Irradiation at 185 and 254 nm: Importance of Hydrodynamic Conditions on the Decomposition Rate. *Separation Science and Technology, 42*(7), 1421-1432.

Dotson, A., Westerhoff, P., & Krasner, S. W. (2009). Nitrogen enriched dissolved organic matter (DOM) isolates and their affinity to form emerging disinfection by-products. *Water Science and Technology, 60*(1), 135-143.

Dotson, A. D., Keen, V. S., Metz, D., & Linden, K. G. (2010). UV/H_2O_2 treatment of drinking water increases post-chlorination DBP formation. *Water Research, 44*(12), 3703-3713.

Fang, J.-Y., Ling, L., & Shang, C. (2013). Kinetics and mechanisms of pH-dependent degradation of halonitromethanes by UV photolysis. *Water Research, 47*(3), 1257-1266.

Fang, J., Ma, J., Yang, X., & Shang, C. (2010). Formation of carbonaceous and nitrogenous disinfection by-products from the chlorination of Microcystis aeruginosa. *Water Research, 44*(6), 1934-1940.

Gonzalez, M. G., Oliveros, E., Wörner, M., & Braun, A. M. (2004). Vacuum-ultraviolet photolysis of aqueous reaction systems. *Journal of Photochemistry and Photobiology C: Photochemistry Reviews, 5*(3), 225-246.

Goslan, E. H., Gurses, F., Banks, J., & Parsons, S. A. (2006). An investigation into reservoir NOM reduction by UV photolysis and advanced oxidation processes. *Chemosphere, 65*(7), 1113-1119.

Grote, B. (2012). *Application of advanced oxidation processes (AOP) in water treatment*. Paper presented at the 37th Annual Qld Water Industry Operations Workshop, Parklands, Gold Coast, Australia.

Guilherme, S., & Rodriguez, M. J. (2014). Occurrence of regulated and non-regulated disinfection by-products in small drinking water systems. *Chemosphere, 117*, 425-432.

Han, Y., Chen, Z.-L., Tong, L.-N., Yang, L., Shen, J.-M., Wang, B.-Y., . . . Chen, Q. (2013). Reduction of N-Nitrosodimethylamine with zero-valent zinc. *Water Research, 47*(1), 216-224.

Hansen, K. M. S., Zortea, R., Piketty, A., Vega, S. R., & Andersen, H. R. (2013). Photolytic removal of DBPs by medium pressure UV in swimming pool water. *Science of The Total Environment, 443*, 850-856.

Hou, S., Ling, L., Shang, C., Guan, Y., & Fang, J. (2017). Degradation kinetics and pathways of haloacetonitriles by the UV/persulfate process. *Chemical Engineering Journal, 320*, 478-484.

Huang, H., Wu, Q.-Y., Hu, H.-Y., & Mitch, W. A. (2012). Dichloroacetonitrile and Dichloroacetamide Can Form Independently during Chlorination and Chloramination of Drinking Waters, Model Organic Matters, and Wastewater Effluents. *Environmental Science & Technology, 46*(19), 10624-10631.

Huang, H., Wu, Q.-Y., Tang, X., Jiang, R., & Hu, H.-Y. (2016). Formation of haloacetonitriles and haloacetamides and their precursors during chlorination of secondary effluents. *Chemosphere, 144*, 297-303.

Huang, H., Wu, Q. Y., Hu, H. Y., & Mitch, W. A. (2012). Dichloroacetonitrile and dichloroacetamide can form independently during chlorination and chloramination of drinking waters, model organic matters, and wastewater effluents. *Environmental Science and Technology, 46*(19), 10624-10631. doi:10.1021/es3025808

Huo, S., Xi, B., Yu, H., Qin, Y., Zan, F., & Zhang, J. (2013). Characteristics and transformations of dissolved organic nitrogen in municipal biological nitrogen

removal wastewater treatment plants. *Environmental Research Letters, 8*(4), 1-9.

Imoberdorf, G., & Mohseni, M. (2011). Experimental study of the degradation of 2,4-D induced by vacuum-UV radiation. *Water Science and Technology, 63*(7), 1427-1433.

Imoberdorf, G., & Mohseni, M. (2012). Kinetic study and modeling of the vacuum-UV photoinduced degradation of 2,4-D. *Chemical Engineering Journal, 187*, 114-122.

Imoberdorf, G., & Mohseni, M. (2014). Comparative study of the effect of vacuum-ultraviolet irradiation on natural organic matter of different sources. *Journal of Environmental Engineering, 140*(3), 1-9.

Jia, A., Wu, C., & Duan, Y. (2016). Precursors and factors affecting formation of haloacetonitriles and chloropicrin during chlor(am)ination of nitrogenous organic compounds in drinking water. *Journal of Hazardous Materials, 308*, 411-418.

Jo, C. H., Dietrich, A. M., & Tanko, J. M. (2011). Simultaneous degradation of disinfection byproducts and earthy-musty odorants by the UV/H_2O_2 advanced oxidation process. *Water Research, 45*(8), 2507-2516.

Jones, M. N. (1984). Nitrate reduction by shaking with cadmium. *Water Research, 18*(5), 643-646.

Keen, O. S., Love, N. G., & Linden, K. G. (2012). The role of effluent nitrate in trace organic chemical oxidation during UV disinfection. *Water Research, 46*(16), 5224-5234.

Kiattisaksiri, P., Khan, E., Punyapalakul, P., & Ratpukdi, T. (2016). Photodegradation of haloacetonitriles in water by vacuum ultraviolet irradiation: Mechanisms and intermediate formation. *Water Research, 98*, 160-167.

Kim, J., Chung, Y., Shin, D., Kim, M., Lee, Y., Lim, Y., & Lee, D. (2003). Chlorination by-products in surface water treatment process. *Desalination, 151*(1), 1-9.

Krasner, S. W., Mitch, W. A., Westerhoff, P., & Dotson, A. (2012). Formation and control of emerging C- and N-DBPs in drinking water. *Journal - American Water Works Association, 104*(11), E582-E595.

Krasner, S. W., Weinberg, H. S., Richardson, S. D., Pastor, S. J., Chinn, R., Sclimenti, M. J., . . . Thruston, A. D. (2006). Occurrence of a New Generation of Disinfection Byproducts. *Environmental Science & Technology, 40*(23), 7175-7185.

Kutschera, K., Börnick, H., & Worch, E. (2009). Photoinitiated oxidation of geosmin and 2-methylisoborneol by irradiation with 254nm and 185nm UV light. *Water Research, 43*(8), 2224-2232.

Lamsal, R., Walsh, M. E., & Gagnon, G. A. (2011). Comparison of advanced oxidation processes for the removal of natural organic matter. *Water Research, 45*(10), 3263-3269.

Lee, W., & Westerhoff, P. (2005). Dissolved Organic Nitrogen Measurement Using Dialysis Pretreatment. *Environmental Science & Technology, 39*(3), 879-884.

Lee, W., Westerhoff, P., & Croué, J.-P. (2007). Dissolved Organic Nitrogen as a Precursor for Chloroform, Dichloroacetonitrile, N-Nitrosodimethylamine, and Trichloronitromethane. *Environmental Science & Technology, 41*(15), 5485-5490.

Li, M., Qiang, Z., Hou, P., Bolton, J. R., Qu, J., Li, P., & Wang, C. (2016). VUV/UV/Chlorine as an Enhanced Advanced Oxidation Process for Organic Pollutant Removal from Water: Assessment with a Novel Mini-Fluidic VUV/UV Photoreaction System (MVPS). *Environmental Science & Technology, 50*(11), 5849-5856.

Li, M., Wang, C., Yau, M., Bolton, J. R., & Qiang, Z. (2017). Sulfamethazine degradation in water by the VUV/UV process: Kinetics, mechanism and antibacterial activity determination based on a mini-fluidic VUV/UV photoreaction system. *Water Research, 108*, 348-355.

Liao, Y., Brame, J., Que, W., Xiu, Z., Xie, H., Li, Q., . . . Alvarez, P. J. (2013). Photocatalytic generation of multiple ROS types using low-temperature crystallized anodic TiO2 nanotube arrays. *Journal of Hazardous Materials, 260*, 434-441.

Ling, L., Sun, J., Fang, J., & Shang, C. (2016). Kinetics and mechanisms of degradation of chloroacetonitriles by the UV/H$_2$O$_2$ process. *Water Research, 99*, 209-215.

Liu, H., Jeong, J., Gray, H., Smith, S., & Sedlak, D. L. (2012). Algal Uptake of Hydrophobic and Hydrophilic Dissolved Organic Nitrogen in Effluent from Biological Nutrient Removal Municipal Wastewater Treatment Systems. *Environmental Science & Technology, 46*(2), 713-721.

Liu, J.-L., & Li, X.-Y. (2015). Removal of soluble microbial products as the precursors of disinfection by-products in drinking water supplies. *Environmental Technology, 36*(6), 722-731.

Mezyk, S. P., Helgeson, T., Cole, S. K., Cooper, W. J., Fox, R. V., Gardinali, P. R., & Mincher, B. J. (2006). Free Radical Chemistry of Disinfection-Byproducts. 1. Kinetics of Hydrated Electron and Hydroxyl Radical Reactions with Halonitromethanes in Water. *The Journal of Physical Chemistry A, 110*(6), 2176-2180.

Molnar, J. J., Agbaba, J. R., Dalmacija, B. D., Klašnja, M. T., Dalmacija, M. B., & Kragulj, M. M. (2012). A comparative study of the effects of ozonation and TiO2-catalyzed ozonation on the selected chlorine disinfection by-product precursor content and structure. *Science of The Total Environment, 425*, 169-175.

Moussavi, G., Hossaini, H., Jafari, S. J., & Farokhi, M. (2014). Comparing the efficacy of UVC, UVC/ZnO and VUV processes for oxidation of organophosphate pesticides in water. *Journal of Photochemistry and Photobiology A: Chemistry, 290*(1), 86-93.

Muellner, M. G., Wagner, E. D., McCalla, K., Richardson, S. D., Woo, Y.-T., & Plewa, M. J. (2007). Haloacetonitriles vs. Regulated Haloacetic Acids: Are Nitrogen-Containing DBPs More Toxic? *Environmental Science & Technology, 41*(2), 645-651.

Munter, R. (2001). Advanced oxidation processes-current status and prospects. *Proceedings of the Estonian Academy of Sciences, Chemistry, 50*(2), 59-80.

Oppenländer, T. (2003). *Photochemical Purification of Water and Air*: Wiley-VCH.

Park, B., Shin, D., Cho, E., & Khim, J. (2012). Effect of Ultrasonic Frequency and Power Density for Degradation of Dichloroacetonitrile by Sonolytic Ozonation. *Japanese Journal of Applied Physics, 51*(7S), 1-4.

Parsons, S. (2004). *Advanced Oxidation Processes for Water and Wastewater Treatment*: IWA Publishing.

Pehlivanoglu-Mantas, E., & Sedlak, D. L. (2008). Measurement of dissolved organic nitrogen forms in wastewater effluents: Concentrations, size distribution and NDMA formation potential. *Water Research, 42*(14), 3890-3898.

Pereira, V. J., Weinberg, H. S., Linden, K. G., & Singer, P. C. (2007). UV Degradation Kinetics and Modeling of Pharmaceutical Compounds in Laboratory Grade and Surface Water via Direct and Indirect Photolysis at 254 nm. *Environmental Science & Technology, 41*(5), 1682-1688.

Plewa, M. J., Wagner, E. D., Jazwierska, P., Richardson, S. D., Chen, P. H., & McKague, A. B. (2004). Halonitromethane Drinking Water Disinfection Byproducts: Chemical Characterization and Mammalian Cell Cytotoxicity and Genotoxicity. *Environmental Science & Technology, 38*(1), 62-68.

Prarat, P., Ngamcharussrivichai, C., Khaodhiar, S., & Punyapalakul, P. (2011). Adsorption characteristics of haloacetonitriles on functionalized silica-based porous materials in aqueous solution. *Journal of Hazardous Materials, 192*(3), 1210-1218.

Qi, W., & Jiangyong, H. (2016). NDMA formation potential removal in treated effluent by UV/H_2O_2 process *Journal of Water Reuse and Desalination, 06.1*, 156-166.

Ratpukdi, T., Rice, J. A., Chilom, G., & Khan, E. (2008). Rapid Fractionation of Natural Organic Matter in Water Using a Novel Solid Phase Extraction Technique. *Proceedings of the Water Environment Federation, 2008*(9), 6653-6668.

Ratpukdi, T., Siripattanakul, S., & Khan, E. (2010). Mineralization and biodegradability enhancement of natural organic matter by ozone–VUV in comparison with ozone, VUV, ozone–UV, and UV: Effects of pH and ozone dose. *Water Research, 44*(11), 3531-3543.

Reckhow, D. A., MacNeill, A. L., Platt, T. L., MacNeill, A. L., & McClellan, J. N. (2001). Formation and degradation of dichloroacetonitrile in drinking waters. *Journal of Water Supply: Research and Technology - Aqua, 50*(1), 1-13.

Richardson, S. D. (2003). Disinfection by-products and other emerging contaminants in drinking water. *TrAC Trends in Analytical Chemistry, 22*(10), 666-684.

Sadiq, R., & Rodriguez, M. J. (2004). Disinfection by-products (DBPs) in drinking water and predictive models for their occurrence: a review. *Science of The Total Environment, 321*(1), 21-46.

Sarathy, S., & Mohseni, M. (2007). The impact of UV/H_2O_2 advanced oxidation on molecular size distribution of chromophoric natural organic matter. *Environmental Science and Technology, 41*(24), 8315-8320.

Sarathy, S., & Mohseni, M. (2010). Effects of UV/H_2O_2 advanced oxidation on chemical characteristics and chlorine reactivity of surface water natural organic matter. *Water Research, 44*(14), 4087-4096.

Sharpless, C. M., & Linden, K. G. (2003). Experimental and Model Comparisons of Low- and Medium-Pressure Hg Lamps for the Direct and H_2O_2 Assisted UV Photodegradation of N-Nitrosodimethylamine in Simulated Drinking Water. *Environmental Science & Technology, 37*(9), 1933-1940.

Shin, D., Jang, M., Cui, M., Na, S., & Khim, J. (2013). Enhanced removal of dichloroacetonitrile from drinking water by the combination of solar-photocatalysis and ozonation. *Chemosphere, 93*(11), 2901-2908.

Simsek, H., Kasi, M., Ohm, J. B., Blonigen, M., & Khan, E. (2013). Bioavailable and biodegradable dissolved organic nitrogen in activated sludge and trickling filter wastewater treatment plants. *Water Research, 47*(9), 3201-3210.

Stuart W. Krasner, R. C., Yingbo C. Guo, Cordelia J. Hwang, Salvador J. Pastor, Michael J. Sclimenti, Paul Westerhoff, Baiyang Chen, Zaid K. Chowdhury, Shahnawaz Sinha, Bruce E. Rittmann. (2005, 6/12/05 - 6/16/05). *Contribution of wastewater to DBP formation.* Paper presented at the AWWA 124th Annual Conference and Exposition: The World's Water Event, ACE 2005, San Francisco, CA, United States.

Szabó, R. K., Megyeri, C., Illés, E., Gajda-Schrantz, K., Mazellier, P., & Dombi, A. (2011). Phototransformation of ibuprofen and ketoprofen in aqueous solutions. *Chemosphere, 84*(11), 1658-1663.

U.S.EPA. (1995). Method 551.1 Determination of chlorination disinfection by-products, chlorinated solvents, and halogenated pesticides/herbicides in drinking water by liquid–liquid extraction and gas chromatograph with

electron-capture detection (Revision 1.0). Cincinnati, Ohio, USA: United States Environmental Protection Agency.

Wang, D., Bolton, J. R., Andrews, S. A., & Hofmann, R. (2015). UV/chlorine control of drinking water taste and odour at pilot and full-scale. *Chemosphere, 136*, 239-244.

Wang, G. S., Liao, C. H., Chen, H. W., & Yang, H. C. (2006). Characteristics of Natural Organic Matter Degradation in Water by UV/H$_2$O$_2$ Treatment. *Environmental Technology, 27*(3), 277-287.

Webster, T. S., Condee, C., & Hatzinger, P. B. (2013). Ex situ treatment of N-nitrosodimethylamine (NDMA) in groundwater using a fluidized bed reactor. *Water Research, 47*(2), 811-820.

Weng, S., Li, J., & Blatchley, E. R. (2012). Effects of UV254 irradiation on residual chlorine and DBPs in chlorination of model organic-N precursors in swimming pools. *Water Research, 46*(8), 2674-2682.

Westerhoff, P., & Mash, H. (2002). Dissolved organic nitrogen in drinking water supplies: a review. *Journal of Water Supply: Research and Technology - Aqua, 51*(8), 415.

WHO. (2011). Guidelines for Drinking-water Quality, fourth ed. Geneva, Switzerland: World Health Organization.

Xiao, Y., Fan, R., Zhang, L., Yue, J., Webster, R. D., & Lim, T.-T. (2014). Photodegradation of iodinated trihalomethanes in aqueous solution by UV 254 irradiation. *Water Research, 49*, 275-285.

Xiao, Y., Zhang, L., Yue, J., Webster, R. D., & Lim, T.-T. (2015). Kinetic modeling and energy efficiency of UV/H$_2$O$_2$ treatment of iodinated trihalomethanes. *Water Research, 75*, 259-269.

Xie, Y. (2004). *Disinfection byproducts in drinking water: formation, analysis, and control*. Boca Raton, Florida: Lewis Publishers.

Xu, B., Chen, Z., Qi, F., & Yang, L. (2008). Photodegradation of N-nitrosodiethylamine in water with UV irradiation. *Chinese Science Bulletin, 53*(21), 3395-3401.

Xu, B., Ye, T., Li, D.-P., Hu, C.-Y., Lin, Y.-L., Xia, S.-J., . . . Gao, N.-Y. (2011). Measurement of dissolved organic nitrogen in a drinking water treatment plant:

Size fraction, fate, and relation to water quality parameters. *Science of The Total Environment, 409*(6), 1116-1122.

Xu, B., Zhu, H.-Z., Lin, Y.-L., Shen, K.-Y., Chu, W.-H., Hu, C.-Y., . . . Bi, X.-Y. (2012). Formation of Volatile Halogenated By-Products During the Chlorination of Oxytetracycline. *Water, Air, & Soil Pollution, 223*(7), 4429-4436.

Yang, X., Fan, C., Shang, C., & Zhao, Q. (2010). Nitrogenous disinfection byproducts formation and nitrogen origin exploration during chloramination of nitrogenous organic compounds. *Water Research, 44*(9), 2691-2702.

Yang, X., Guo, W., & Shen, Q. (2011). Formation of disinfection byproducts from chlor(am)ination of algal organic matter. *Journal of Hazardous Materials, 197*, 378-388.

Yang, X., Shang, C., & Westerhoff, P. (2007). Factors affecting formation of haloacetonitriles, haloketones, chloropicrin and cyanogen halides during chloramination. *Water Research, 41*(6), 1193-1200.

Yang, X., Shen, Q., Guo, W., Peng, J., & Liang, Y. (2012). Precursors and nitrogen origins of trichloronitromethane and dichloroacetonitrile during chlorination/chloramination. *Chemosphere, 88*(1), 25-32.

Yao, H., Pei, J., Wang, H., & Fu, J. (2017). Effect of Fe(II/III) on tetracycline degradation under UV/VUV irradiation. *Chemical Engineering Journal, 308*, 193-201.

Yimeng, Z., Wenhai, C., Ting, X., Daqiang, Y., Bin, X., Pan, L., & Na, A. (2017). Impact of pre-oxidation using H_2O_2 and ultraviolet/H_2O_2 on disinfection byproducts generated from chlor(am)ination of chloramphenicol. *Chemical Engineering Journal, 317*, 112-118.

Yuval, A., Eran, F., Janin, W., Oliver, O., & Yael, D. (2017). Photodegradation of micropollutants using V-UV/UV-C processes; Triclosan as a model compound. *Science of The Total Environment, 601*, 397-404.

Zhou, C., Gao, N., Deng, Y., Chu, W., Rong, W., & Zhou, S. (2012). Factors affecting ultraviolet irradiation/hydrogen peroxide (UV/H_2O_2) degradation of mixed N-nitrosamines in water. *Journal of Hazardous Materials, 231*, 43-48.

Zoschke, K., Börnick, H., & Worch, E. (2014). Vacuum-UV radiation at 185 nm in water treatment – A review. *Water Research, 52*, 131-145.

APPENDIX A. ANALYTICAL METHODS

Appendix A contains 8 texts, 10 figures, and 5 tables (lists as below).

Text A.1.   HANs extraction method

The concentrations of HANs were analyzed after a liquid-liquid extraction (LLE) which modified from U.S. EPA method 551.1 (U.S.EPA., 1995) by adjusting the amount of sodium sulfate anhydrous crystal (Na_2SO_4, Carlo Erba, France) and methyl-t-butyl ether (MTBE, HPLC grade, RCI Labscan, Thailand)). Twenty-five milliliters of the sample were put in a 40 mL clear glass vial with polypropylene screw cap and Telfon®faced septum. Five grams of Na_2SO_4 were added to increase the ionic strength of the aqueous matrix. Na_2SO_4 was calcined at 400ºC in muffle furnace for 30 min before use. Then, 2.5 mL of MTBE were added as an extraction solvent. After that, the vial was sealed, vigorously shaken for 2 min, and left idle for 4 min. The MTBE layer was transferred into a 2 mL amber vial. The sample extract was stored in a freezer (<-10°C) until analysis within 7 days. The HANs extraction process is shown in Figure A.1.

Text A.2.   GC-ECD conditions for HANs analysis in Chapter 4

For HANs analysis, 1 µL of the extraction solvent (MTBE) was injected into a gas chromatography-electron capture detector (GC-ECD, Agilent 4890D, USA). The column used in this part was a SPB^{TM}-608 fused silica capillary column (15 m × 0.53 mm I.D. × 0.5µm film thickness, Supelco, USA). Helium (He) was a carrier gas and nitrogen (N_2) was a make-up gas. The flow rate of He gas was approximately 8.6 ml min^{-1}. Total flow rate (He + N_2 gas) was approximately 48 ml min^{-1}. The temperature of injector and detector was set at 150°C and 250°C, respectively. The temperature program was set at 40°C for 2.5 min, and then ramped up to 240°C for 1 min at a rate of 40°C min^{-1}. The retention times for MCAN, DCAN, TCAN and DBAN were 1.8, 2.0, 1.2, and 4.5 min, respectively. The detection limits of MCAN, DCAN, TCAN, and DBAN were 0.25, 0.1, 0.5, and 0.1 µg L^{-1}, respectively. Summary of GC-ECD conditions are presented in Table A.1.

Text A.3.   GC-ECD conditions for HANs analysis in Chapter 5

For this part, an HP-5 fused silica capillary column (30 m $\times$ 0.25 mm I.D. $\times$ 0.25 µm film thickness, Agilent, USA) was used as GC-ECD (Agilent 4890D, USA) column. The column head pressure was 2 psi. Carrier gas flow rate (He gas) and total gas flow rate (He + N_2 gas) were 1.3 ml min^{-1}, and 40 ml min^{-1}, respectively. The injection and detector temperature were set at 200 and 270°C, respectively. The GC temperature program consisted of an initial temperature of 35°C for 5 min, then ramped to 240°C at 40°C min^{-1} and held for 1 min. The detection limit of MCAN was 0.1 µg L^{-1} while other HANs species was 0.05 µg L^{-1}. Summary of GC-ECD conditions are presented in Table A.1.

Text A.4.   GC/MS conditions for analysis of HANs intermediates in Chapter 4

The degradation intermediates of HANs were identified by a GC/Mass spectrometer (GC/MS, Agilent 7890B, USA). The GC/MS column used was HP-5ms silica capillary column (30 m$\times$0.25 mm$\times$0.25 µm, Agilent J&W, USA). The column head pressure was 15 psi. The flow rate of carrier gas (He) was approximately 1.5 mL min^{-1}. Total flow rate was approximately 40 mL min^{-1}. The injection volume was 1.5 µL in a split mode at the split ratio of 10:1. The temperature of injector was 150°C. An oven isothermal program was held at 35°C for 6 min, then ramped up to 100°C for 5 min (10°C min^{-1}), and finally ramped up to 200°C for 4 min (10°C min^{-1}). The temperature of the transfer line was 200°C. The mass spectrometer was performed in a full scan mode and collected data from m/z 35-300 amu with 1.9 min of solvent delay. Electron impact ionization was 70 eV and an ion source temperature was 230°C.

Text A.5.   Determination of H$_2$O$_2$ concentration by titanium oxalate method

Titanium oxalate method was found to be unaffected by organic matter and/or chloramine in water. This method is recommended for the determination of H$_2$O$_2$ in water samples treated by AOPs. The concept of the method is the reaction of H$_2$O$_2$ with titanium to form colored peroxotitanium complex (yellowish-orange) in the presence of sulfuric acid. The concentration of H$_2$O$_2$ can be measured by spectrophotometer at 390 nm (Brandhuber & Korshin, 2009). The H$_2$O$_2$ stock solution must be standardized to determine the actual concentration of H$_2$O$_2$ before use (Figure A.2). The weight concentration of H$_2$O$_2$ can be calculated from an Equation (A.1).The steps of H$_2$O$_2$ analysis by titanium oxalate method are shown in Figure A.3. Details of reagents used is described in Table A.2.

$$H_2O_2 \ (mg \ L^{-1}) \quad = \quad T \times N \times 1700 \ \mu g \ mL^{-1} \tag{A.1}$$

Where,   T =   Volume of KMnO$_4$ titrant (mL)

N =   Concentration of KMnO$_4$ (0.1 N)

Text A.6.   Determination of ammonia-nitrogen (NH$_3$-N) by phenate method

Phenate method (4500-NH$_3$ F. Phenate Method) was used for determining the concentration of NH$_3$-N in water sample (APHA, 2012). The principle of the method is the reaction of ammonia, hypochlorite, and phenol catalyzed by sodium nitroprusside to form an intensely blue compound or indophenol, which measured at 640 nm by spectrophotometer (a light path of 1 cm). The color is stable for 24 hr. Details for the method are presented in Table A.3 and Figure A.4, respectively.

Text A.7.   Determination of nitrite (NO$_2$-N) by colorimetric method

The 4500-NO$_2$- B. colorimetric method was modified to determine the concentration of NO$_2$-N in water sample (APHA, 2012). The principle of the method is the formation of a red/pink azo dye produced at pH 2.0 to 2.5 by diazotized sulfanilamide coupled with N-(l-naphthyl)-ethylenediamine dihydrochloride (NED dihydrochloride). The sample was measured at 640 nm. Details of this method are presented in Table A.4 and Figure A.5, respectively.

Text A.8.   Determination of nitrate (NO$_3$-N) by spongy cadmium reduction method

Analysis of NO$_3$-N by spongy cadmium reduction method was modified from (Jones, 1984). In this method, NO$_3$-N is reduced almost quantitatively to nitrite (NO$_2$-N) in the presence of cadmium (Cd). After converting NO$_3$-N to NO$_2$-N, the sample was then analyzed by colorimetric method at 540 nm as described in Figure A.5. The reagents preparation and analysis procedures are shown Table A.5 and Figure A.6, respectively.
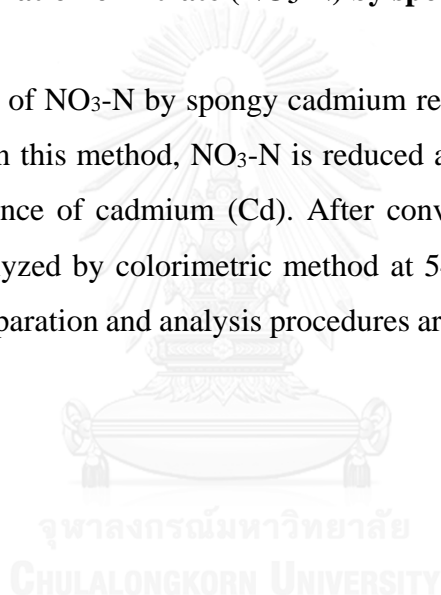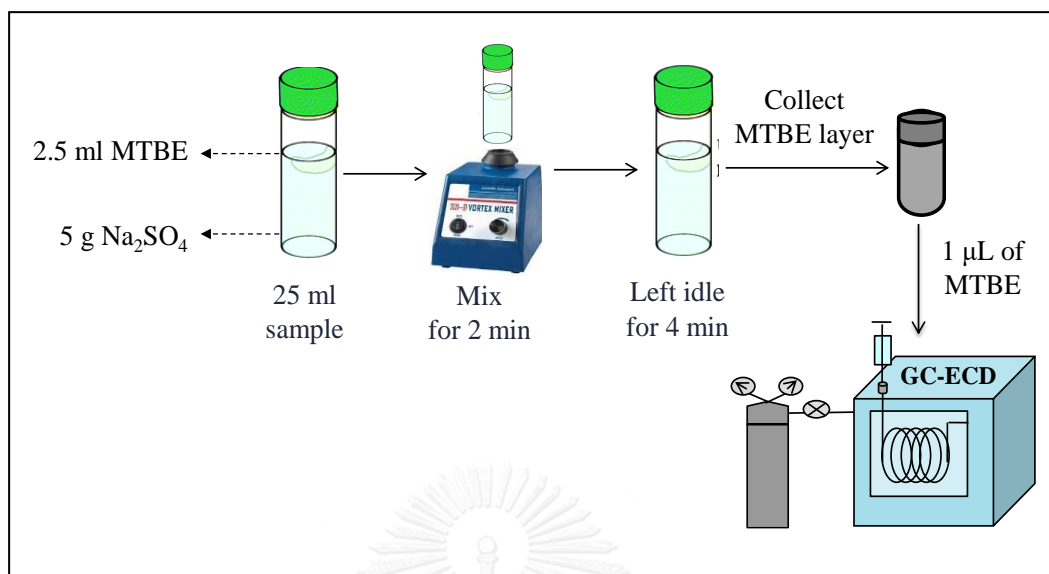
Figure A.1 HANs extraction process

Add 50 ml of DI water into a 250 ml Erlenmeyer flask

Add 10 ml of H_2SO_4 solution A to the flask

Add 10 ml of H_2O_2 stock solution to the flask

Titrate with 0.1 N $KMnO_4$ to the appearance of a faint permanent pinkness

(The pinkness of added $KMnO_4$ will fade in the initial phase of titration, and it appears at the end point)

Calculate the weight concentration of H_2O_2
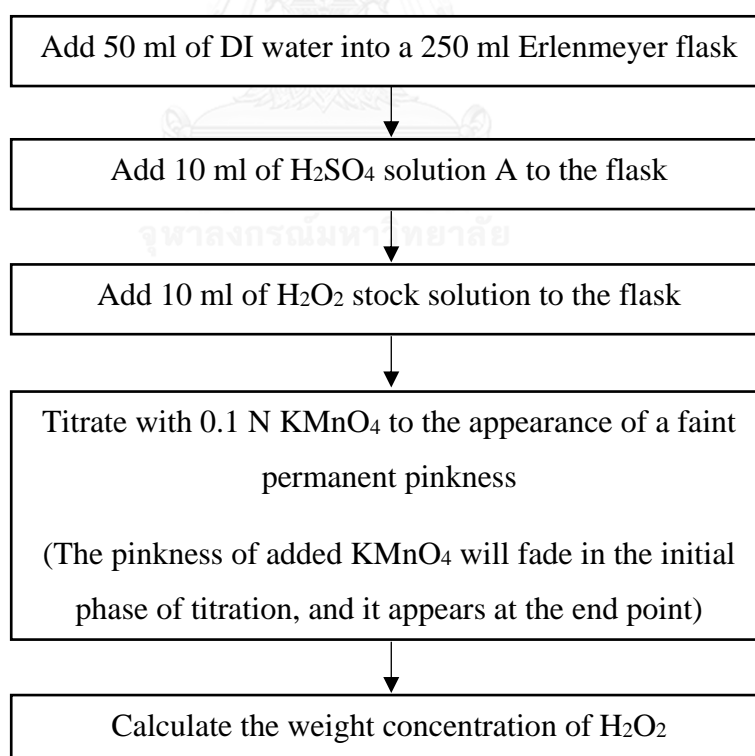
Figure A.2 Standardization of H_2O_2 stock solution

```
┌──────────────────────────────────────────────────────────┐
│     Pipette 10 mL of sample into 25 ml of volumetric flask │
└──────────────────────────────────────────────────────────┘
                             │
                             ▼
┌──────────────────────────────────────────────────────────┐
│              Add 1 mL of sulfuric acid B                   │
└──────────────────────────────────────────────────────────┘
                             │
                             ▼
┌──────────────────────────────────────────────────────────┐
│        Add 1 mL of potassium titanium oxalate solution    │
└──────────────────────────────────────────────────────────┘
                             │
                             ▼
┌──────────────────────────────────────────────────────────┐
│            Adjust volume to 25 mL by DI water              │
└──────────────────────────────────────────────────────────┘
                             │
                             ▼
┌──────────────────────────────────────────────────────────┐
│                        Mix well                            │
└──────────────────────────────────────────────────────────┘
                             │
                             ▼
┌──────────────────────────────────────────────────────────┐
│            Allow color to develop for ~ 5 min              │
└──────────────────────────────────────────────────────────┘
                             │
                             ▼
┌──────────────────────────────────────────────────────────┐
│      Measure the absorbance at 390 nm (1 cm cuvette)       │
└──────────────────────────────────────────────────────────┘
                             │
                             ▼
┌──────────────────────────────────────────────────────────┐
│    Calculate H2O2 concentration from calibration curve     │
└──────────────────────────────────────────────────────────┘
```
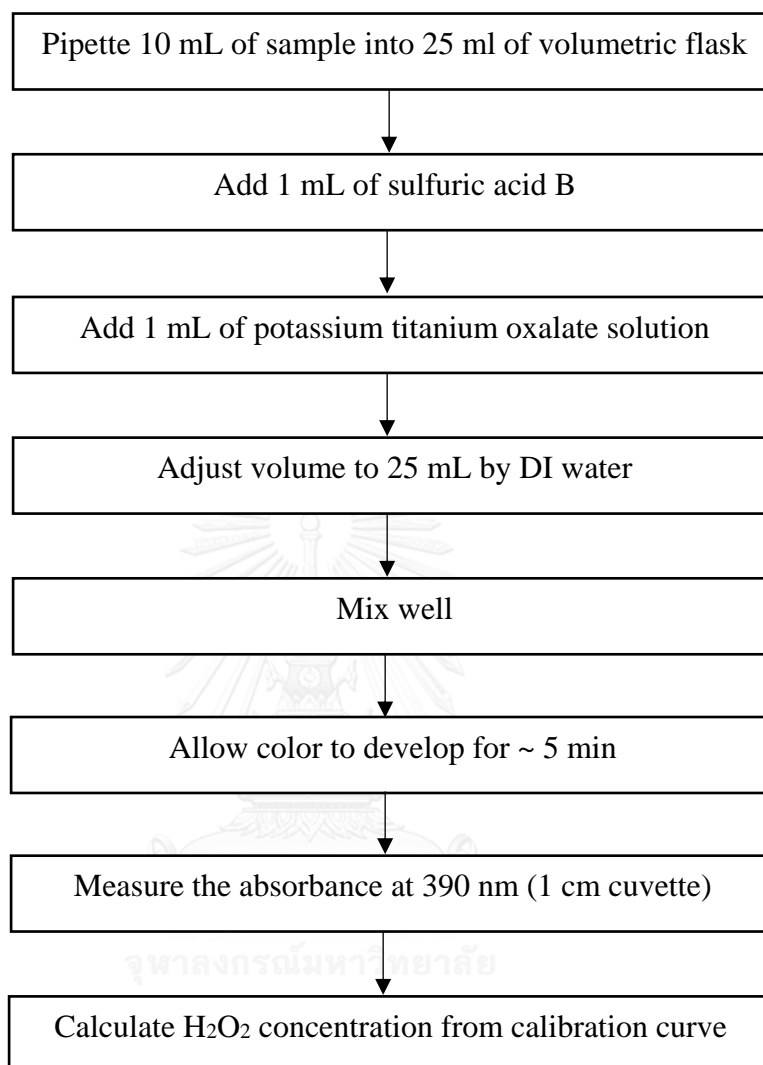
Figure A.3 Determination of H_2O_2 concentration by titanium oxalate method

Add 0.2 ml
Sodium nitrousside
(2)

Add 0.2 ml .... Add 0.5 ml
Phenol solution   Oxidizing solution
(1)   (3)

5 ml
sample

Incubation 1 h (Dark, Room temperature)

Measure the absorbance at 640 nm (1 cm cuvette)

Calculate concentration from calibration curve
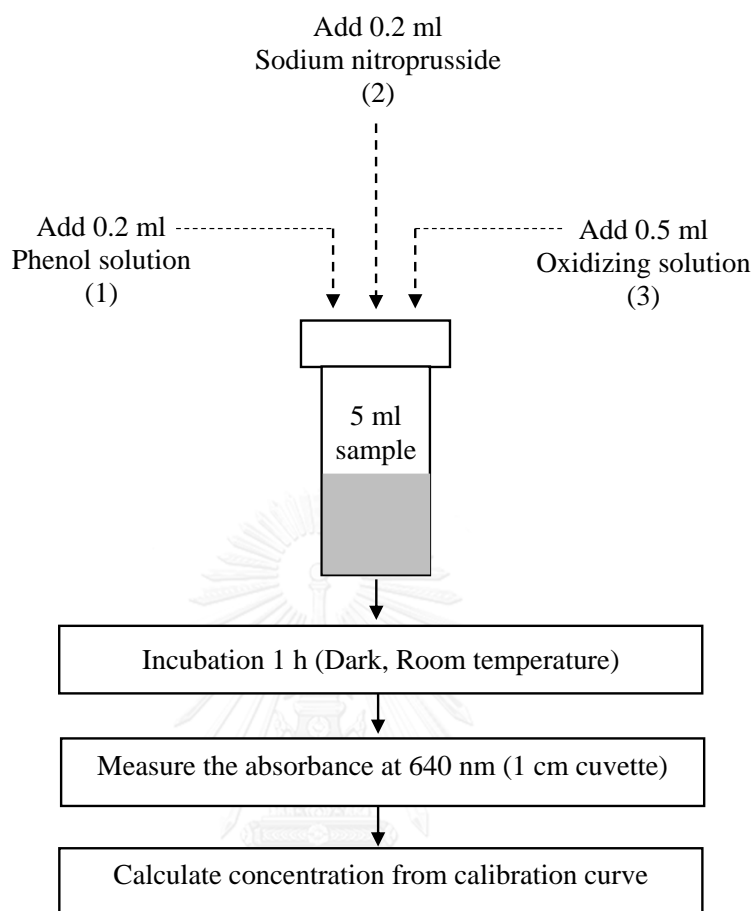
Figure A.4 Determination of NH_3-N by phenate method

Add 0.25 ml color reagent

5 ml
sample

Incubation 10 min (Dark, Room temperature)

Measure the absorbance at 540 nm (1 cm cuvette)

Calculate concentration from calibration curve
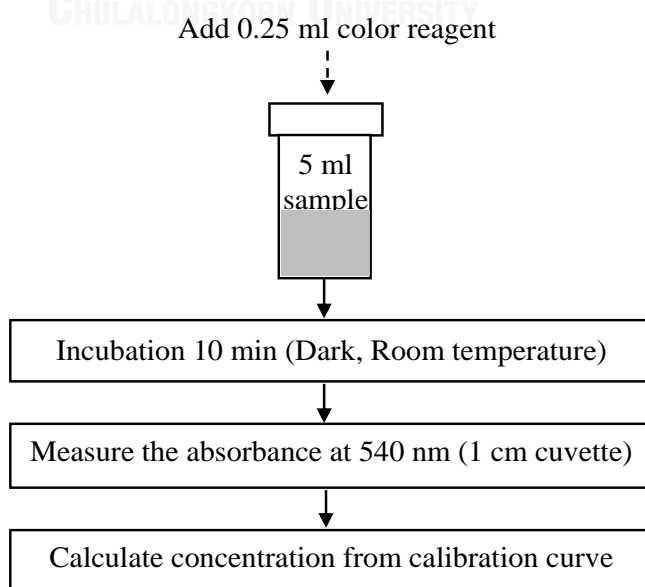
Figure A.5 Determination of NO_2-N by colorimetric method

Add ~ 1 g SpCd ------------- ------------- Add 2 ml NH$_4$Cl solution

10 ml Sample

Centrifuge at 250 rpm, 25°C for 60 min

Pipet 5 ml sample to new vial

Samples filtration with 0.45 µm cellulose acetate syringe filter

Add 0.5 ml color reagent

Incubation 10 min (Dark, Room temperature)

Measure the absorbance at 540 nm (1 cm cuvette)

Calculate concentration from calibration curve
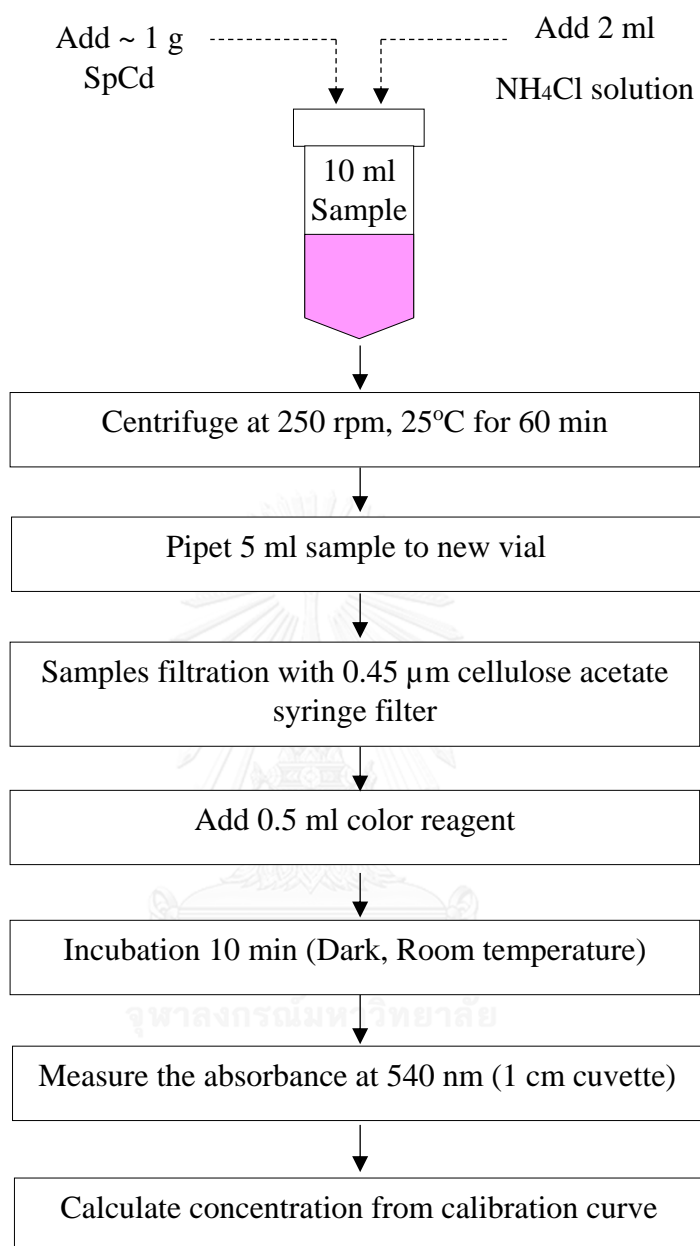
Figure A.6 Determination of NO$_3$-N by spongy cadmium reduction method

H$_2$O$_2$

$y = 0.0119x - 0.0001$

$R^2 = 0.9998$
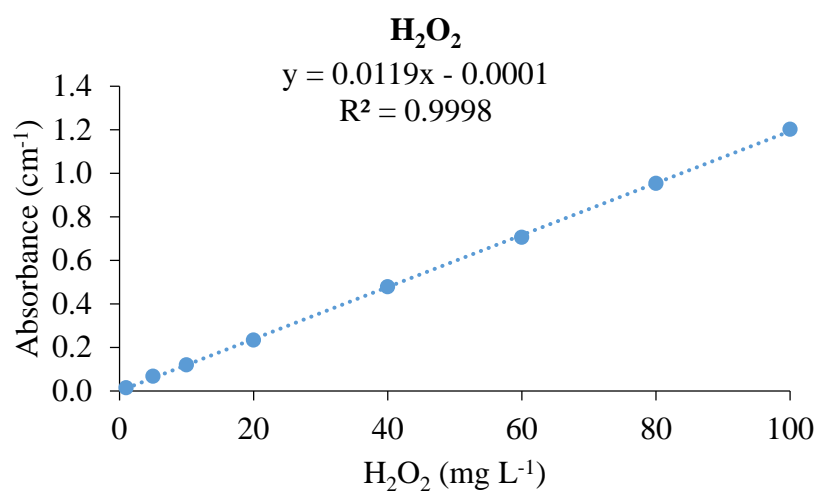
Figure A.7   Calibration curve of H$_2$O$_2$

NH$_3$-N

$y = 1.1837x + 0.002$

$R^2 = 0.9998$
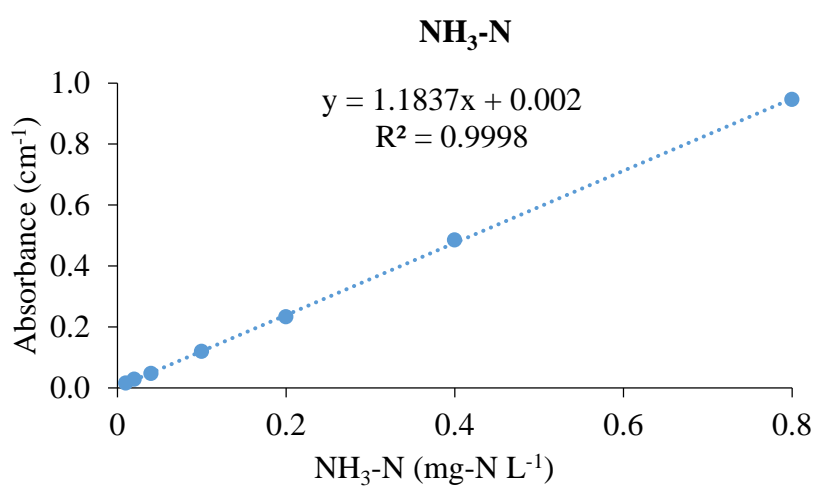
Figure A.8   Calibration curve of NH$_3$-N

NO$_2$-N

$$y = 2.9325x + 0.0008$$
$$R^2 = 0.9995$$

Absorbance (cm^{-1})

NH$_3$-N (mg-N L^{-1})
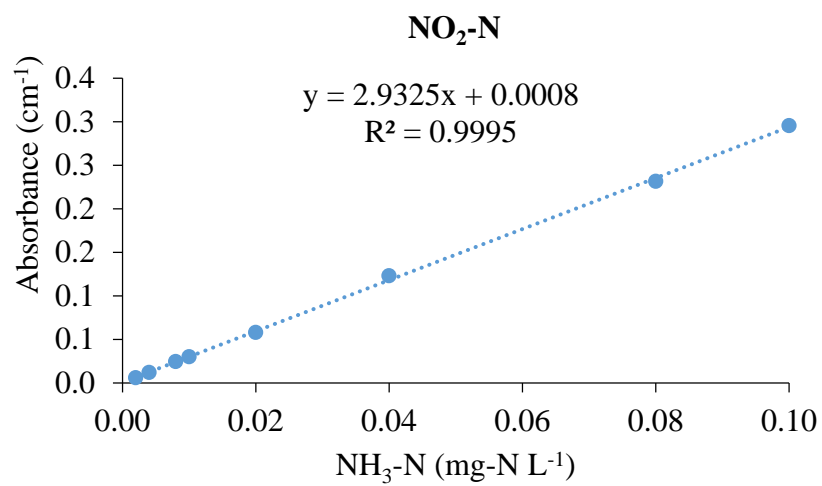
Figure A.9   Calibration curve of NO$_2$-N

NO$_3$-N

$$y = 2.1847x + 0.0062$$
$$R^2 = 0.9998$$

Absorbance (cm^{-1})

NH$_3$-N (mg-N L^{-1})
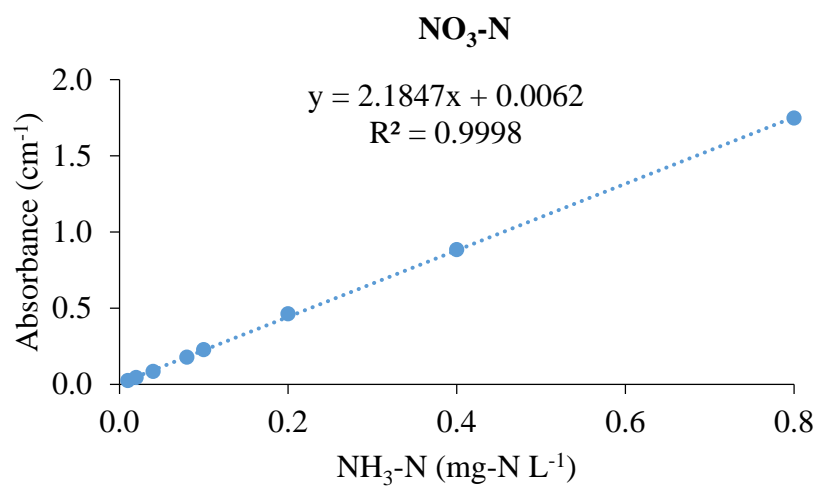
Figure A.10   Calibration curve of NO$_3$-N

Table A.1 GC-ECD (Agilent 4890D) conditions for HANs analysis

Conditions	Type of columns	
	SPB^{TM}-608	HP-5
Column size	15 m length $\times$ 0.53 mm I.D. $\times$ 0.5μm film thickness	30 m length $\times$ 0.25 mm I.D. $\times$ 0.25 μm film thickness
Brand	Supelco, USA	Agilent, USA
Head pressure	2 psi	15 psi
Carrier gas flow rate (He gas)	8.6 ml min^{-1}	1.5 ml min^{-1}
Total gas flow rate (He+ N$_2$ gas)	50 ml min^{-1}	40 ml min^{-1}
Injection mode	Splitless	Splitless
Injector temperature	150°C	200°C
ECD temperature	250°C	270°C
Oven temperature program	40°C, 2.5 min; 40°C min^{-1}; 240°C, 1 min	35°C, 5 min; 40°C min^{-1}; 240°C, 1 min
Retention time of HANs	MCAN: 1.8 min DCAN: 2.0 min TCAN: 1.2 min DBAN: 4.5 min	MCAN: 4.6 min DCAN: 5.5 min TCAN: 4.5 min DBAN: 8.3 min
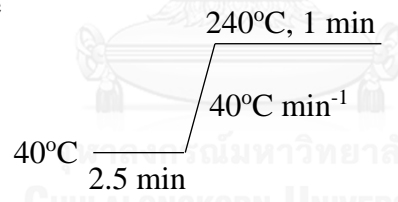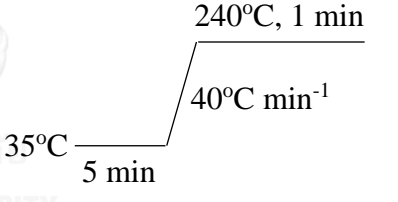
Table A.2 Reagents used for determining H_2O_2 by titanium oxalate method

Reagents	Preparation
Potassium permanganate ($KMnO_4$) solution (0.1N)	- Dissolve 3.2 g of $KMnO_4$ in DI water - Adjust to a final volume of 1000 ml
Potassium titanium oxalate ($K_2TiO(C_2O_4)_2.2H_2O$) solution (50 g/L)	- Dissolve 50 g of $K_2TiO(C_2O_4)_2.2H_2O$ in DI water - Warming slight (by hot plate) - Allow the solution to cool - Adjust to a final volume of 1000 ml
Sulfuric acid (H_2SO_4) solution A (1+9)	- Slowly add 50 ml of concentrated H_2SO_4 to 450 mL DI water in 1 L of beaker - Continuously stir and allow the solution to cool
Sulfuric acid (H_2SO_4) solution B (1+17)	- Slowly add 20 ml of concentrated H_2SO_4 to 340 mL DI water in 1 L of beaker - Continuously stir and allow the solution to cool

Table A.3 Reagents used for determining NH_3-N by phenate method

Reagents	Preparation	Note
1. Phenol solution	Mix 5 ml of liquefied phenol with ethanol to a final volume of 50 ml.	Weekly preparation
2. Sodium nitroprusside solution 0.5% w/v	Dissolve 0.25 g of sodium nitroprusside in 50 ml of DI water.	Monthly preparation
3. Alkaline citrate solution 20% w/v	Dissolve 20 g of trisodium citrate and 1 g of NaOH in 100 ml of DI water	Monthly preparation
4. Oxidizing solution	Mixing 25 ml of alkaline citrate solution with 6.25 ml of sodium hypochlorite (Hyter 5-6%)	Daily preparation

Remark:

- Store solution in amber bottle at 4ºC.
- Commercial sodium hypochlorite solution should be replace every month.

Table A.4 Reagents used for determining NO_2-N by colorimetric method.

Reagent	Preparation	Note
Color reagent	- Dissolve 2.5 g of sulfanilamide and 0.25 g of NED dihydrochloride in 250 ml DI water - Mix the solution well using stirrer - Slowly add 25 ml of phosphoric acid (85%) to the solution - Adjust to final volume of 250 ml by DI water	Monthly preparation/ Store in amber bottle at 4ºC

Table A.5 Reagents used for determining NO_3-N by spongy cadmium reduction method

Reagents	Preparation
1. Ammonium chloride (NH₄Cl) solution (0.7 M)	- Dissolve 18.7 g of NH_4Cl in DI water - Adjust to pH 8.5 by NH_4OH - Make volume to 500 ml DI water
2. Hydrochloric acid (HCl) (6N)	- Mix 248 ml of HCl with DI water - Allow solution to cool.
3. Cadmium sulfate (CdSO₄) solution (20% w/v)	- Dissolve 27.1 g of $CdSO_4.8H_2O$ in DI water - Make volume to 500 ml DI water
4. Spongy cadmium (SpCd)	- Stand zinc metal sticks in 80 ml $CdSO_4$ solution overnight (~ 12 hr) - Remove zinc stick from SpCd using spatula - Acidify the solution with 6N HCl (~5 drops) - Drain the solution from SpCd - Cover SpCd with 6N HCl - Stir to wash and break the SpCd - Drain the solution from SpCd - Rinse SpCd with DI (~ 10 times) until pH >5 - Store SpCd under DI water

Remark:

The spongy cadmium used can be regenerated by washing with 6N HCl for 2 times, followed by rinsing with DI water (~ 10 times) until the pH >5.

APPENDIX B.

SUPPLEMENTARY DATA OF CHAPTER 4

Appendix B contains 1 text, 13 figures, and 2 tables (lists as below).

Text B.1.   Molar absorptivity, quantum yield, and degradation rate constant

Molar absorptivity (ε) measures a probability of HANs that absorb light at the UV wavelength of 254 nm. Based on the Beer-Lambert law, the molar absorptivity ($M^{-1}cm^{-1}$) of HANs in the wavelength range of 200 to 400 nm (Figure B.1) was calculated according to Equation (B.1) (Pereira, Weinberg, Linden, & Singer, 2007).

$$A = \varepsilon \, [\text{HAN}] \, d \tag{B.1}$$

Where,

A is absorbance (cm^{-1}) of each HAN species,

[HAN] is concentration of HAN (molar),

d is absorption cell path length (1 cm).

Quantum yield (Φ) for direct UV photolysis is a ratio of total number of molecules of contaminant transformed to total number of molecules of photon absorbed by contaminant (Parsons, 2004). As the removal of HANs follows the pseudo first order rate law, the quantum yield (mol E^{-1}) of HANs degradation by direct UV photolysis can be calculated using Equation (B.2) (Xiao et al., 2015).

$$\Phi = \frac{k_{obs,HANs}}{2.303 \, I_0 \varepsilon L} \tag{B.2}$$

Where,

$k_{obs,HANs}$ is an observed removal rate of HANs (min^{-1}),

I_0 is a light intensity ($E \, L^{-1} \, s^{-1}$),

L is an effective optical path length of the photoreactor (6.89 cm) which was determined using a H_2O_2 actinometer.

In the VUV system, $k_{obs,HANs}$ involves the reaction of direct photolysis (k_d) by photon absorption and indirect photolysis by $OH^{\bullet}$ (k_i), which can be expressed by Equations (B.3) and (B.4).

$$-\frac{dC}{dt} = (k_{obs})[\text{HANs}] \tag{B.3}$$

$$-\frac{dC}{dt} = (k_d + k_i)[HANs] \qquad (B.4)$$

Where,

k_d is the pseudo-first order rate constant of direct photolysis (min^{-1})

k_i is the pseudo-first order rate constant of $OH^\bullet$-assisted indirect photolysis (min^{-1}).

The indirect photolysis (k_i) can be referred to a function of the second order rate constants of HANs with $OH^\bullet$ ($k_{OH\bullet/HANs}$) and a steady state level of $OH^\bullet$ ($[OH^\bullet]_{ss}$) (Equation (B.6)) (Pereira, Weinberg, Linden, & Singer, 2007; Xiao et al., 2015). Substituting Equation (B.5) into Equation (B.4), the overall degradation rate constant of HANs can be expressed by Equation (A.6).

$$k_i = k_{OH^\bullet,HANs} \times [OH^\bullet]_{ss} \qquad (B.5)$$

$$-\frac{dC}{dt} = \left(k_d + \left(k_{OH^\bullet/HANs} \times [OH^\bullet]_{ss}\right)\right) \times [HANs] \qquad (B.6)$$

To differentiate between direct photolysis and indirect oxidation (by $OH^\bullet$), the VUV experiments were performed with the addition of $OH^\bullet$ scavenger (TBA). The addition of TBA leads to the activity suppression of $OH^\bullet$; therefore, this condition represents the direct photolysis by photon absorption at 185 and 254 nm (k_d). The direct photolytic efficiency from these two wavelengths can be separated by comparing the kinetics rate of HANs degraded by VUV (185+254 nm) and UV lamps (only 254 nm). The indirect photo-oxidation due to $OH^\bullet$ (k_i) can be obtained by subtracting $k_{obs,HANs}$ with k_d.

For comparison the efficiency of direct photolysis of HANs, fluence-based degradation rate constants (k_f) was determined by normalize the time-based degradation rate constant (k_d) with energy of the lamp at a specific wavelength. The k_f value allows for direct comparisons among photodegradation rate constants obtained with different photoreactor, which can be calculated from Equation (B.7) (Xiao et al., 2014).

$$k_f = \frac{k_d}{q_p \cdot \frac{hc}{\lambda}} \tag{B.7}$$

Where,

k_f is the fluence-based degradation rate constant (cm^2 mJ^{-1}),

k_d is the pseudo-first order rate constant of direct photolysis (s^{-1}),

q_p is the photon flux emitted by the lamps (E s^{-1} cm^{-2}),

hc/λ is the photon energy at a specific wavelength (kJ mol^{-1}).

The competition kinetics was employed to determine the second order rate constants between a probe compound of $OH^\bullet$ and single HANs (Pereira, Weinberg, Linden, & Singer, 2007; Xiao et al., 2015). As described above, MB was used as a probe compound at a concentration of 10 µM in this study. Under VUV, HANs can be degraded by direct photolysis as well as indirect photolysis. Thus, the effect of direct photolysis (k_d) cannot be neglected. The second order rate constants of $OH^\bullet$ reacting with HANs ($k_{OH^\bullet/HANs}$) can be obtained from Equation (B.8) (Pereira, Weinberg, Linden, & Singer, 2007; Xiao et al., 2015).

$$k_{OH^\bullet/HANs} = k_{OH^\bullet/MB}\left(\frac{k_{obs,HANs} - k_{d,HANs}}{k_{obs,MB} - k_{d,MB}}\right) \tag{B.8}$$

Where,

$k_{obs,HANs}$ is observed pseudo first order rate constants of HANs (min^{-1}),

$k_{obs,MB}$ is observed pseudo first order rate constants of MB (min^{-1}).

$k_{d,MB}$ is a pseudo first order rate constant of MB removal by direct photolysis (min^{-1}),

$k_{OH^\bullet/MB}$ is a second order rate constant of MB with $OH^\bullet$ (2.1×10^{10} mol^{-1} s^{-1}) (Keen, Love, & Linden, 2012).
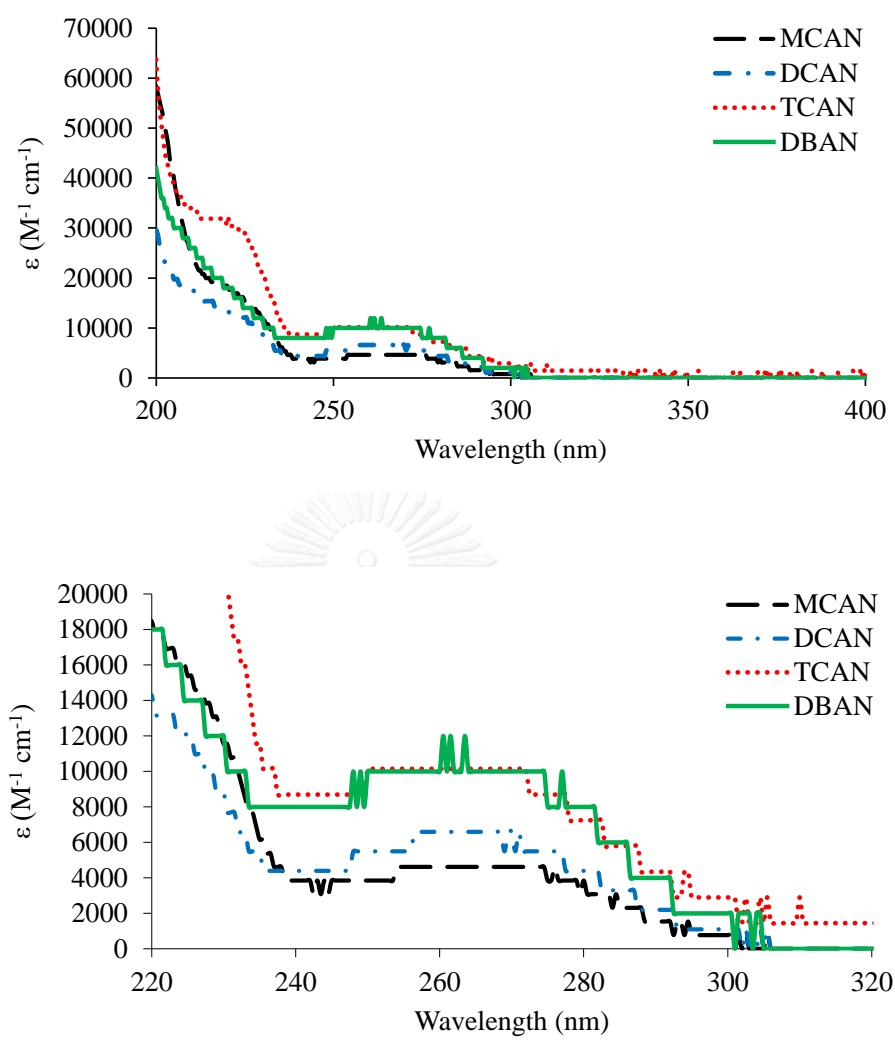
Figure B.1 Molar absorptivity (ε) of HANs at concentrations ranging from 0.5 to 1.3 μM (100 μg L^{-1})

GC/MS spectrum of MCAN intermediate
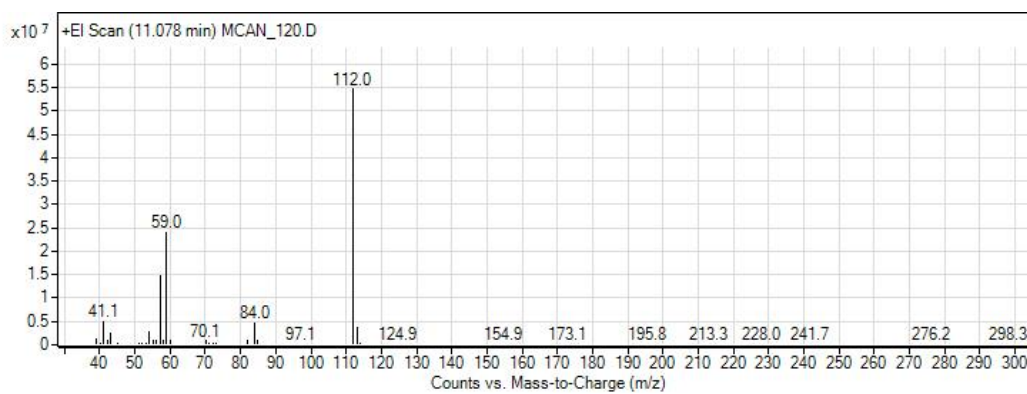
Figure B.2 GC/MS spectrum of MCAN intermediate: 4H-1,2,4-Triazol-3-amine,4-ethyl-
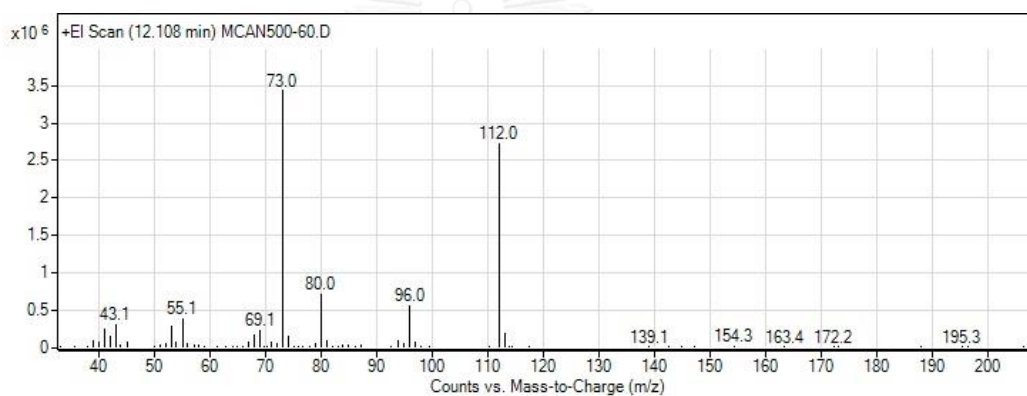
Figure B.3 GC/MS spectrum of MCAN intermediate: 4-Penten-2-one, 3-methyl-, O-methyloxime

GC/MS spectrum of DCAN intermediate
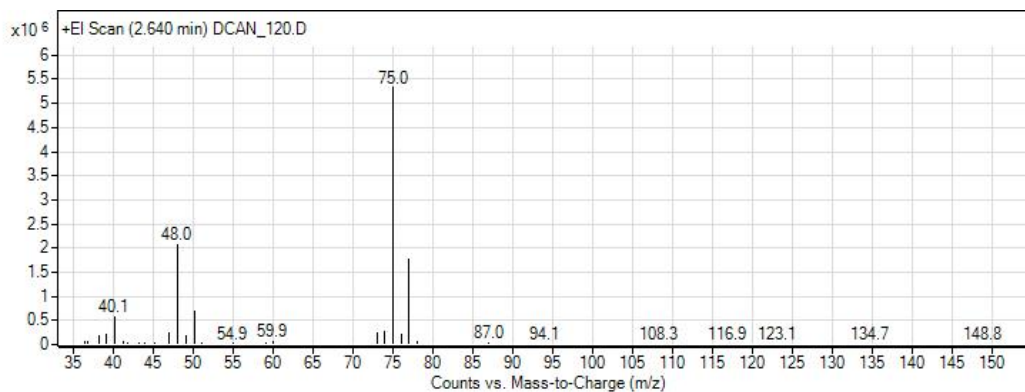
Figure B.4 GC/MS spectrum of DCAN intermediate: Monochloroacetonitrile
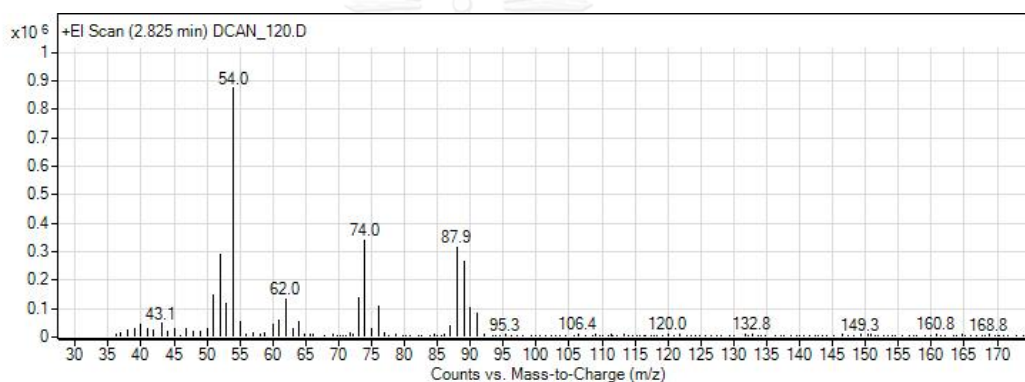
Figure B.5 GC/MS spectrum of DCAN intermediate: 2-Chloropropionitrile
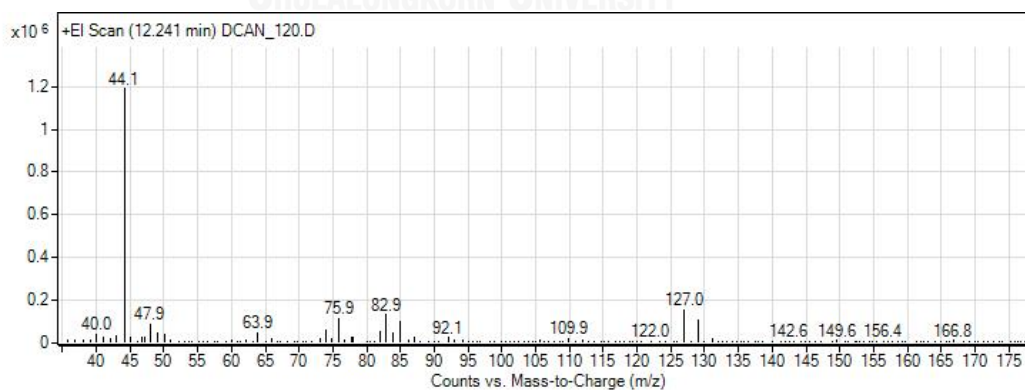
Figure B.6 GC/MS spectrum of DCAN intermediate: Dichloroacetamide

GC/MS spectrum of TCAN intermediate
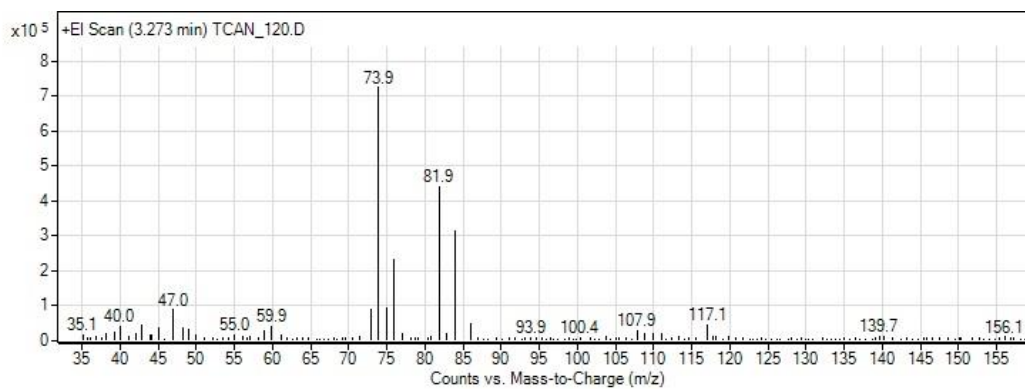
Figure B.7 GC/MS spectrum of TCAN intermediate: Dichloroacetonitrile
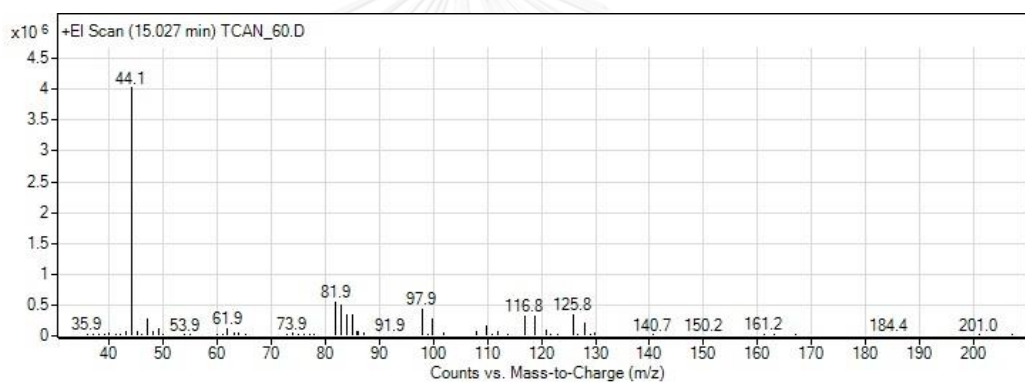
Figure B.8 GC/MS spectrum of TCAN intermediate: 2,2,2-Trichloroacetamide

GC/MS spectrum of DBAN intermediate
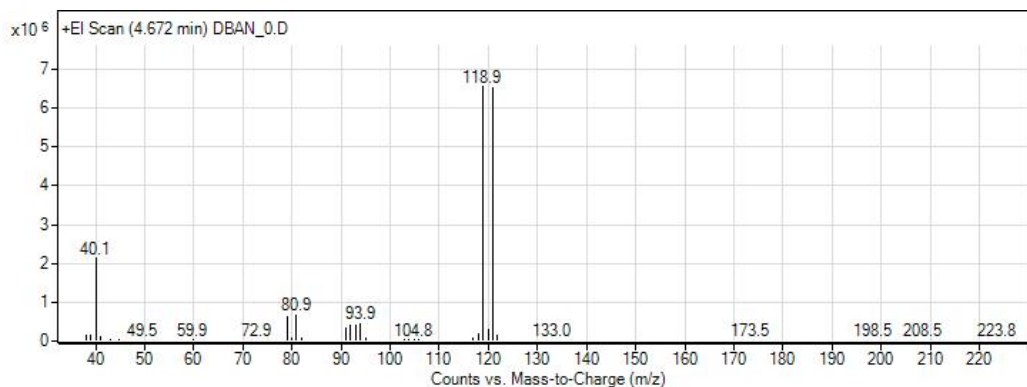
Figure B.9 GC/MS spectrum of DBAN intermediate: Monobromoacetonitrile
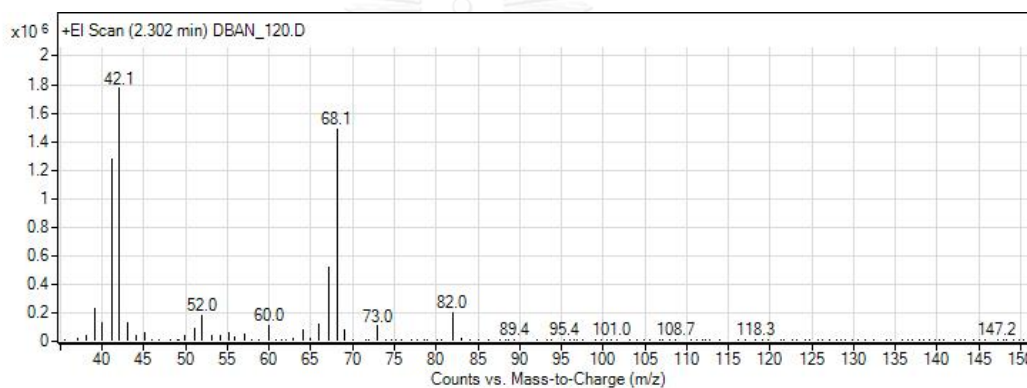
Figure B.10 GC/MS spectrum of DBAN intermediate: 2,2-Dimethylpropanenitrile
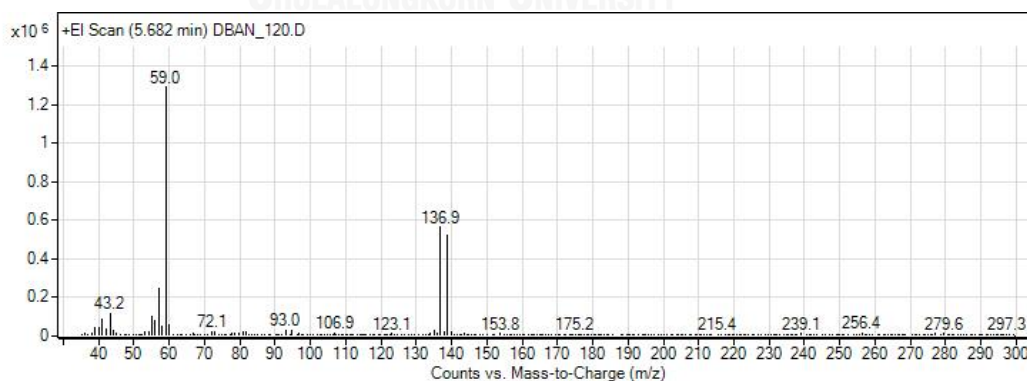
Figure B.11 GC/MS spectrum of DBAN intermediate: 1-Bromo-2-methyl-2-propanol
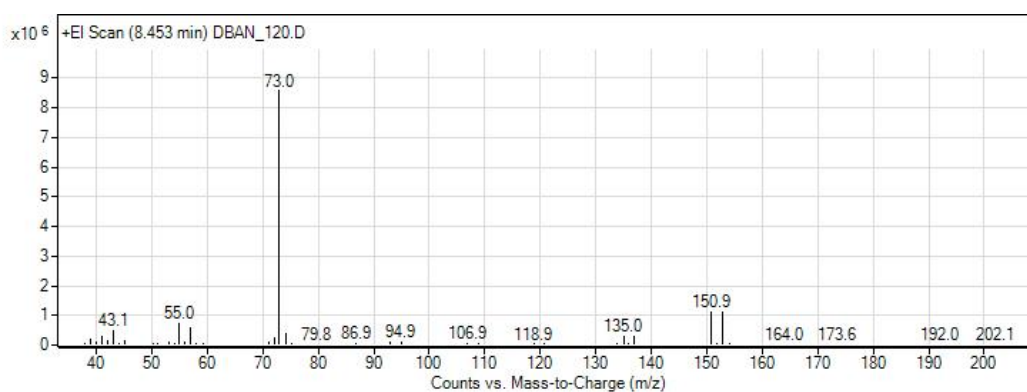
Figure B.12 GC/MS spectrum of DBAN intermediate: 1-Bromo-2-methyl-2-butanol
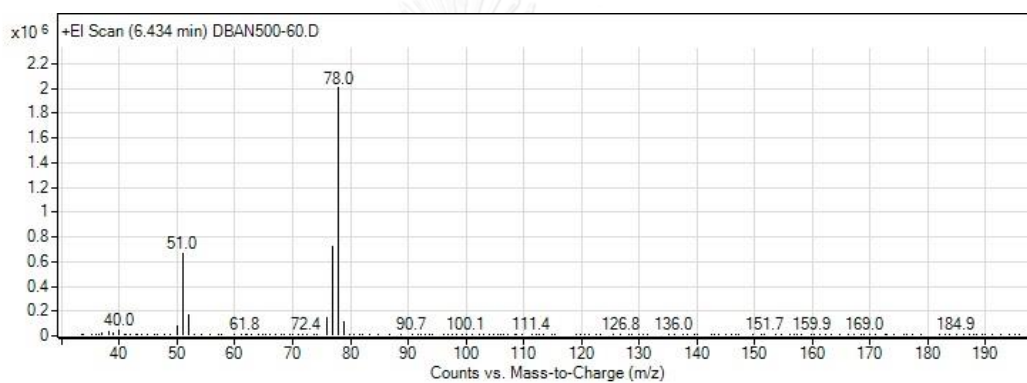
Figure B.13 GC/MS spectrum of DBAN intermediate: Fumaronitrile

Table B.1 Removal efficiency (%) at different reaction time (min) and degradation rate constants of HANs ($k_{obs,HANs}$)

HANs	Solution	Treatment conditions	Removal efficiency (%)				$k_{obs,HANs}$ ($\times 10^{-2}$ min^{-1})	R^2
			10 min	15 min	30 min	120 min		
MCAN	Mixed	UV	7	9	11	20	0.21	0.691
	Mixed	VUV	15	20	36	77	1.25	0.993
	Mixed	VUV+Air	15	19	30	59	0.81	0.942
	Mixed	VUV+N$_2$	94	99	ND	ND	27.84	0.986
	Single	UV	6	7	8	16	0.16	0.681
	Single	VUV	20	24	51	85	1.73	0.967
	Single	VUV+TBA	8	14	24	63	0.82	0.996
DCAN	Mixed	UV	8	12	14	22	0.26	0.592
	Mixed	VUV	20	26	49	88	1.81	0.993
	Mixed	VUV+Air	15	28	32	75	1.22	0.978
	Mixed	VUV+N$_2$	99	ND	ND	ND	42.55	0.969
	Single	UV	8	8	12	19	0.12	0.653
	Single	VUV	33	41	58	92	2.31	0.965
	Single	VUV+TBA	16	26	29	96	2.21	0.927
TCAN	Mixed	UV	19	20	23	45	0.55	0.689
	Mixed	VUV	31	40	66	93	2.51	0.949
	Mixed	VUV+Air	41	62	73	92	2.67	0.813
	Mixed	VUV+N$_2$	77	81	ND	ND	26.92	0.999
	Single	UV	13	14	28	70	1.02	0.987
	Single	VUV	38	53	73	97	4.38	0.994
	Single	VUV+TBA	19	43	74	99	4.12	0.951
DBAN	Mixed	UV	96	98	100	ND	21.32	0.769
	Mixed	VUV	97	99	ND	ND	33.64	0.971
	Mixed	VUV+Air	90	99	99	ND	17.58	0.857
	Mixed	VUV+N$_2$	100	ND	ND	ND	66.26	0.775
	Single	UV	98	99	ND	ND	33.10	0.878
	Single	VUV	98	99	ND	ND	33.50	0.831
	Single	VUV+TBA	94	98	100	ND	31.61	1.000

Remark:

VUV+Air	= VUV with air purging
UV+N$_2$	= VUV with nitrogen gas (N$_2$) purging
VUV+TBA	= VUV with *tert*-butanol (TBA) addition
ND	= No data

จุฬาลงกรณ์มหาวิทยาลัย
CHULALONGKORN UNIVERSITY

Table B.2 Intermediates of each HAN in the single solution during VUV process

Parent HANs	Intermediate compounds			
	Retention time (min)	Name	Chemical structure	Exact mass (m/z)
MCAN	11.078	4H-1,2,4-Triazol-3-amine,4-ethyl- ($C_4H_8N_4$)		112
	12.108*	4-Penten-2-one, 3-methyl-, O-methyloxime ($C_7H_{13}NO$)		127
DCAN	2.640	Monochloroacetonitrile (C_2H_2ClN)		75
	2.825	2-chloropropionitrile ($CH_3CHClCN$)		90
	12.241	Dichloroacetamide ($C_2H_3Cl_2NO$)		128
TCAN	3.273	Dichloroacetonitrile (C_2HCl_2N)		109
	15.027	2,2,2-Trichloroacetamide ($C_2H_2Cl_3NO$)		162

Parent HANs	Intermediate compounds			
	Retention time (min)	Name	Chemical structure	Exact mass (m/z)
DBAN	4.672	Monobromoacetonitrile (C_2H_2BrN)	$Br-\underset{\underset{H}{\mid}}{\overset{\overset{H}{\mid}}{C}}-C\equiv N$	120
	2.302	2,2-dimethylpropanenitrile (C_5H_9N)	$H_3C-\underset{\underset{CH_3}{\mid}}{\overset{\overset{CH_3}{\mid}}{C}}-C\equiv N$	83
	5.682	1-Bromo-2-methyl-2-propanol (C_4H_9BrO)	$H_3C-\underset{\underset{CH_3}{\mid}}{\overset{\overset{OH}{\mid}}{C}}-\underset{\underset{H}{\mid}}{\overset{\overset{H}{\mid}}{C}}-Br$	153
	8.453	1-Bromo-2-methyl-2-butanol ($C_5H_{11}BrO$)	$H_3C-\underset{\underset{H}{\mid}}{\overset{\overset{H}{\mid}}{C}}-\underset{\underset{OH}{\mid}}{\overset{\overset{CH_3}{\mid}}{C}}-\underset{\underset{H}{\mid}}{\overset{\overset{H}{\mid}}{C}}-Br$	167
	6.434 *	Fumaronitrile ($C_4H_2N_2$)	$N\equiv C-\underset{\underset{H}{\mid}}{C}=\underset{\underset{H}{\mid}}{C}-C\equiv N$	78

Remark:

   *Intermediate detected when initial concentration of parent compounds were 500 mg L^{-1}.

APPENDIX C.
SUPPLEMENTARY DATA OF CHAPTER 5

Appendix C contains 28 figures, and 5 tables (lists as below).

C.1 H_2O_2 residual

Figure C.1 H_2O_2 residual of SW samples treated by VUV/H5 (5 mg L^{-1} H_2O_2)

Figure C.2 H_2O_2 residual of SW samples treated by VUV/H10 (10 mg L^{-1} H_2O_2)
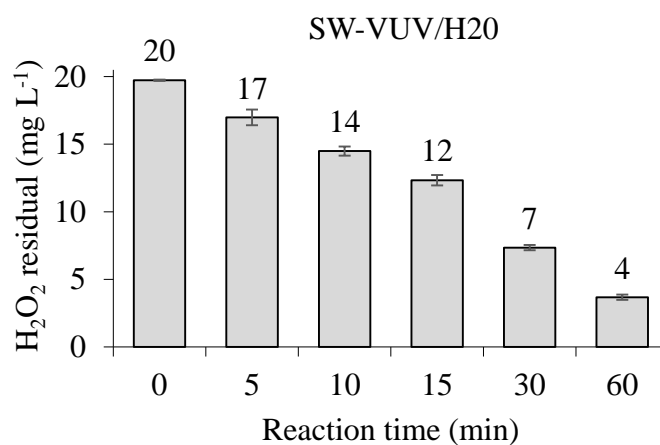
Figure C.3 H_2O_2 residual of SW samples treated by VUV/H20 (20 mg L^{-1} H_2O_2)
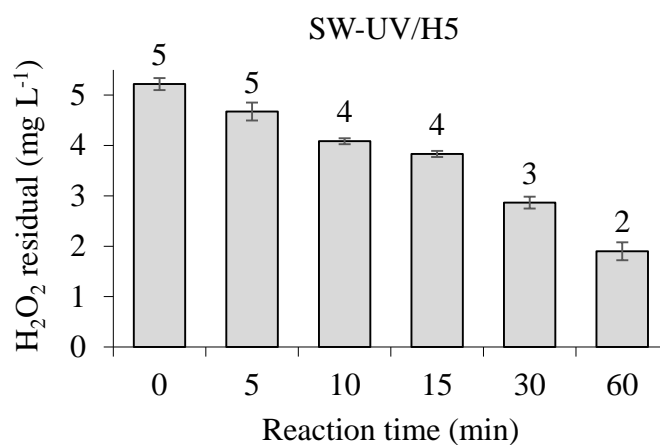
Figure C.4 H_2O_2 residual of SW samples treated by UV/H5 (5 mg L^{-1} H_2O_2)
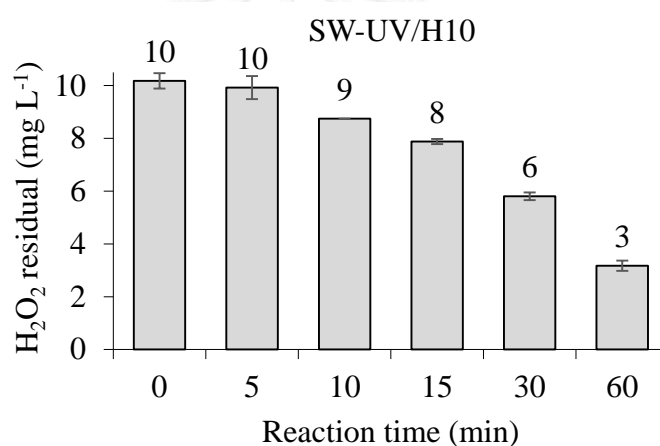
Figure C.5 H_2O_2 residual of SW samples treated by UV/H10 (10 mg L^{-1} H_2O_2)
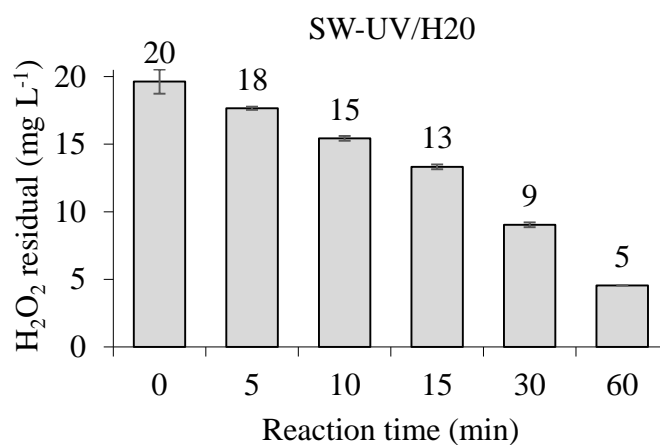
Figure C.6 H_2O_2 residual of SW samples treated by UV/H20 (20 mg L^{-1} H_2O_2)
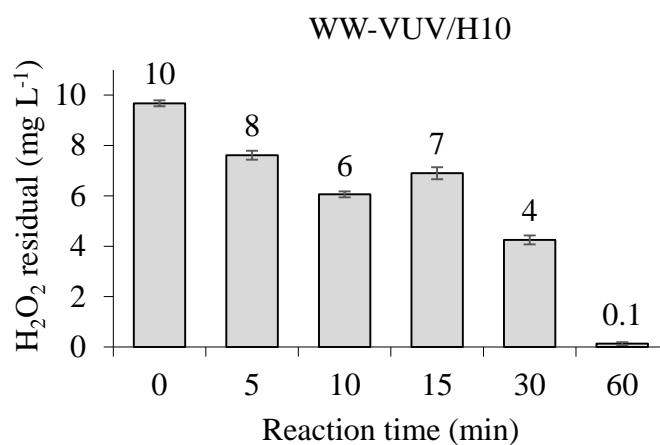
WW-VUV/H10

Figure C.7 H$_2$O$_2$ residual of WW samples treated by VUV/H10 (10 mg L^{-1} H$_2$O$_2$)
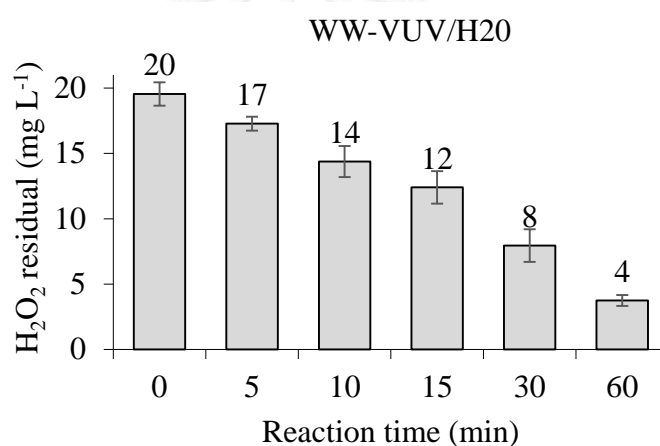
WW-VUV/H20

Figure C.8 H$_2$O$_2$ residual of WW samples treated by VUV/H20 (20 mg L^{-1} H$_2$O$_2$)
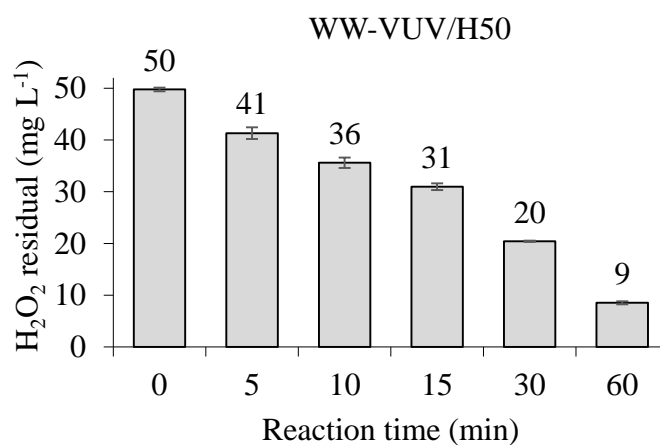
WW-VUV/H50

Figure C.9 H$_2$O$_2$ residual of WW samples treated by VUV/H50 (50 mg L^{-1} H$_2$O$_2$)
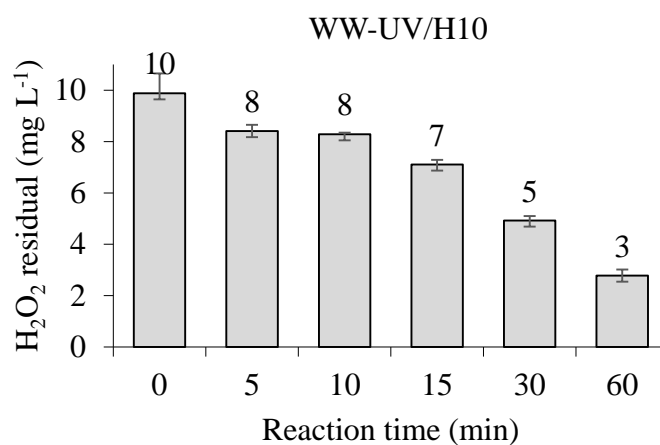
Figure C.10 H_2O_2 residual of WW samples treated by UV/H10 (10 mg L^{-1} H_2O_2)
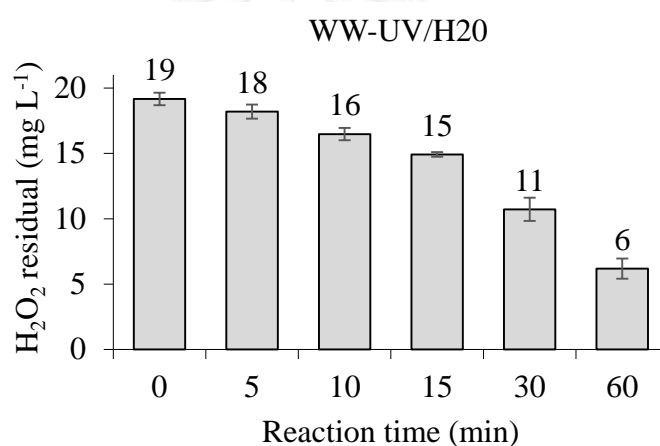
Figure C.11 H_2O_2 residual of WW samples treated by UV/H20 (20 mg L^{-1} H_2O_2)
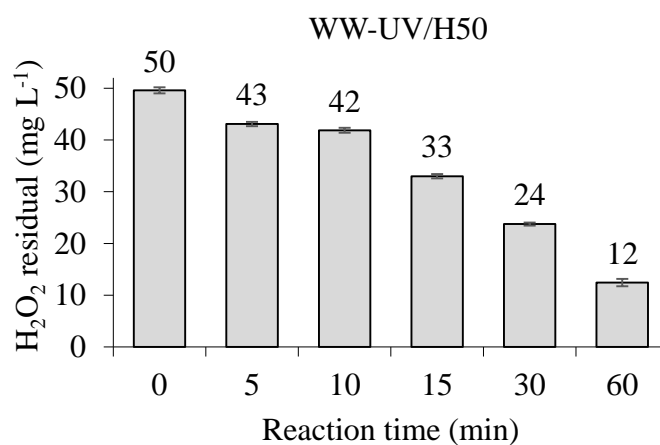
Figure C.12 H_2O_2 residual of WW samples treated by UV/H50 (50 mg L^{-1} H_2O_2)

C.2.   Reduction of UV$_{254}$
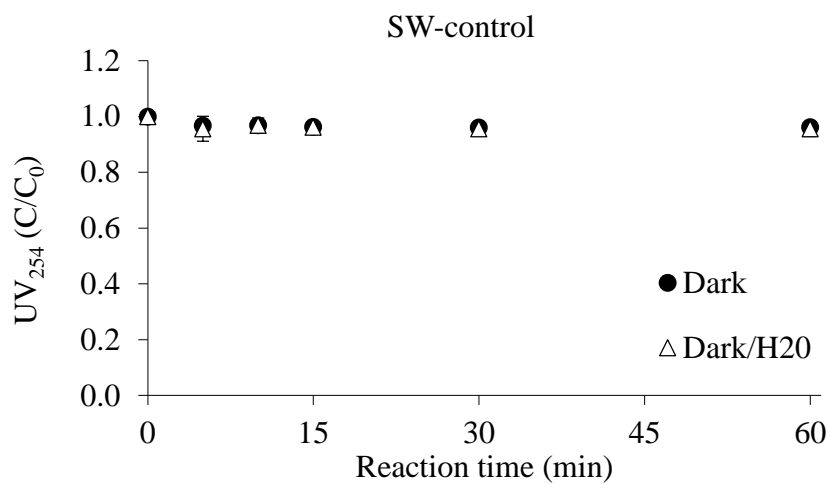
Figure C.13 Normalized UV$_{254}$ value (C/C$_0$) of untreated SW sample (Dark) and
treated SW sample with 20 mg L^{-1} H$_2$O$_2$ (Dark/H20)
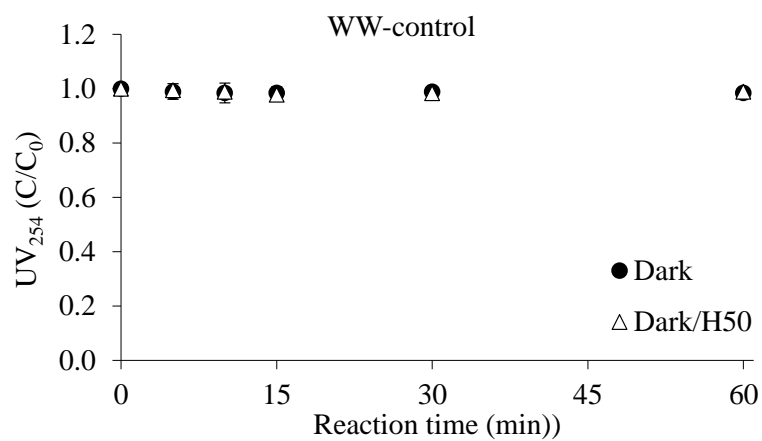
Figure C.14 Normalized UV$_{254}$ value (C/C$_0$) of untreated WW sample (Dark) and
treated WW sample with 50 mg L^{-1} H$_2$O$_2$ (Dark/H50)
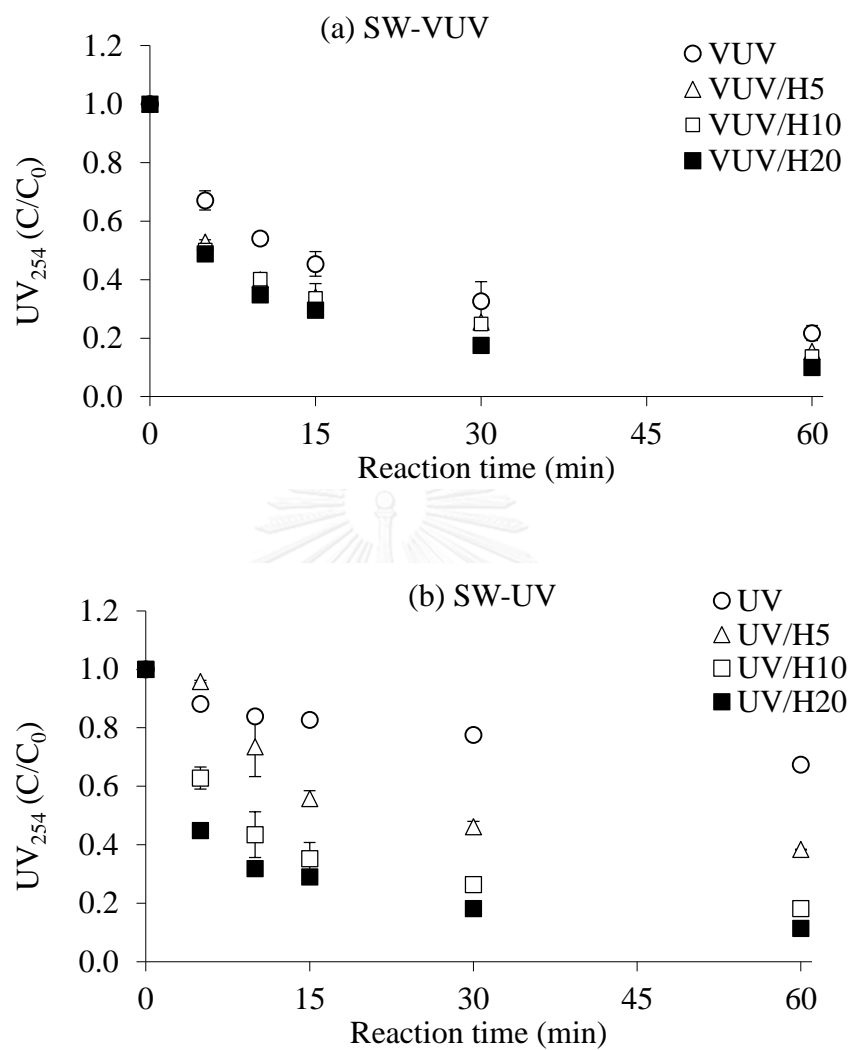
Figure C.15 Normalized UV_{254} value (C/C_0) of SW samples treated by (a) VUV, VUV/H_2O_2 and (b) UV, UV/H_2O_2 (H5, H10, and H20 represent H_2O_2 concentration at 5, 10, and 20 mg L^{-1}, respectively)
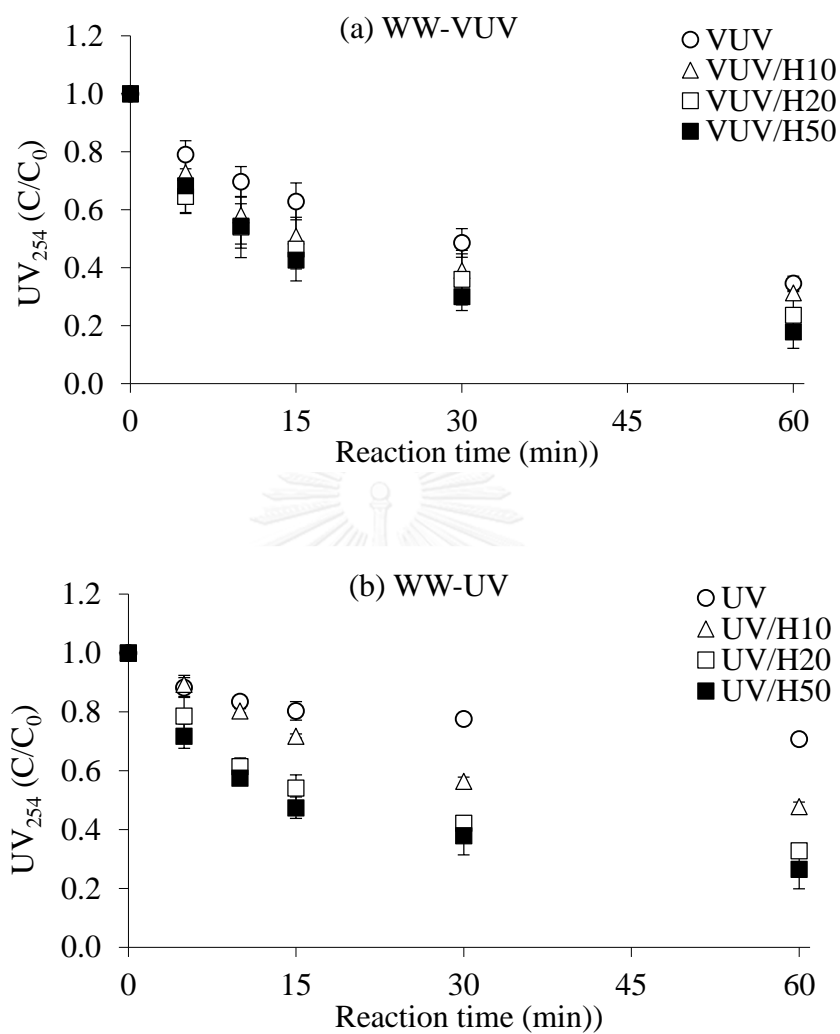
Figure C.16 Normalized UV_{254} value (C/C_0) of WW samples treated by (a) VUV, VUV/H_2O_2 and (b) UV, UV/H_2O_2 (H10, H20, and H50 represent H_2O_2 concentration at 10, 20, and 50 mg L^{-1}, respectively)

C.3. Reduction of DOC and DON of unirradiated samples

SW-control
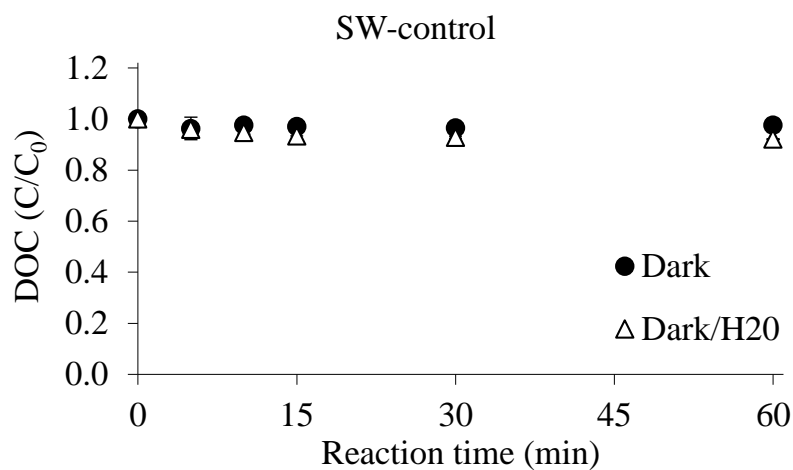
Figure C.17 Normalized DOC concentration (C/C$_0$) of unirradiated SW sample without H$_2$O$_2$ (Dark) and with 20 mg L^{-1} H$_2$O$_2$ (Dark/H20)

SW-control
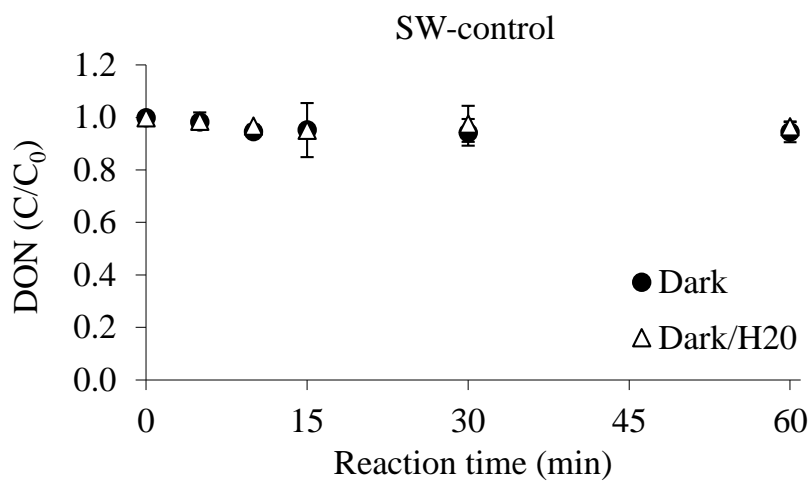
Figure C.18 Normalized DON concentration (C/C$_0$) of unirradiated SW sample without H$_2$O$_2$ (Dark) and with 20 mg L^{-1} H$_2$O$_2$ (Dark/H20)
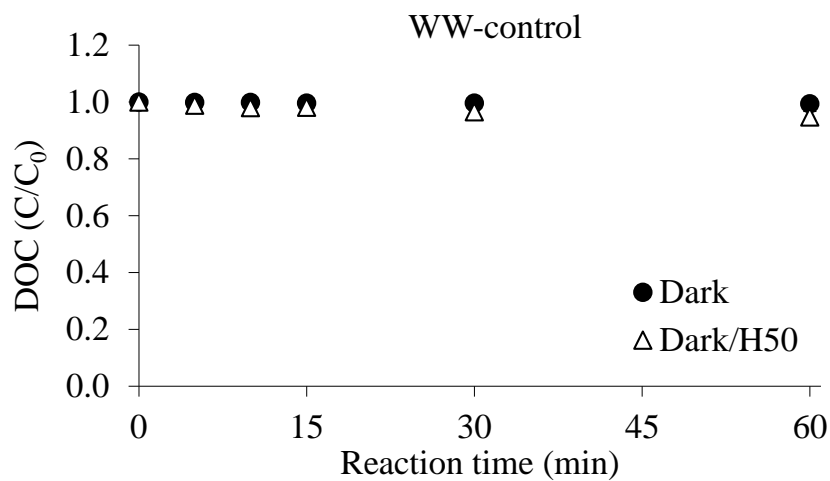
Figure C.19 Normalized DOC concentration (C/C_0) of unirradiated WW sample without H_2O_2 (Dark) and with 50 mg L^{-1} H_2O_2 (Dark/H50)
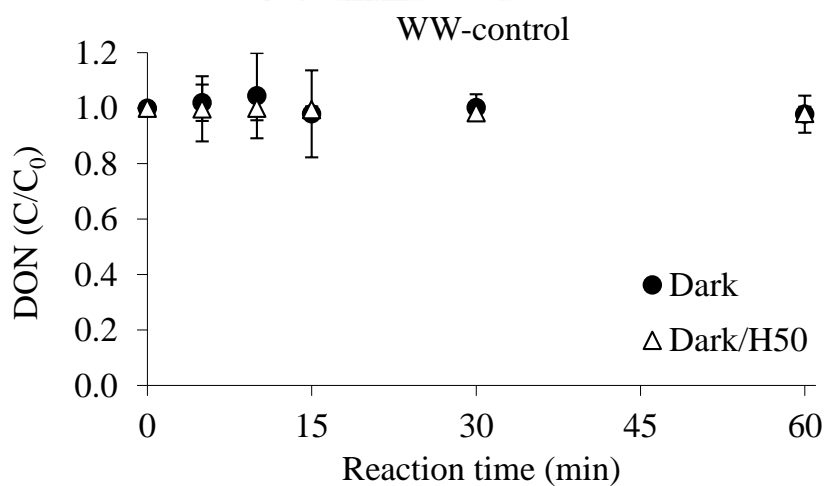
Figure C.20 Normalized DON concentration (C/C_0) of unirradiated WW sample without H_2O_2 (Dark) and with 50 mg L^{-1} H_2O_2 (Dark/H50)

C.4. FEEM

(a) VUV/H5
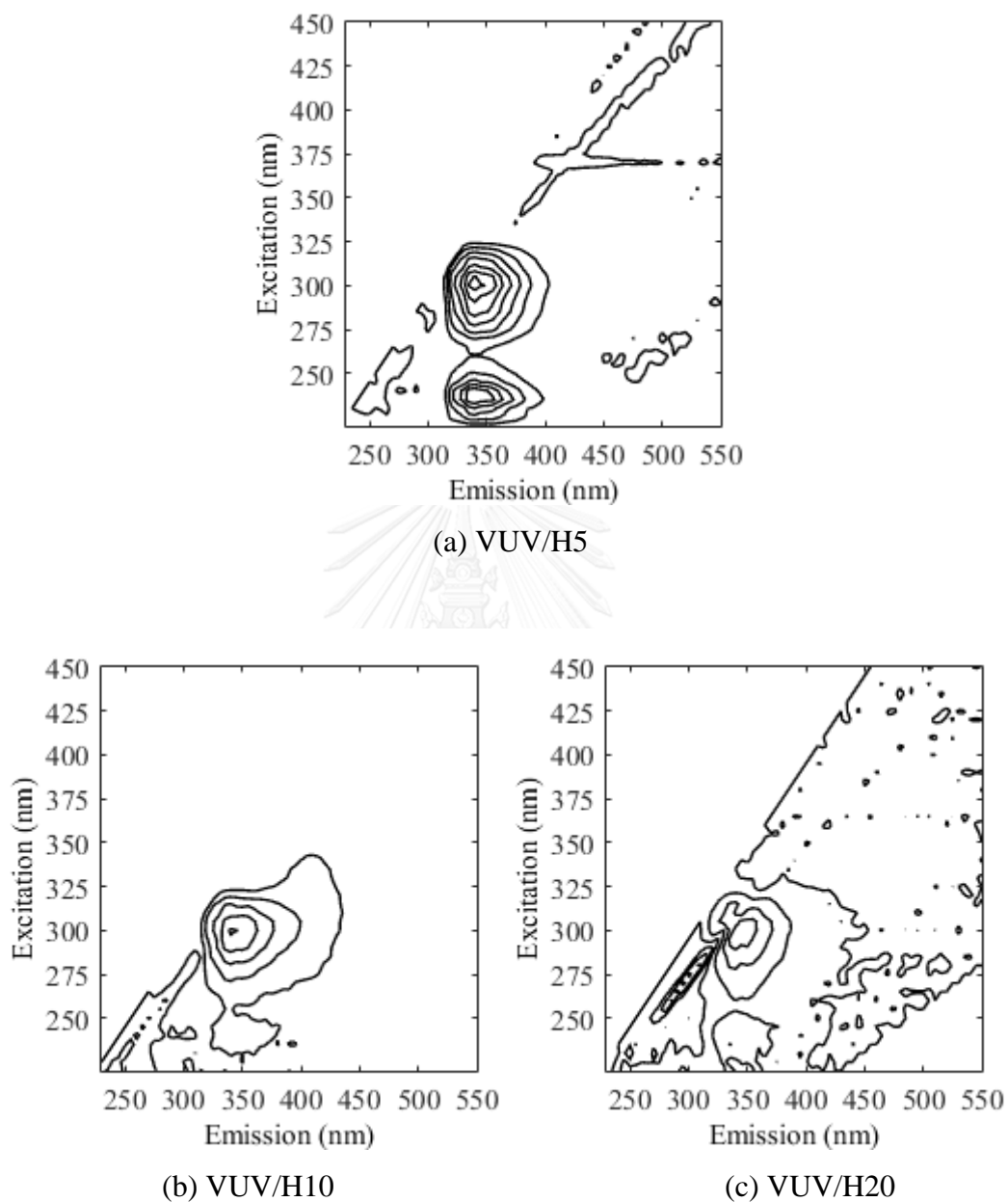
(b) VUV/H10

(c) VUV/H20

Figure C.21 FEEM of SW sample treated by VUV/H_2O_2 at 60 min

(H5, H10, and H20 represent H_2O_2 concentration at 5, 10, and 20 mg L^{-1}, respectively)
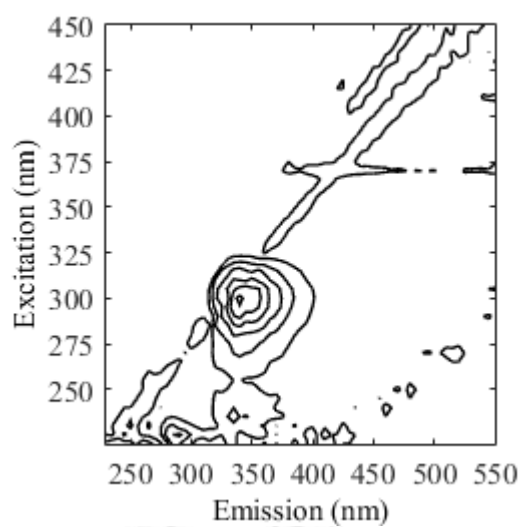
(a) UV/H5
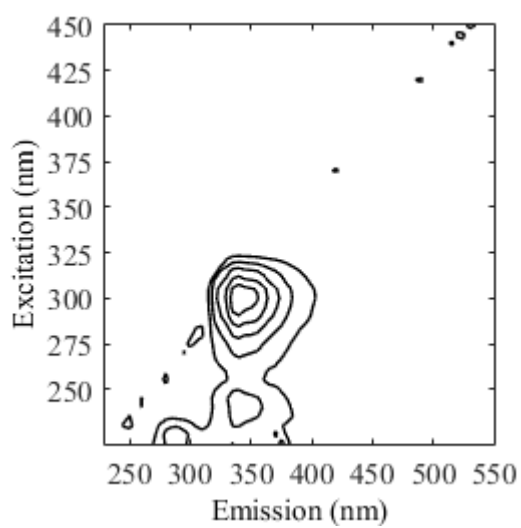
(b) UV/H10
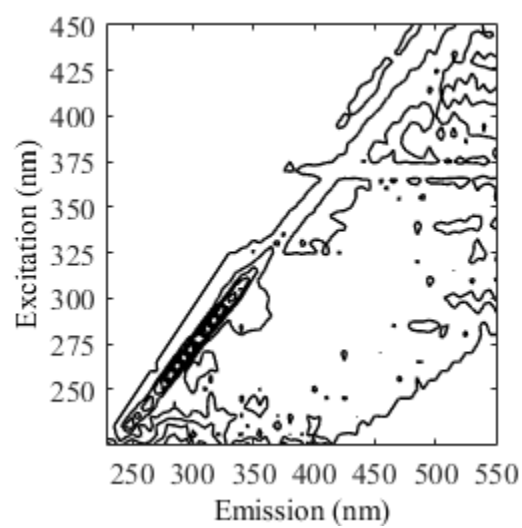
(c) UV/H20

Figure C.22 FEEM of SW sample treated by UV/H_2O_2 at 60 min

(H10, H20, and H50 represent H_2O_2 concentration at 10, 20, and 50 mg L^{-1},
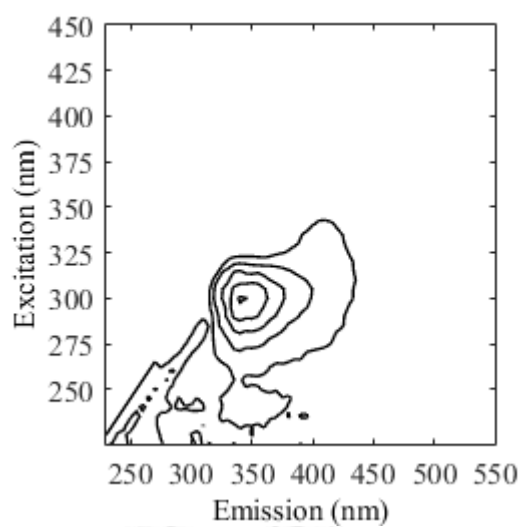
respectively)

(a) VUV/H10
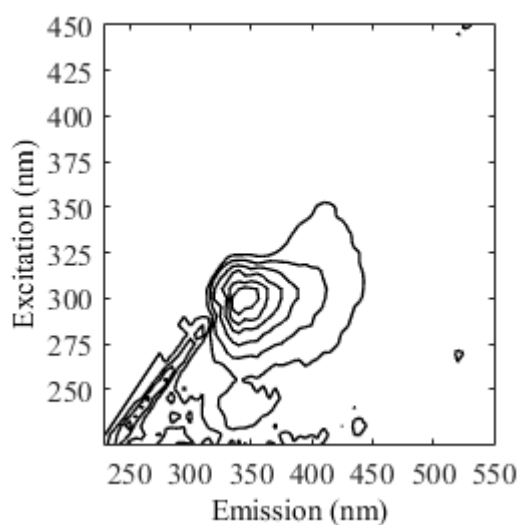
(b) VUV/H20
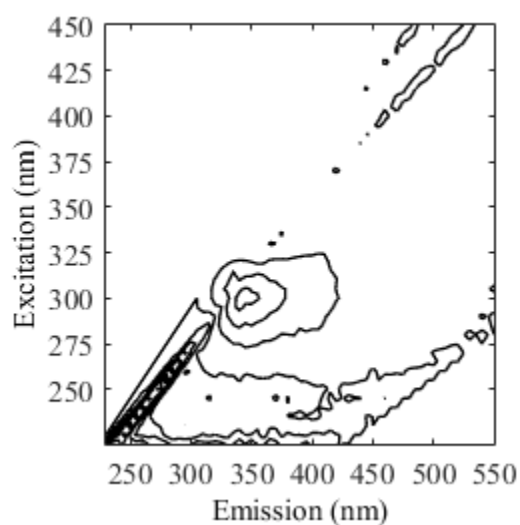
(c) VUV/H50

Figure C.23 FEEM of WW sample treated by VUV/H_2O_2 at 60 min

(H10, H20, and H50 represent H_2O_2 concentration at 10, 20, and 50 mg L^{-1},

respectively)

(a) UV/H10

(b) UV/H20

(c) UV/H50
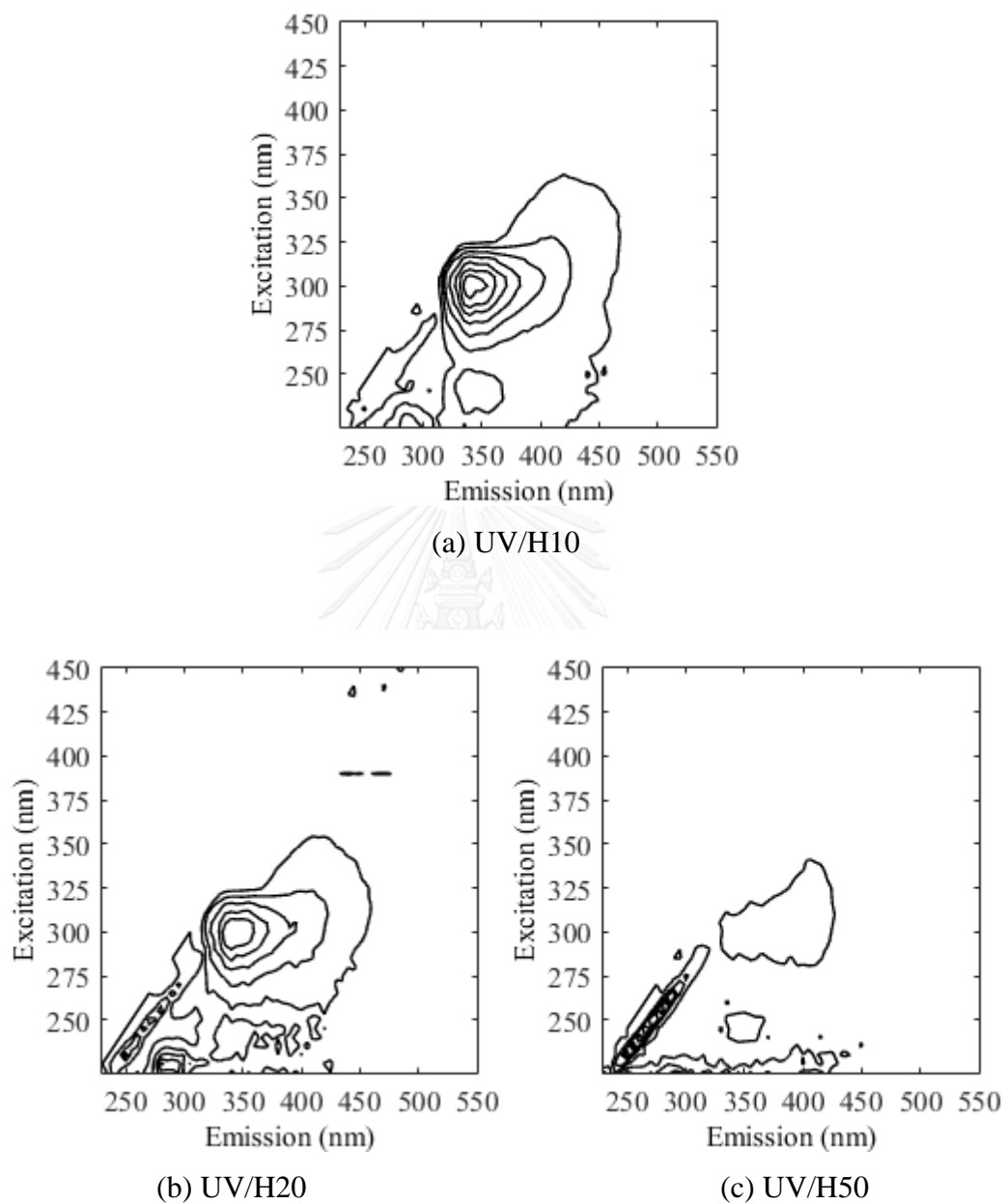
Figure C.24 FEEM of WW sample treated by UV/H_2O_2 at 60 min

(H10, H20, and H50 represent H_2O_2 concentration at 10, 20, and 50 mg L^{-1},

respectively)

Table C.1 Peak intensities of SW samples treated by VUV and VUV/H_2O_2 at 60 min

Ex/Em (nm)	Peak	Components	Peak intensity (QSU)			
			VUV	VUV/H5	VUV/H10	VUV/H20
295/340	B	Trytophan	2.10	1.03	0.85	0.59
270/420	C	Humic acid	4.21	0.37	0.13	0.19

Table C.2 Peak intensities of SW samples treated by UV and UV/H_2O_2 at 60 min

Ex/Em (nm)	Peak	Components	Peak intensity (QSU)			
			UV	UV/H5	UV/H10	UV/H20
295/340	B	Trytophan	2.10	1.79	0.59	0.49
270/420	C	Humic acid	4.21	3.34	0.03	0.14

Table C.3 Peak intensities of WW samples treated by VUV and VUV/H_2O_2 at 60 min

Ex/Em (nm)	Peak	Components	Peak intensity (QSU)			
			VUV	VUV/H10	VUV/H20	VUV/H50
220/295	A	Aromatic protein	5.54	1.37	0.17	0.11
290/340	B	Trytophan	14.05	5.67	5.50	5.21
315/405	C	Humic acid	9.08	1.11	0.34	0.21

Table C.4 Peak intensities of WW samples treated by UV and UV/H_2O_2 at 60 min

Ex/Em (nm)	Peak	Components	Peak intensity (QSU)			
			UV	UV/H10	UV/H20	UV/H50
220/295	A	Aromatic protein	5.54	2.51	0.46	0.30
290/340	B	Trytophan	14.05	6.93	1.30	0.50
315/405	C	Humic acid	9.08	5.24	0.54	0.24

(a) SW-VUV, VUV/H_2O_2-Peak B

$y = 1.2817x + 1.5958$
$R^2 = 0.9622$

(b) SW-VUV, VUV/H_2O_2-Peak C

$y = 0.4238x + 2.434$
$R^2 = 0.7852$
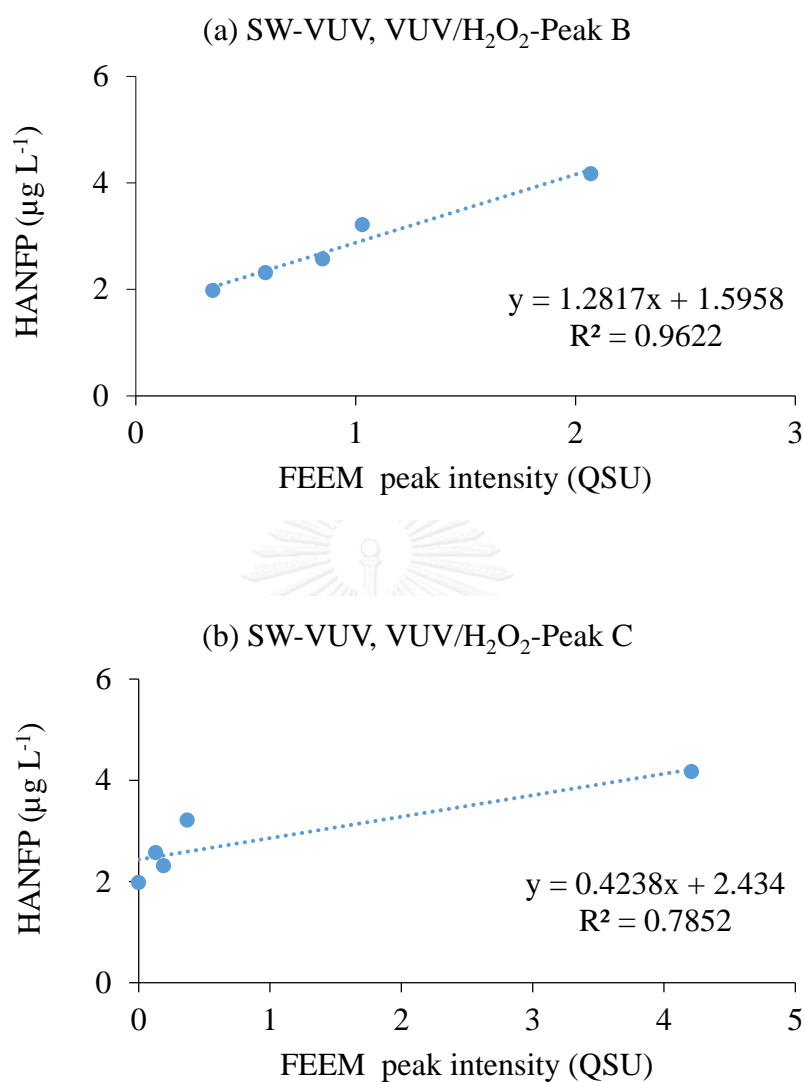
Figure C.25 Correlation between HANFP and FEEM peak intensities of SW samples at 60 min of VUV and VUV/H_2O_2: (a) Peak B: Tryptophan, and (b) Peak C: Humic acid

(a) SW-UV, UV/H$_2$O$_2$-Peak B

$$y = 0.9242x + 1.938$$
$$R^2 = 0.9134$$

HANFP (µg L^{-1})

FEEM peak intensity (QSU)

(b) SW-UV, UV/H$_2$O$_2$-Peak C

$$y = 0.3941x + 2.2409$$
$$R^2 = 0.8794$$

HANFP (µg L^{-1})

FEEM peak intensity (QSU)
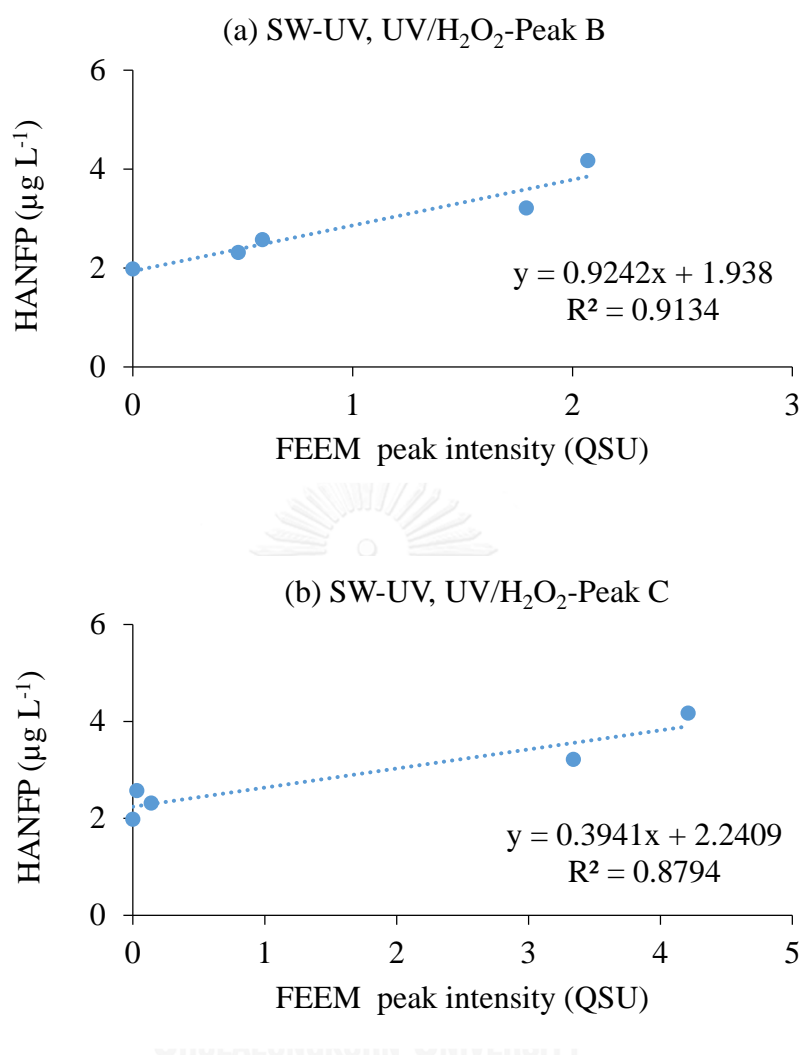
Figure C.26 Correlation between HANFP and FEEM peak intensities of SW samples at 60 min of UV and UV/H$_2$O$_2$: (a) Peak B: Tryptophan, and (b) Peak C: Humic acid
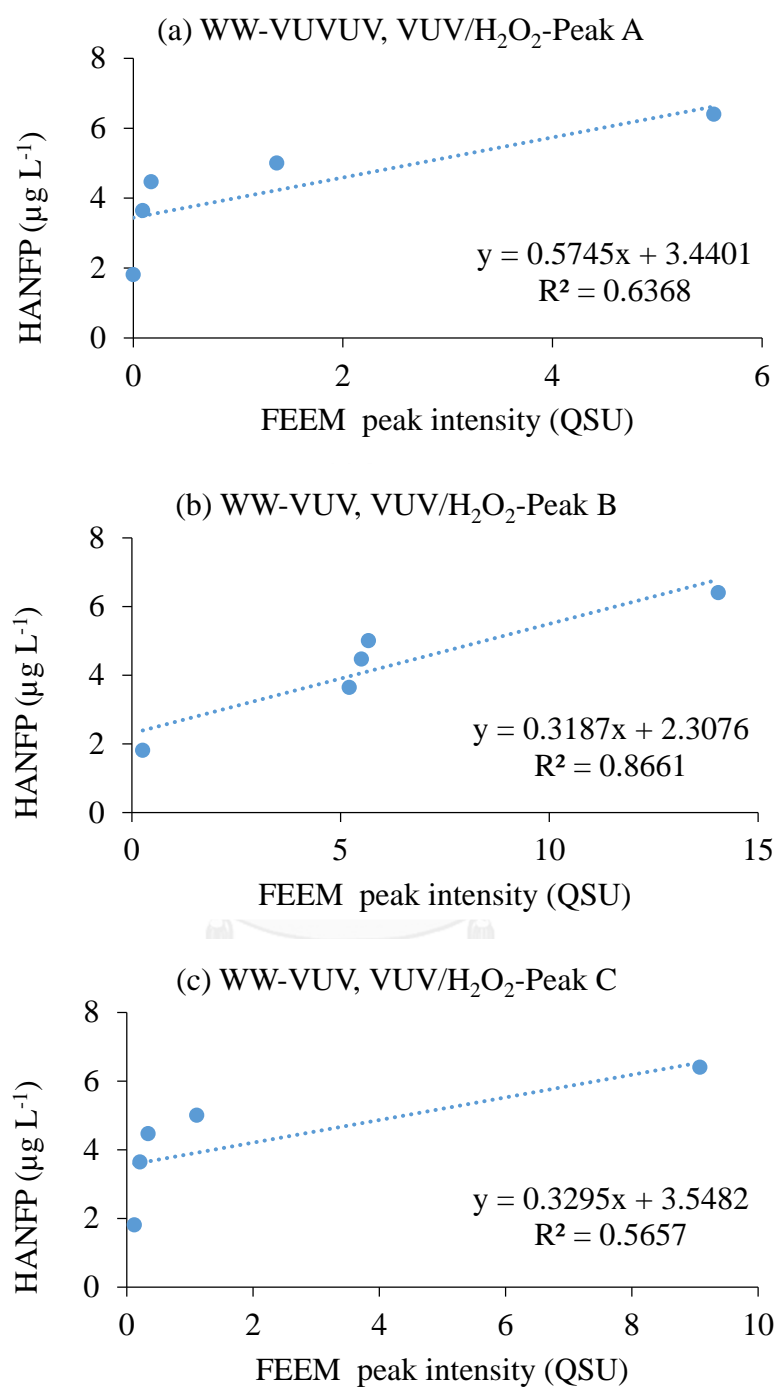
Figure C.27 Correlation between HANFP and FEEM peak intensities of SW samples
at 60 min of VUV and VUV/H_2O_2: (a) Peak A: Aromatic protein, (b) Peak B:
Tryptophan, and (c) Peak C: Humic acid
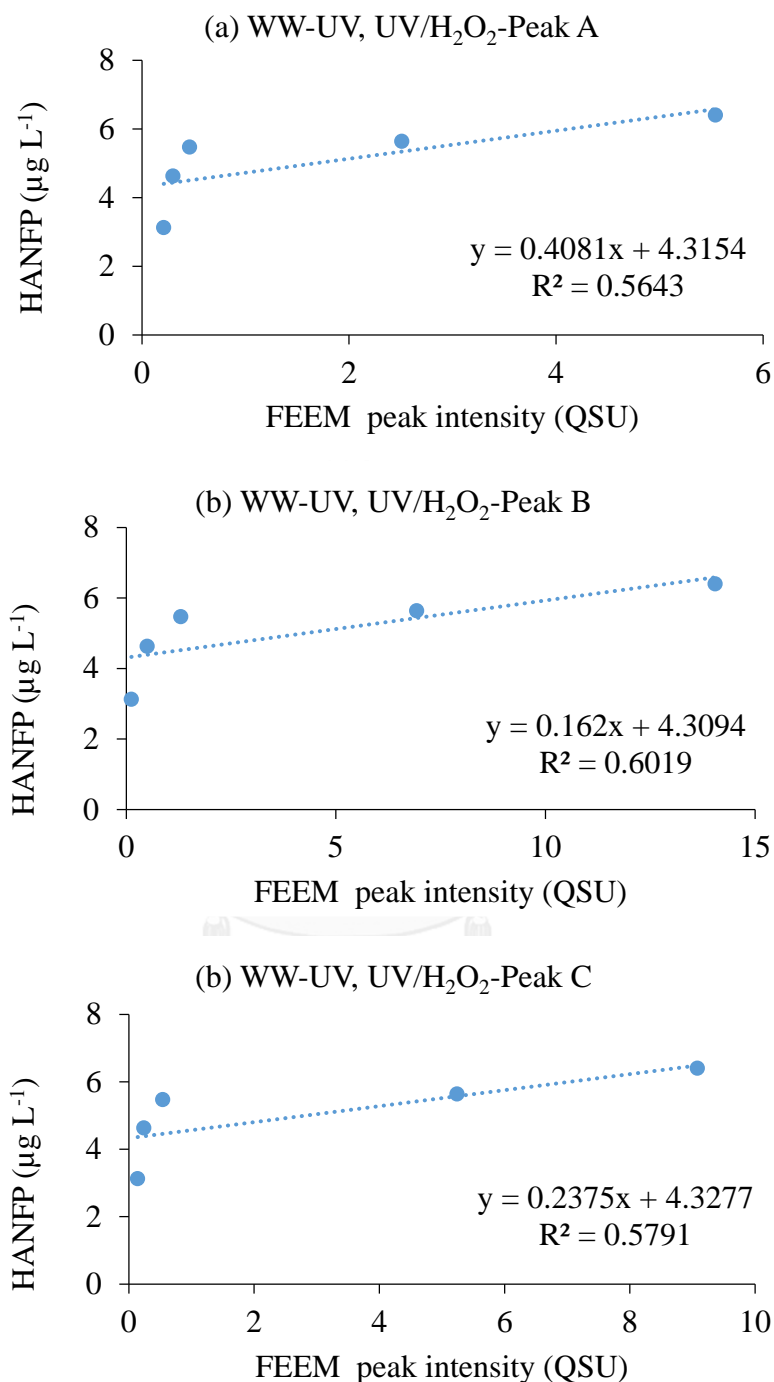
Figure C.28 Correlation between HANFP and FEEM peak intensities of SW samples

at 60 min of UV and UV/H_2O_2: (a) Peak A: Aromatic protein, (b) Peak B:

Tryptophan, and (c) Peak C: Humic acid

Table C.5 Correlation between HANFP and FEEM peaks intensities of SW and WW samples at 60 min of VUV and UV treatments

FEEM peaks	Surface water (SW)		Treated wastewater effluent (WW)	
	VUV/H2O$_2$	UV/H$_2$O$_2$	VUV/H$_2$O$_2$	UV/H$_2$O$_2$
	R^2	R^2	R^2	R^2
Peak A	-	-	0.6368	0.5643
Peak B	0.9622	0.9134	0.8661	0.6019
Peak C	0.7852	0.8794	0.5657	0.5791

Remark:

Peak A: Aromatic protein

Peak B: Tryptophan and protein like-compound

Peak C: Humic acid-like compound

C.5. Reduction of Specific UV$_{254}$ absorbance (SUVA)

$$\text{SUVA (L mg-C}^{-1}\text{ m}^{-1}) = (\text{UV}_{254} / \text{DOC}) \times 100 \qquad\qquad (\text{C.1})$$
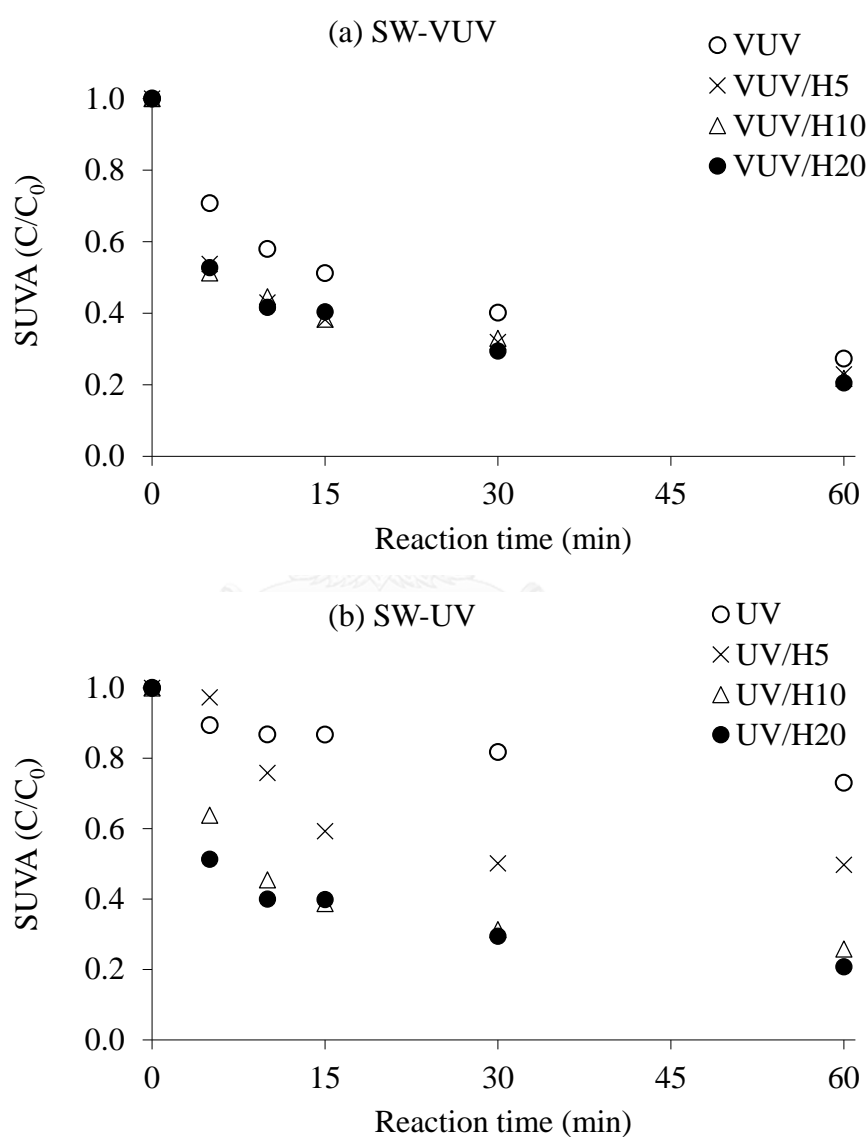
Figure C.29 Normalized SUVA value (C/C$_0$) of SW samples treated by (a) VUV, VUV/H$_2$O$_2$ and (b) UV, UV/H$_2$O$_2$ (H5, H10, and H20 represent H$_2$O$_2$ concentration at 5, 10, and 20 mg L^{-1}, respectively)
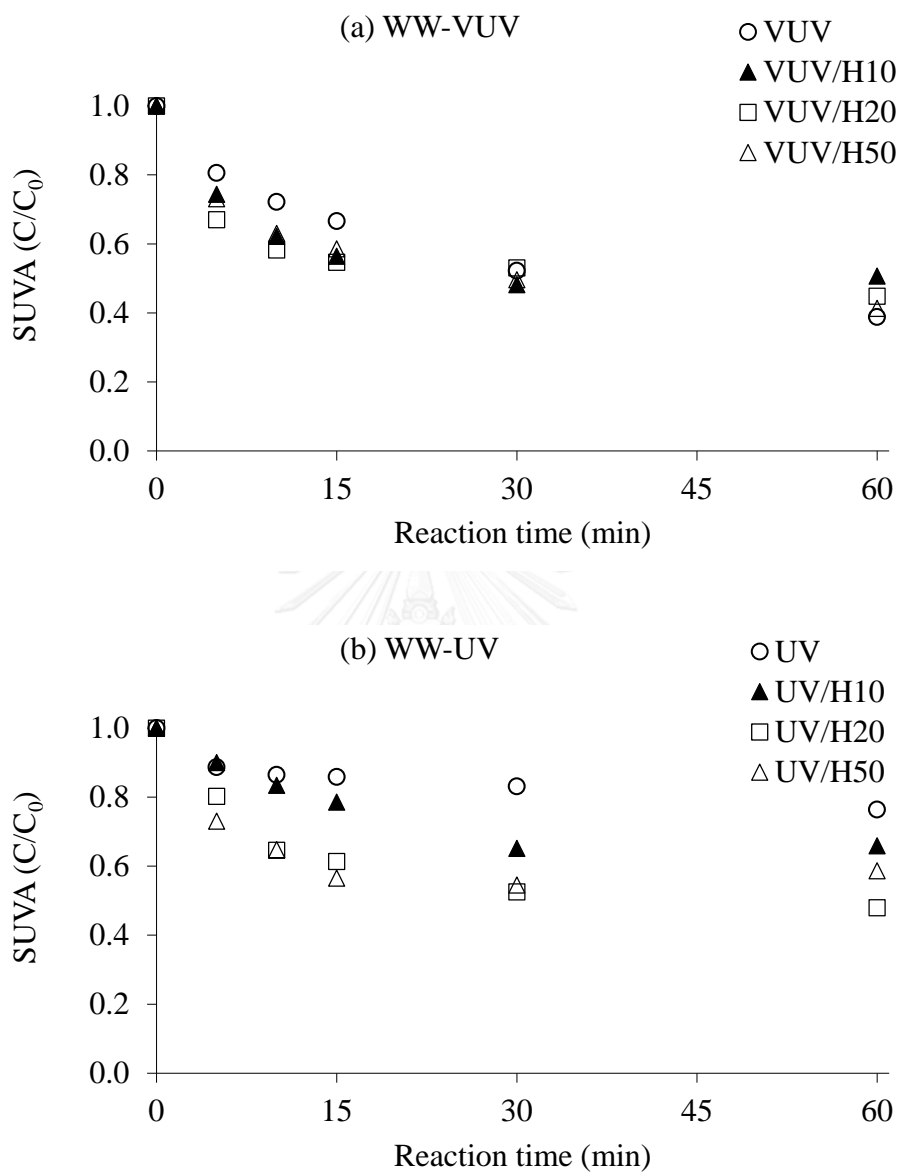
Figure C.30 Normalized SUVA value (C/C$_0$) of WW samples treated by (a) VUV, VUV/H$_2$O$_2$ and (b) UV, UV/H$_2$O$_2$ (H10, H20, and H50 represent H$_2$O$_2$ concentration at 10, 20, and 50 mg L^{-1}, respectively)

VITA

Miss Pradabduang Kiattisaksiri was born on December 13, 1985 in Chaiyaphum province, Thailand. She graduated high school in Kanjanapisek Wittayalai Chaiyaphum School in 2003. After that she studied Bachelor degree at Faculty of Science and Technology, Thammasat University, Thailand. She received her Bachelor Degree of Science in Health Science (major Environmental Health) in academic year 2007. Two year later, she received her Master's degree of Science in Environmental Management, the International Postgraduate Program in Hazardous Substance and Environmental Management (IP-HSM), Graduate School, Chulalongkorn University, Thailand, in 2009. After that she worked as an environmental officer at Center of Excellence on Hazardous Substance Management (HSM) for 1 year before started PhD life. She attended Doctoral studies in the same program with MSc degree, and finished the Degrees of Doctor of Philosophy Program in Environmental Management in 2016.